

DESIGN AND SIMULATION OF A BIPED WALKING MACHINE

Ramesh R Bale

BE Honours (University of Mysore)

May 1994

*A thesis submitted for the degree of Master of Engineering (Research)
of the Australian National University*

Department of Engineering
Faculty of Engineering and Information Technology
The Australian National University

Acknowledgements

I would like to sincerely thank my supervisor, Dr Jon Kieffer for his excellent and thorough guidance throughout my masters program. The support and encouragement given by him during this research is much appreciated. This acknowledgment would not be complete without reference to my friends who have been there for me during the last 2 years, especially Perry Blackmore and Ken Yamazaki. Finally, I thank my beloved wife Meenu for her support and patience.

Statement of Originality

The information presented in this thesis is the result of original research and has not been submitted for the purpose of obtaining a higher degree at any university or institution.

The work in this thesis is based on the research presented in publication [1].

The research described in this thesis is the result of a collaborative effort with my Masters supervisor Dr. Jon Kieffer.



Ramesh R. Bale

May 13, 1994 .

Nomenclature

$g :$	Acceleration due to gravity, $\frac{m}{sec^2}$.
$J_\ell, J_b, J_m :$	Mass moment of inertia of the leg assemblies, body and rotor about the hip axis, $\frac{kg}{m^2}$.
$J_0 :$	$J_0 = J_\ell + m\ell^2$, Effective mass moment of inertia of support leg about point of ground contact, $\frac{kg}{m^2}$.
$\ell :$	Leg length, m.
$L :$	Step length, m.
$m_\ell, m_b :$	Mass of the leg assemblies and body respectively, kg.
$m :$	$m = m_\ell + m_b$, Mass of the biped, kg.
$\tau_i :$	Torque at joints $i \in (0, 1)$, Nm.
$\tau_m :$	Motor torque, Nm.
$N :$	Gear ratio of the reduction unit.
$\theta_0, \dot{\theta}_0, \ddot{\theta}_0 :$	Position, velocity and acceleration of the stance leg with respect to the vertical, rad, $\frac{rad}{sec}$, $\frac{rad}{sec^2}$.
$\theta_m, \dot{\theta}_m, \ddot{\theta}_m :$	Position, velocity and acceleration of the rotor with respect to the stance leg, rad, $\frac{rad}{sec}$, $\frac{rad}{sec^2}$.
$\theta_1, \dot{\theta}_1, \ddot{\theta}_1 :$	Position, velocity and acceleration of the body with respect to the stance leg, rad, $\frac{rad}{sec}$, $\frac{rad}{sec^2}$.
$\eta :$	Efficiency of the reduction unit.
$K_t :$	Torque constant of the motor, $\frac{Nm}{Ampere}$.
$K_b :$	Back emf constant of the motor, $\frac{Volts}{rad/sec}$.
$V_b :$	Motor back emf, Volts.
$i :$	Motor current, Ampere.
$R :$	Motor terminal resistance, Ohms.
$u :$	Motor control voltage, Volts.
$V_{max} :$	Maximum motor control voltage, Volts.
No Load Speed :	No load speed of the motor, $\frac{rad}{sec}$.
$L_m :$	Motor terminal inductance, Henry.

b :	Body radius, m.
A_{ob} :	Area enclosed between the legs and the floor below the body, m^2 .
A_{ob}^* :	Dimensionless area enclosed between the legs and the floor below the body.
θ_{0max} :	Maximum value of θ_0 from which the biped can recover to the balanced vertical position, rad.
θ_{opt} :	Value of θ_0 which maximizes area A_{ob}^* for a given body radius b , rad.
T_{sim} :	Simulation time, sec.
α :	Angle considered for stability criteria along the roll axis, rad.
N_{FS} :	Factor of safety in design.
SY_i :	Yield strength of the material of link $i \in$ (leg, body), $\frac{N}{m^2}$.
ρ :	Mass density of the aluminium alloy, $\frac{kg}{m^3}$.
w_s :	Width of the biped based on the stability criteria, m.
w_r :	Width of the body or rim, m.
h_r :	Rim thickness of the body, m.
t_d :	Disc thickness of the body, m.
d_g :	Reduction unit shaft diameter.
E :	Young's modulus of aluminium alloy, $\frac{N}{m^2}$.
$\frac{\Delta \ell}{\ell}$:	Allowable deflection per unit length of the leg.
d_ℓ :	Outside diameter of the leg cross section , m.
t_ℓ :	Cross sectional thickness of the leg, m.
w_ℓ :	Width of the foot, m.
motor Mass :	Mass of the motor, kg.
motor Diameter :	Diameter of the motor, m.
gear Mass :	Mass of the reduction unit, kg.
gear Diameter :	Diameter of the reduction unit, m.
motor Length :	Length of the motor, m.
gear Length :	Length of the reduction unit, m.

m_a :	Mass of the actuators = $2 \times (\text{motor mass} + \text{gear mass})$, kg.
Stall Torque :	Stall torque of the motor, Nm.
C_p :	Specific heat of copper, $\frac{J}{kg \text{ } ^\circ C}$.
C_{th} :	Thermal capacitance of the motor, $\frac{J}{^\circ C}$.
R_{th} :	Thermal resistance of the motor, $\frac{^\circ C}{J} \text{sec}$.
T_a :	Ambient temperature, $^\circ C$.
T_{motor} :	Motor temperature, $^\circ C$.
i_{max} :	Maximum motor current, Ampere.
F_n, F_t :	Normal and tangential foot forces.
μ :	Coefficient of friction between the support foot and the ground surface.
ν :	Poisson's ratio of aluminium alloy.
t_{Fab} :	Fabrication thickness, m.
$T_{motor \text{ max.}}$:	Maximum motor temperature, $^\circ C$.
$V_{supply \text{ max.}}$:	Maximum motor supply voltage, Volts.
$i_{supply \text{ max.}}$:	Maximum motor supply current, Ampere.
M_{gis} :	Maximum gear input speed, $\frac{rad}{sec}$.
ℓ_{min} :	Minimum leg length, m.

Abstract

This report covers the design of a biped walking machine. The design is based on concepts proposed in [1] which reduce the complexity of the biped's governing dynamics to a trivial level. The aim is to use commercial actuators in the design of a small, light, low-cost biped that can step over relatively large obstacles. The approach is based on system modelling, design optimization and verification by computer simulation. The resulting biped weighs 2.1 kg and has a leg length (0.23 m) to stride (0.246 m) ratio of 0.93.

Contents

Acknowledgments	i
Nomenclature.	iii
Abstract	vi
1 Introduction	1
1.1 General Background	1
1.1.1 Existing Biped Robots	1
1.2 Motivation for this Work	4
1.2.1 Dynamically Simple Biped	4
1.3 Focus of Research	5
1.4 Overview of Thesis	5
2 Conceptual Description of the Machine	6
2.1 Introduction	6
2.2 Concepts for Biped Design	6
2.2.1 Walking Gaits	8
2.2.2 Physical Implementation	10
2.3 Type of Machine Considered for the Detailed Design	13
2.4 Design Objectives	13
3 Governing Equations	15
3.1 Introduction	15
3.2 Definition of Planes	15
3.3 Assumptions in Mathematical Modelling	16
3.4 Dynamic Equations of Motion	17
3.5 Motor Equations	18
3.6 Motor Equations After Gear Reduction	20

3.7	Dynamic Equations in terms of Control Voltage-u	20
3.8	State-Space Representation	21
3.9	Thermal Model for the Motor	23
3.9.1	Introduction	23
3.9.2	Assumptions in Motor Thermal Model	23
3.9.3	Thermal Model Equations	23
3.9.4	Practical issues of Thermal modelling	25
3.10	Foot Force and Friction Equations	26
4	Formulation of the Design Optimization Problem	27
4.1	Introduction	27
4.2	Optimization Criteria	27
4.2.1	Introduction	27
4.2.2	Largest Obstacle Crossing Criteria	29
4.2.3	Optimization Strategy	32
4.3	Actuator Constraints	33
4.3.1	Introduction	33
4.3.2	Actuator Performance Limits	33
4.3.3	Actuator Dimensions	35
4.3.4	Other Actuator Parameters	36
4.4	Gear Box Constraints	36
4.4.1	Gear Box Properties	36
4.4.2	Gear Box Speed Constraint	36
4.5	Foot Force Constraint and Friction Limits	37
4.5.1	Foot Force Constraint	37
4.5.2	Friction Limits	37
4.6	Stability in the Lateral Plane	37
4.7	Material Selection	39
4.8	Body Design Constraints	41
4.8.1	Introduction	41
4.8.2	Design Objective	41
4.8.3	Hub Dimensions	42
4.8.4	Constraints on the Body Radius b	42
4.8.5	Constraints on Disc Thickness t_d	44

4.8.6	Constraints on Rim Width w_r and Rim Thickness h_r	48
4.8.7	Mass of the Body	49
4.8.8	Mass Moment of Inertia of the Body	49
4.9	Design Constraints of the Leg Assemblies	49
4.9.1	Introduction	49
4.9.2	Objectives and Assumptions	50
4.9.3	Leg Stress and Deflection Constraints	51
4.9.4	Constraint on the Leg Length ℓ and Width of the Foot w_ℓ	52
4.9.5	Mass of the Leg Assemblies	53
4.9.6	Mass Moment of Inertia of the Leg Assemblies	53
4.10	Summary of the Design Optimization Problem	55
5	Solution to the Design Optimization Problem	57
5.1	Introduction	57
5.2	Motor Operation Scheme	57
5.3	Maximum Stance Angle	59
5.3.1	Assumptions	59
5.3.2	Solution to Maximum Stance Angle θ_{0max}	59
5.4	Solution to Optimized Biped	61
5.4.1	Solution to Body Design	63
5.4.2	Solution to Design of Leg Assemblies	65
5.5	Verification by Simulation	66
5.5.1	Controller Design	66
5.5.2	Simulation	68
6	Results	70
6.1	Actuator Set Selection	70
6.1.1	Motor Muscle	70
6.1.2	Motor Constant and Combined Motor Parameter	71
6.1.3	Stall Torque	73
6.1.4	Criteria For Selecting Actuator Sets	73
6.2	Optimization Results	73
6.2.1	Biped Design with Maxon DC Motors	74
6.2.2	Biped Design with Pittman Brushless DC Motors	74
6.2.3	Biped Design with Maxon Brushless EC Motors	76

6.2.4	Biped Considered for the Detailed Design	77
7	Specifications of the Best Biped	78
7.1	Introduction	78
7.2	Commercially-available Components	78
7.2.1	Motor	78
7.2.2	Motor Control Unit	80
7.2.3	Encoder	80
7.2.4	Planetary Gearhead	82
7.2.5	Output Resolution	82
7.2.6	Rate Gyro	83
7.2.7	Electrolytic Tilt Sensor	85
7.3	Custom-manufactured Components	86
7.4	Cost Estimate	87
7.5	Overall Specifications of the Best Biped	88
8	Verification of the Final Design through Simulation	90
8.1	Introduction	90
8.2	Behaviour of the Best Biped Under Control	90
8.3	Verification of the Motor Thermal Model	96
9	Conclusion	98
10	Recommendations	100
	Bibliography	102
A	Single-Leg Support Phase Equations	105
A.1	Introduction	105
A.2	Inverted Pendulum Model	105
B	Optimum Step Angle $\theta_{optimum}$	108
B.1	Introduction	108
B.2	Unique Step Length	108
B.2.1	Optimum Stance Angle Corresponding to Unique Step Length . . .	110

C	MATLAB ALGORITHM	111
C.1	Introduction	111
C.2	Main Script File ‘OptAllscript’	111
C.2.1	MotorFiles	113
C.2.2	Optimize	114
C.2.3	SetBipedScript	115
C.2.4	SetGearset	116
C.2.5	Set ℓ min	116
C.2.6	Stability	116
C.2.7	BodyDesign	116
C.2.8	LegDesign	119
C.2.9	Alalloytubes	121
C.2.10	Al6106-T6	122
C.2.11	SetTuberset	122
C.2.12	put_GLOBAL_DATA	122
C.2.13	find_bol_opt	123
C.2.14	theta_minus_theta	124
C.2.15	get_GLOBAL_DATA	124
C.2.16	LinearModel_Order3	125
C.2.17	MaxTheta0	126
C.2.18	doublesort	126
C.2.19	SetBestScript	127
C.2.20	SimGDscript	127
C.2.21	pend	128
C.2.22	uofx	129
D	Motor Data for Maxon_990	130
D.1	Introduction	130
D.2	MAXON_990.m File Used in MATLAB Routine	130
E	Motor Data for Pittman_3112_43	132
E.1	Introduction	132
E.2	PITTMAN3112.43.m File Used in MATLAB Routine	132

F Motor Data for Maxon_136	134
F.1 Introduction	134
F.2 MAXON_136.m File Used in MATLAB Routine	134

List of Figures

2-1	Biped Machine- one foot per leg.	7
2-2	Biped Machine- two feet per leg.	7
2-3	Notations used for Deriving Biped Dynamic Equations in [1].	7
2-4	Wheel Gait.	8
2-5	Inchworm Gait.	9
2-6	Single-Leg Support Phase.	9
2-7	Dual-Leg Support Phase.	10
2-8	Biped Walking Machine.	11
2-9	Potentiometer for Measuring Stance Angle.	12
3-1	Definition of Planes.	16
3-2	Single-Leg support Phase Notations.	17
3-3	Electro-Mechanical Model of the DC Motor Assembly.	18
3-4	Foot Forces.	26
4-1	Maximum Slope that the Biped can Climb	28
4-2	Measure of Ability to Cross Large Obstacles.	28
4-3	Variation of Area A_{ob} due to increase in the Body Radius.	29
4-4	Area A_{ob} as $\theta_0 \rightarrow \theta_{0largest}$	29
4-5	Relation between θ_0 and step length L	30
4-6	Area A_{ob} Vs θ_0	31
4-7	Dimensionless Area A_{ob}^* Vs $\frac{b}{l}$	32
4-8	Stability in Lateral Plane.	38
4-9	Design Parameters of the Body.	42
4-10	Limiting Speed of the Disc.	44
4-11	Braking Force on the Body.	45
4-12	Body in Bending Mode.	46

4-13 Leg Assembly.	50
4-14 Design Parameters of the Leg.	51
4-15 Biped Leg Assumed for Design Optimization.	53
5-1 Torque Vs Speed Curve of a typical DC Motor.	58
5-2 Configuration of the Body without Rim.	65
5-3 Representation of State Feedback Control	69
6-1 Motor Constant K_m Vs Motor Mass.	71
6-2 Combined Parameter $\frac{K_m}{R_{th}}$ Vs Motor Mass.	72
6-3 BOLOpt. for 19 Maxon DC Motors.	75
6-4 BOLOpt. for 10 Pittman Brushless DC Motors.	76
6-5 BOLOpt. for 6 Maxon Brushless EC Motors.	77
7-1 Gyrostar.	83
8-1 θ_0 Vs. Time.	91
8-2 $\dot{\theta}_0$ Vs. Time.	91
8-3 $\dot{\theta}_1$ Vs. Time.	92
8-4 θ_1 Vs. Time.	92
8-5 Normal Force Vs. Time.	93
8-6 Coefficient of Friction Vs. Time.	94
8-7 Control u Vs. Time.	94
8-8 Current Vs. Time.	95
8-9 Back emf Vs. Time.	95
8-10 Temperature of the Motor Vs. Time.	96
C-1 Flow Chart of OptAllscript.	112

Chapter 1

Introduction

1.1 General Background

Motivation for building walking machines arrives from the need for vehicles that can travel on difficult terrain where existing vehicles cannot go. About half the earth's surface is inaccessible to wheeled or tracked vehicles [2]. Compared to the legged locomotion, wheeled locomotion is only attractive on prepared or naturally hard and even surfaces. In principle, legged locomotion should be mechanically superior over a considerable range of soil conditions [2] and is certainly superior for crossing obstacles. This is well illustrated by the fact that the majority of the terrain cited as inaccessible to wheeled and tracked vehicles presents little difficulty to animals using legged locomotion [2]. It should be possible to build walking vehicles that can travel to the places legged animals are already able to reach. Legs also promise improved vehicular mobility where ground is soft, steep or slippery, or where existing paths are narrow or discontinuous [3]. Walking robots may have advantages in extreme environments such as in nuclear power plants. The biped locomotion robot is expected to be very useful in houses and factories designed for smooth human locomotion [4]. Also, legged locomotion results in less soil damage.

1.1.1 Existing Biped Robots

Kato and his colleagues built one of the earliest biped robots which started walking in 1973. It was statically stable at all times relying on keeping its center of gravity above at least one of its large feet. Later, Kato and coworkers developed a locomotion gait for bipeds referred to as quasi-dynamic walking. Its main feature was that the transition of support from one foot to the other was very quick resulting in no obvious two-foot support. Later,

dynamic walking of a biped robot called “WL-10RD” was realized by the same group of scientists [5]. Fursho and Sano developed a nine-link biped with a sensor based control which weighs 25 kg and has a leg length (0.97 m) to stride (0.25 m) ratio of 3.9. In total, this robot has eight degrees of freedom [4]. Raibert built a two-legged machine that could run [6]. It tipped all the time to keep a dynamic balance that was similar to Miura’s machine [5]. A physical biped robot similar to the one built by Miura and Shimoyama was built and studied by Katoh and Mori. The emphasis was on a control method of dynamic locomotion that gave an asymptotic stability of the trajectory [5]. Miyazaki and Arimoto constructed a biped robot and studied its locomotion. They noticed that in some cases the degrees of freedom of a biped robot became larger than the number of actuators during dynamic walking [5]. Research on biped robots has been conducted at Clemson University since 1984. A practical biped robot named SD-2 was designed and constructed with eight degrees of freedom. Each hip joint has two degrees of freedom and each ankle joint has two degrees of freedom as well [5]. Tad McGeer designed and demonstrated a passive two-dimensional biped for walking down inclines. During each step, small motors lift the swing feet clear of the ground but otherwise this machine is just a pair of coupled pendula walking without active control [7].

Hirofumi Miura and Iso Shimoyama have developed five kinds of bipeds. They are named Biper-1, 2, 3, 4 and 5. All of them are statically unstable but can perform a dynamically stable walk with suitable control. Biper-1 and Biper-2 only walk sideways. Biper-3 is a stilt type robot whose foot contact occurs at a point and can walk sideways, backwards and forward. Biper-4’s legs have the same degrees of freedom as human legs. Biper-5 is similar to Biper-3 but in case of Biper-5, all apparatus such as the computer are mounted on it [8]. Some of the biped robots designed and built by research groups in Japan are as given in Tables 1.1.1, 1.1.2 and 1.1.3 [4].

Table 1.1.1: Research Groups in Japan on Biped Robot(Part 1A).

Research Groups	Robots(Degree of Freedom P:Pitch,R:Roll,Y:Yaw)	Control Method, Approach Method, Actuator, etc
Kato, I. and Takanishi A. (Waseda Unvi.)	1972 WL-5(P:6,R:2,Y:2,Body:1) 1981 WL-9DRmk2(P:6,R:4) 1984 WL-10RD(P:6,R:4,Y:2) 1987 WL-12(P:6,Body:3)	Anthropomorphous Robot, Electro-Hyroservo, Mechanical impedance control.
Miura.H and Simoyama,I. (Tokyo Univ.)	1980 Biper-3(P:1,R:2) 1981 Biper-4(P:5,R:2)	3D stilt-type Biped, Multi-Processor control system.

Table 1.1.2: Research Groups in Japan on Biped Robot(Part 1B).

Research Groups	Robots(Degree of Freedom P:Pitch,R:Roll,Y:Yaw)	Control Method, Approach Method, Actuator, etc
Ito,M., Narikiyo,T., and Takeichi,K. (Nagoya Univ.)	1984 Ayumi(P:6)	Control Theoretic Approach, Analysis and synthesis of Double-support phase, Dynamic walking using High Gain Feed back.
Funabashi, H. (Tokyo Inst. of Tech.)	1982 MEG-2(legs:1,Body:1)	Sophisticated link Mechanism, Generation of Walking pattern by a motor.

Table 1.1.3: Research Groups in Japan on Biped Robot(Part 1C).

Research Groups	Robots(Degree of Freedom P:Pitch,R:Roll,Y:Yaw)	Control Method, Approach Method, Actuator, etc
Mita.T. (Chiba Univ.)	1980 CW-1(P:6) 1983 CW-2(P:6) 1984 CW-3D(P:6,R:4,Body:1)	Control Theoretic Approach, Optimal Regulator, Biped Locomotion with Kick action, Digital Control Theory.
Kato, R. and Mori, M. (Toa Univ. and Tokyo Inst. of Tech.)	1979 BIPMAN(P:2,The length of the leg is variable)	Pattern Generator Using Coupled Van der Pol's Equation.
Sato, S. (Shibaura Inst. of Tech.)	1985 ASSHY-15(Arms:10,Body:2, Legs:12)	Hydraulic Actuator, Anthropomorphous Robot.

1.2 Motivation for this Work

For biped walking machines built to date [2]-[11] control complexity increases with the number of links and generality of mass distributions. Most successful machines rely on non-anthropomorphic simplifications to reduce dynamic complexity [1]. The simple dynamics of Raibert's hopping/running machine [6] allowed him and his coworkers to develop elegant controls and to investigate fundamental aspects of legged locomotion with minimal control complexity.

1.2.1 Dynamically Simple Biped

Groundwork for our dynamically simple biped walking machine was laid out in Reference 1. This paper introduced the possibility of realizing three link, two motor, planar bipeds that have mass centers invariantly fixed at the hip axis and bodies that serve as reaction wheels. It has provided four main results : (1) derivation of governing dynamic equations, constraints, and conditions for periodic walking, (2) analytical solutions to the problem of gait synthesis for periodic walking, (3) realistic examples providing evidence that such

machines can be successfully implemented using existing commercial actuators. This study formed the basis and motivation for this work.

1.3 Focus of Research

Design optimization and simulations are the main targets of this work adhering to the following main objectives : (1) to achieve a light compact biped of ≤ 0.5 m height and weighing ≤ 5 kg mass, (2) maximizing step length, (3) maximizing the obstacle that the biped can step over, (4) minimizing the total mass of the biped. Since performance of this system depends on control as well as mechanical design, some fundamental aspects of control must be considered in the design optimization [12]. Hence, an integrated approach has been followed to arrive at an appropriate match between system hardware design and controller design.

1.4 Overview of Thesis

Chapter 2 describes the proposed class of bipeds, their walking gaits, their physical implementation and design objectives. Chapter 3 develops the governing equations of motion. Also, it presents constraints to avoid lifting and slipping. Chapter 4 covers design optimization by first deriving criteria for optimization and then establishes all the major design constraints. Chapter 5 presents solution to the design optimization problem. Chapter 6 presents various results obtained from design optimization and simulation routine which was implemented in MATLAB. Also, it points out the best biped. Chapter 7 presents the specifications of the components as well as overall specifications of the best biped after completing detailed design of the best biped. Chapter 8 verifies the final design through simulation and discusses the simulation results. Chapter 9 concludes this work. Chapter 10 presents recommendations.

Chapter 2

Conceptual Description of the Machine

2.1 Introduction

The proposed biped is based on concepts first dealt in reference [1] in which a whole class of dynamically-simple bipeds were introduced. The objective of this work is to develop a detailed design for one member of that set. This chapter begins by reviewing the concepts proposed in [1], then identifies the particular type of machine we have chosen to design in detail. The final section describes our design goals.

2.2 Concepts for Biped Design

The concepts proposed in [1] apply to a variety of biped designs. Figure 2-1 shows a biped with one foot per leg. Figure 2-2 shows a biped with two feet per leg. Both these versions are composed of three links (a body plus two identical legs) that are serially-interconnected at the hip by coaxial revolute joints which are driven independently by separate motors. The main concept on which these dynamically-simple bipeds are based on is that the mass centers of each link is coincident with hip axis h-h. This feature makes the combined mass center configuration-invariant which results in dynamic simplicity of the biped.

The dynamic equations for these class of bipeds are reduced to such a trivial level of complexity that they may be the simplest of all bipeds attempted so far. The governing equations derived in [1] using the notations shown in Figure 2-3 are as given below.

$$\ddot{\psi}_0 = \frac{mg\ell}{J_0} \sin \psi_0 - \frac{1}{J_0} \tau_1 \quad (2.2.1)$$

$$\ddot{\psi}_1 = \frac{1}{J_b} (\tau_1 - \tau_2) \quad (2.2.2)$$

$$\ddot{\psi}_2 = \frac{1}{J_\ell} \tau_2 \quad (2.2.3)$$

Equations (2.2.1) - (2.2.3) show that dynamic equations are not coupled and two of the three equations are linear. Nonlinear equation (2.2.1) is the same as an inverted pendulum despite the fact that control torque τ_1 is applied at the hip (between stance leg and the body) rather than the base of the pendulum. This means that the body torques the ankle without placing a heavy actuator near the ankle or a drive system to transmit torque from the body to the foot. The system has three degrees of freedom (ψ_0, ψ_1, ψ_2) but only two inputs (τ_1, τ_2).

2.2.1 Walking Gaits

Without knees or equivalent mechanisms for shortening the legs, the proposed biped will stub its toe if standard anthropomorphic gaits are used. Hence two types of gaits : (1) wheel gaits in which legs rotate over the top rather than reciprocate (Figure 2-4), and (2) inchworm gaits where the legs perform alternating steps that contract and expand the distance between the feet (Figure 2-5) were proposed. Both of the proposed gaits can be divided into single-leg and dual-leg support phases as shown in Figures 2-6 and 2-7 respectively. These phases alternate in the course of walking.

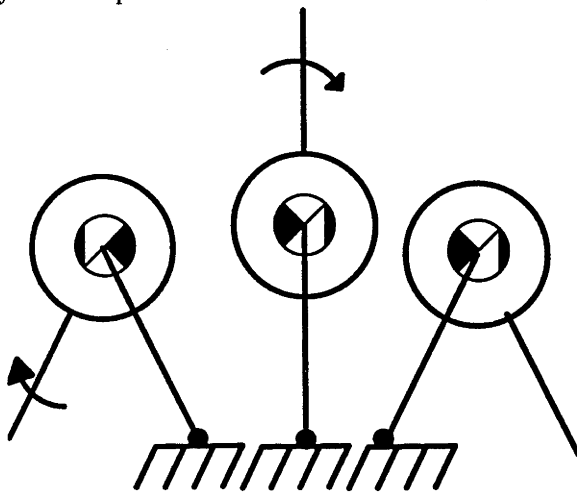


Figure 2-4: Wheel Gait.

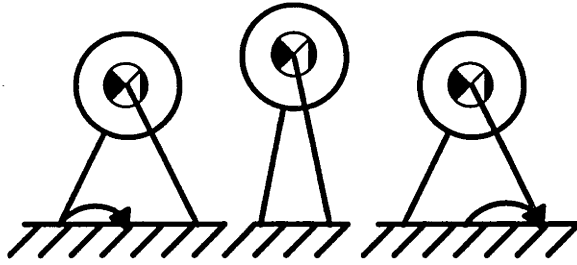


Figure 2-5: Inchworm Gait.

Two important issues in single-leg support phase are (1) balancing of the biped, (2) swing-leg control. The detailed design developed in this thesis is based on the idea that swing-leg control will not be a major problem for the following reasons : (1) design of the swing-leg will be such that it does not introduce any unbalanced torque at the hip joint, (2) the legs will be kept as light as possible so that they only introduce a small amount of disturbance to balance control in single-leg support phase, (3) because the swing-leg is not in contact with the floor it can easily undergo continuous path control similar to that of a robot manipulator [4].

Single-leg Support Phase Balance

Control of balance in the single-leg support phase is considered to be same as the problem of balancing an inverted pendulum. Torque is applied at the tip rather than at the base, but the governing equations are the same.

The idea that walking is considered to be series of inverted pendulum motions with appropriate conditions of connection was previously used by [8] in the controller design for their Biper-3 robot. However, the analogy is less precise.

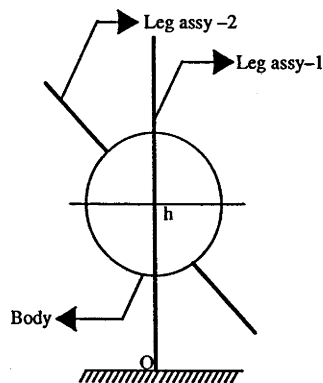


Figure 2-6: Single-Leg Support Phase.

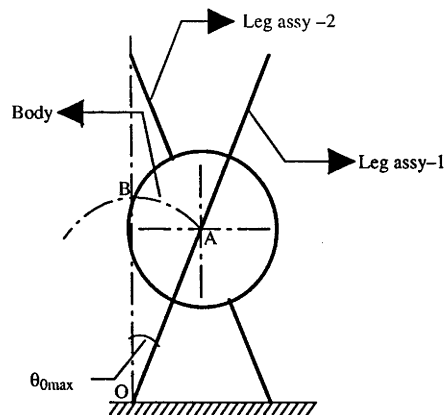


Figure 2-7: Dual-Leg Support Phase.

Dual-leg Support Phase

The dual-leg support phase (Figure 2-7) can be either instantaneous or finite time. In reference [1] we developed conditions for periodic walking using instantaneous support transfer. In this work we have chosen instead to use a finite time dual support phase because : (1) it is better to initiate walking from static dual support phase rather than statically unstable position, (2) we feel that it will be easier to set up initial conditions appropriate for next step in a statically-stable dual support condition, (3) we feel that it will allow larger steps because large impact losses occur for large steps with instantaneous support transfer.

2.2.2 Physical Implementation

Even though our machine is based on planar kinematics, it's implementation must be three dimensional. It should be noted here that animal locomotion is also primarily a planar activity even though animals are three dimensional systems [6]. These bipeds can be realized in three dimension by implementations that are stabilized within the plane by passive means such as Raibert's tethering scheme [6] or by using sufficiently wide feet.

Figure 2-8 shows the finalized design of the proposed biped developed in this study. We refer to it here only to clarify some issues of physical implementation. It mainly consists of a body plus two leg assemblies. These are serially interconnected at the hip by coaxial revolute joints that are actuated by electric motors. Body is attached to a pair of reduction units via their shafts through a coupling. Each reduction unit is driven by an electric motor. Each of the leg assembly is attached to a reduction unit housing.

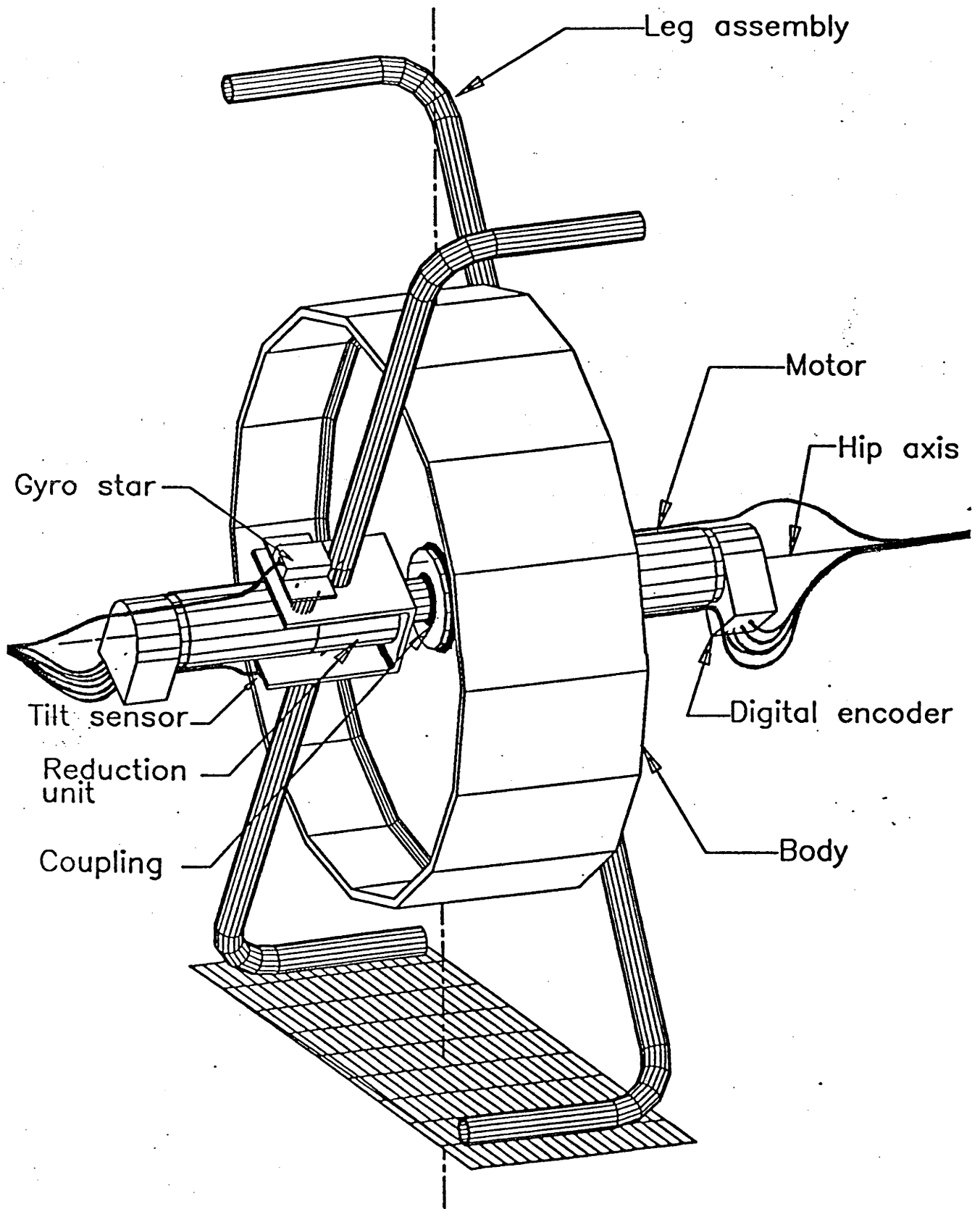


Figure 2-8: Biped Walking Machine.

Actuators

Electric DC motors and brushless DC motors with reduction gears were considered for the design. This choice is made because they are inexpensive, compact, clean, easy and versatile to control compared with alternatives such as hydraulic actuators.

Power Supply and Control Unit

Power will be supplied to motors through their respective power supply units kept off board. Computers and motor controller units are also kept off-board. Power and signals will be wired to each of the leg assembly with a separate harness that terminates coaxially with the leg's hip joint. Sufficient slackness will be allowed in the wiring harness to avoid torsional loading due to twisting that will occur during wheel gait walking. For this laboratory biped the harness will be guided by a person while the robot is walking. This precaution will prevent twisting of wires.

Sensing

Unlike a manipulator, locomotion robots are not fixed to the floor which makes it difficult to measure position and speed. Also, it is important to accurately detect/measure the stance angle with respect to vertical and the body spin rate for feedback control system design. Neglecting the swing leg, the body spin rate, stance angle and the rate of the stance leg angle are the three feedback states. Accurate digital encoders attached to the motor shafts will detect the position of the body with respect to stance leg. Stance leg angle will be detected as discussed below. The body position can be determined by these two signals and differentiated to determine the body spin rate.

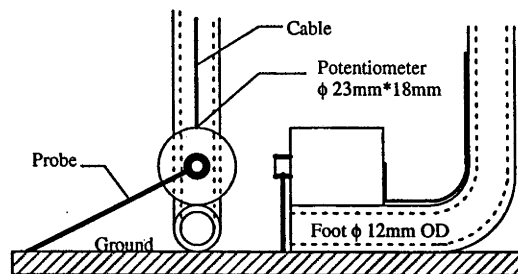


Figure 2-9: Potentiometer for Measuring Stance Angle.

Several methods for measuring the stance angle have been considered : (1) conventional potentiometers, (2) compact, light rate gyros, (3) compact, light bubble tilt sensors. A

conventional spring loaded potentiometer can be mounted on each foot as shown in Figure 2-9. The disadvantages of this method are : (1) increased mass of the biped, (2) increased mass moment of inertia of the leg about the hip axis which increases the disturbance in single-leg support phase balance, (3) flexible probe may introduce some instability in the system, (4) complicates the design. Hence, potentiometers are not considered for measuring the stance angle.

As an alternative, we opted to use light, compact and accurate rate gyros and bubble inclinometers. Gyros can measure the angular velocity $\dot{\theta}_0$. Orientation θ_0 can be obtained by integrating velocity over time. Bubble inclinometers when connected in an appropriate electrical circuit will provide an output voltage proportional to tilt angle and a phase indicative of tilt direction. Since the time constant of bubble inclinometers are of the order of 300ms, feedback from rate gyros will be used to maintain dynamic stability (balance) in single-leg support phase. The bubble inclinometers will be used to estimate the ground slope and to correct for drift error in the rate gyros.

2.3 Type of Machine Considered for the Detailed Design

In this study, we choose to focus on designing a biped with two feet per leg as shown in the Figure 2-2. We prefer this design over one foot per leg because it reduces the total mass of the biped. Balancing mass to maintain CG at the hip axis is completely avoided due to symmetrical mass distribution of the leg about hip axis in this design. The mass moment of inertia of the leg about the hip axis is greater than that in case of one foot per leg. However swing angle of the leg will reduce by 180° for wheel gait walking thus limiting the disturbance during single-leg support phase balance.

2.4 Design Objectives

Broadly speaking, the objective is to design a small prototype biped that can be used to explore control algorithms for dynamic walking. Also, to illustrate the special advantages of bipeds over conventional wheeled vehicles. We also feel the biped should be capable of stepping over large obstacles relative to it's size.

To meet these design objectives, we have chosen to optimize the biped design with respect to a single control task. That task is to raise itself from a stationary dual-leg support phase (OA, Figure 2-7) to balance in a single-leg support condition (OB, Figure

2-7). The optimization criteria, as explained in Chapter 4, is to maximize the size of an obstacle that the biped can step over in performing such a manoeuvre. We focus on this single particular task in order to simplify the design process. However, we feel that optimal performance with respect to this task will ensure that it has good general performance capability.

Chapter 3

Governing Equations

3.1 Introduction

The design of the biped will be based on the single control task of bringing the biped from a stationary dual-leg support phase to balance in a single-leg support condition (Chapter-2). Hence, a mathematical model for the single-leg support phase will play an important role in our design. This chapter begins by defining the axes and planes used for modelling the single-leg support phase. Section 3.3 presents assumptions made in arriving at the mathematical model. Section 3.4 presents the dynamic equations of motion for the single-leg support phase. Section 3.5 defines mechanical and electrical equations of a typical DC motor and establishes motor torque as a function of motor voltage and speed. Section 3.6 presents equations for modelling the gear reducer. Section 3.7 combines results of sections 3.4, 3.5 and 3.6 to establish dynamic equation for the single-leg support phase as a function of motor control voltage 'u'. Section 3.8 puts these results in an equivalent state-space form. Section 3.9 derives a thermal model for the motor and also shows how the model can be incorporated in the state equation. Final section covers the friction equations, establishes foot force equations and presents the condition to avoid slipping.

3.2 Definition of Planes

We have called the plane of walking as “sagittal plane” which is defined as a plane vertical to the ground in the direction of walking (Figure 3-1). The plane perpendicular to the direction of walking is the lateral plane (Figure 3-1). In addition to these planes yaw, roll and pitch axes are defined as shown in Figure 3-1.

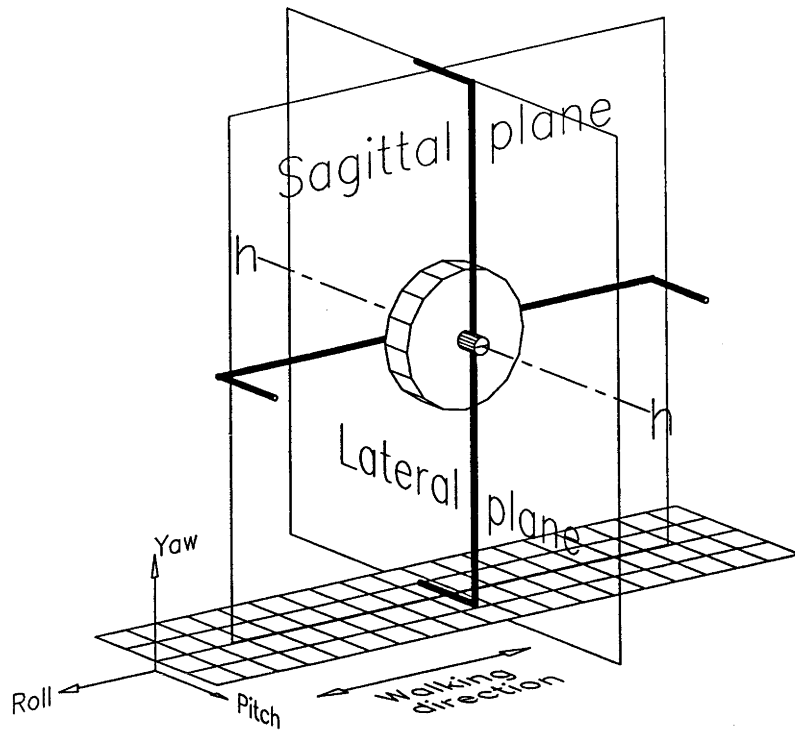


Figure 3-1: Definition of Planes.

3.3 Assumptions in Mathematical Modelling

A mathematical model of a dynamic system is defined as a set of equations that represents the dynamics of the system accurately or at least, fairly well. One of the most important problems in control engineering is to obtain a reasonably accurate mathematical model of a physical component. Note that to be useful, a mathematical model must be neither too complicated nor too simplified. A mathematical model must represent the essential aspects of the physical component. The predictions of system behaviour based on the mathematical model must be reasonably accurate. Keeping the above points in view the assumptions made in deriving equations in further sections are as given below.

- (1) Motion of the biped is only in the sagittal plane (No motion about Roll or Yaw axes).
- (2) The frictional forces in the joints are neglected.
- (3) Feet are modelled as point of contact in the sagittal plane and considered as a pin joint that is fixed to the ground but free to move about the pitch axis. Note that although the mathematical model assumes that the foot is pinned to the ground, we also derive foot force and slipping conditions that are used

to verify that the foot remains fixed to ground.

(5) The low inductance and damping values of the DC motor are neglected. Note that this assumption is verified (Chapter 8) by checking that the electrical time constant for chosen motors is very small with respect to system dynamics.

(6) Change in motor parameters (K_b , K_t , R) due to temperature rise is assumed negligible. Temperature of the motor will be simulated to see whether the temperature rise is significant or not (Chapter 8).

(7) Stiffness of the gear shaft is infinite and there is neither backlash nor elastic deformation.

(8) Further assumptions were made to develop a thermal model of the motor as discussed in Section 3.9.2.

3.4 Dynamic Equations of Motion

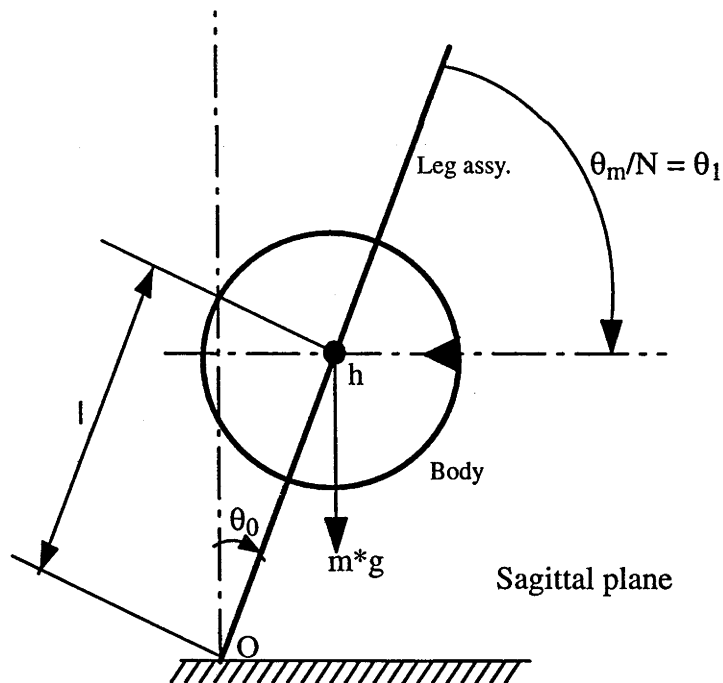


Figure 3-2: Single-Leg support Phase Notations.

We have followed Lagrange's approach to derive single-leg support phase equations. Notations used in deriving these equations are shown in Figure 3-2. By substituting the kinetic and potential energies of each link into Lagrange's equation, the following dynamic equations of motion in the single-leg support phase were derived. Details are given in

Appendix A. Also, recall notation conventions presented in Section 'Nomenclature'.

$$\tau_0 = (J_0 + J_b + J_m)\ddot{\theta}_0 + (J_b + NJ_m)\ddot{\theta}_1 - mlg \sin \theta_0 \tag{3.4.1}$$

$$\tau_1 = (J_b + NJ_m)\ddot{\theta}_0 + (J_b + N^2J_m)\ddot{\theta}_1 \tag{3.4.2}$$

Where

$$m = m_b + m_\ell \tag{3.4.3}$$

3.5 Motor Equations

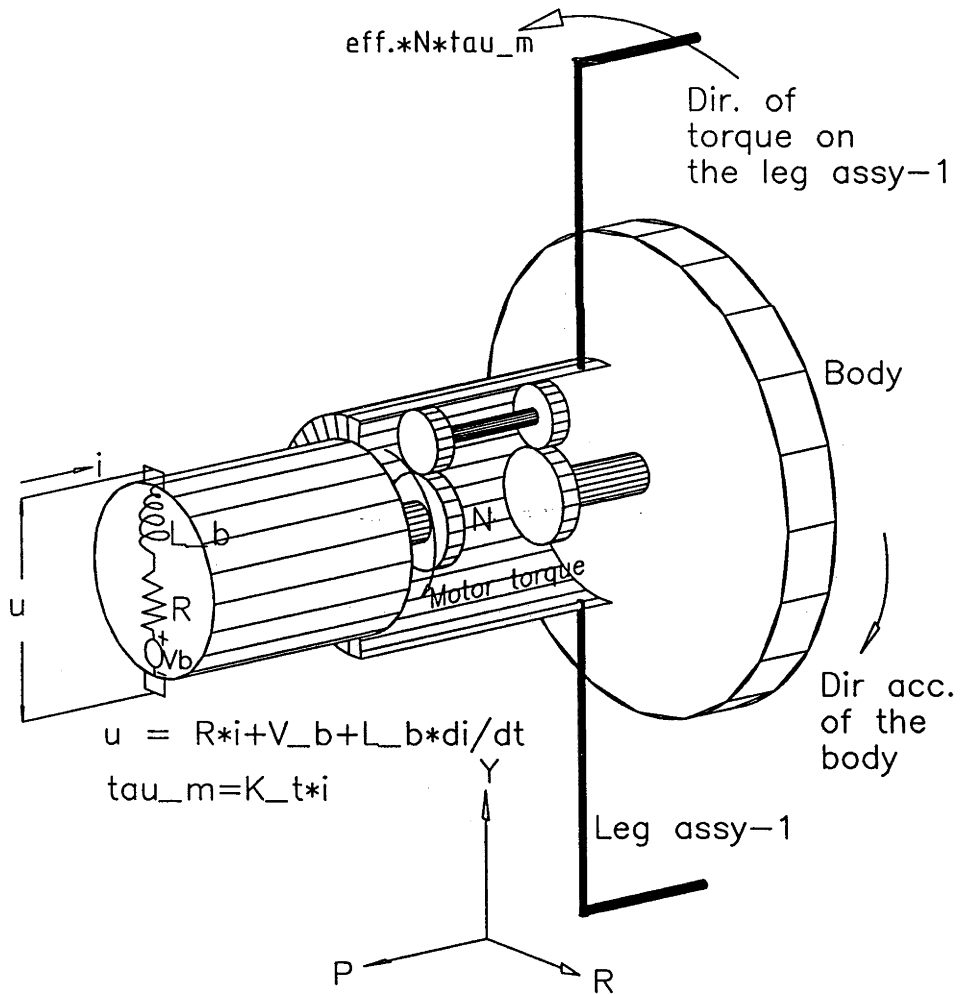


Figure 3-3: Electro-Mechanical Model of the DC Motor Assembly.

Electro-mechanical model of a typical DC motor assembly is shown in Figure 3-3. Permanent magnet DC servo motors convert electrical energy into mechanical energy through the

interaction of two magnetic fields. One field is produced by a permanent magnet assembly and the other is produced by an electrical current flowing in the motor windings. These fields result in a torque which tends to rotate the rotor. As the rotor rotates, the current in the windings is commuted to produce continuous torque output. The mechanical and electrical equations are as given below.

$$\tau_m = K_t i \quad (3.5.1)$$

$$u = Ri + V_b + L_m \frac{di}{dt} \quad (3.5.2)$$

Where K_t , torque constant, is the measure of torque per unit current produced by the motor. The motor back emf constant K_b is a measure of the voltage per unit speed generated when the rotor is turning. The magnitude and polarity of K_b are functions of rotor velocity $\dot{\theta}_m$ and direction of rotation respectively. The motor back emf is as given below.

$$V_b = K_b \dot{\theta}_m \quad (3.5.3)$$

The term $L_m \frac{di}{dt}$ is neglected because motor electrical time constant is significantly less than system dynamics (see Chapter 8 for verification). Torque-current relationship in case of brushless DC motor [12] is as given below.

$$\tau_m = \frac{3}{2} K_0 I_0 \quad (3.5.4)$$

The equation (3.5.4) indicates a linear relationship between the output torque and the desired motor current I_0 . Hence, motor torque in case of brushless DC motor can be expressed by equation (3.5.1) which is the same as a conventional DC motor. The torque-current characteristics of a brushless DC motor are the same as those of DC motor [12]. By combining equations (3.5.2), (3.5.1) and (3.5.3), motor torque can be expressed as given below.

$$\tau_m = \frac{K_t u}{R} - \frac{K_t K_b \dot{\theta}_m}{R} \quad (3.5.5)$$

3.6 Motor Equations After Gear Reduction

Electric motors generally produce maximum power at relatively high speeds and low torque. Therefore, in order to acquire high torque at low speeds appropriate reduction units must be used. Most small commercial DC motors come with a choice of planetary or harmonic drive reduction units. For the biped, it is essential that any unit be symmetrically balanced to avoid vibration due to unbalanced forces. Usually, the speed reduction and magnification of the torque will be in several stages. The gearhead efficiency decreases with higher number of stages. Efficiency of the gearhead is as given below.

$$\eta = \eta_1 \eta_2 \eta_3 \dots$$

Considering a reduction ratio of N , the position, velocity and acceleration of the rotor ($\theta_m, \dot{\theta}_m, \ddot{\theta}_m$) can be expressed in terms of position, velocity and acceleration of the body relative to the stance leg as follows.

$$\theta_m = N\theta_1 \quad (3.6.1)$$

$$\dot{\theta}_m = N\dot{\theta}_1 \quad (3.6.2)$$

$$\ddot{\theta}_m = N\ddot{\theta}_1 \quad (3.6.3)$$

Torque τ_1 can be expressed in terms of the motor torque as given below.

$$\tau_1 = \eta N \tau_m \quad (3.6.4)$$

Substituting equation (3.6.2) in (3.5.5) and using equation (3.6.4), torque τ_1 can be rewritten as given below.

$$\tau_1 = \eta \frac{K_t N u}{R} - \eta \frac{K_t K_b N^2 \dot{\theta}_1}{R} \quad (3.6.5)$$

3.7 Dynamic Equations in terms of Control Voltage-u

We have decided to use motor supply voltage u as the control. Therefore, we replace τ_1 in equation (3.4.2) with expression (3.6.5) which gives τ_1 as a function of u and $\dot{\theta}_1$. We also set torque τ_0 at the point of foot contact to zero. This results in the following dynamic model of the single-leg support phase in terms of control voltage.

$$\begin{bmatrix} \ddot{\theta}_0 \\ \ddot{\theta}_1 \end{bmatrix} = M^{-1} \begin{bmatrix} mlg & 0 \\ 0 & -\eta \frac{K_t K_b N^2}{R} \end{bmatrix} \begin{bmatrix} \sin \theta_0 \\ \dot{\theta}_1 \end{bmatrix} + M^{-1} \begin{bmatrix} 0 \\ \eta \frac{K_t N}{R} \end{bmatrix} u \quad (3.7.1)$$

Where

$$M = \begin{bmatrix} (J_0 + J_b + J_m) & (J_b + NJ_m) \\ (J_b + NJ_m) & (J_b + N^2 J_m) \end{bmatrix} \quad (3.7.2)$$

3.8 State-Space Representation

The state-space representation is an important step in Modern Control theory. Modern control theory is based on the description of the system in terms of 'n' first order differential equations which may be combined into one first order vector matrix differential equation. It is worth noting here that the conventional control theory is based on the input-output relationship or transfer function. As the system gets complex, the mathematical representation of the system using these conventional methods becomes difficult. But state-space representation i.e. use of vector matrix notation greatly simplifies the mathematical representation of the system of equations.

The state-space representation is well suited for optimal control problems and for multiple-input and multiple-output systems. The state-space representation of a system is convenient in implementation of computer aided design algorithms. Also, lately it has become a standard practice to represent all systems in state-space form.

Representation of the Single-Leg Support Phase Dynamics in the State-Space Form :-

Dynamic equations for the single-leg support phase will be represented by state-space form because of the advantages discussed in the above two paragraphs. The steps followed to reduce the single-leg support dynamic equations into a state-space form is as given below.

Let, the four states of the system be as given below.

$$x_1 = \theta_0 \quad (3.8.1)$$

$$x_2 = \dot{\theta}_0 \quad (3.8.2)$$

$$x_3 = \dot{\theta}_1 \quad (3.8.3)$$

$$x_4 = \theta_1 \quad (3.8.4)$$

Also, from equations (3.7.1) and (3.7.2), matrices S and T can be defined as follows.

$$S = M^{-1} \begin{bmatrix} mlg & 0 \\ 0 & -\eta \frac{K_t K_b N^2}{R} \end{bmatrix} = \begin{bmatrix} S_{11} & S_{12} \\ S_{21} & S_{22} \end{bmatrix} \quad (3.8.5)$$

$$T = M^{-1} \begin{bmatrix} 0 \\ \eta \frac{K_t N}{R} \end{bmatrix} = \begin{bmatrix} T_1 \\ T_2 \end{bmatrix} \quad (3.8.6)$$

By using the above definitions, the second-order differential equation (3.7.1) can be expressed as a first-order differential state equation as given below.

$$\dot{x} = \tilde{A}\tilde{x} + \tilde{B}u \quad (3.8.7)$$

Where

$$\dot{x} = \begin{bmatrix} \dot{x}_1 \\ \dot{x}_2 \\ \dot{x}_3 \\ \dot{x}_4 \end{bmatrix} \quad (3.8.8)$$

$$\tilde{A} = \begin{bmatrix} 0 & 1 & 0 & 0 \\ S_{11} & 0 & S_{12} & 0 \\ S_{21} & 0 & S_{22} & 0 \\ 0 & 0 & 1 & 0 \end{bmatrix} \quad (3.8.9)$$

$$\tilde{x} = \begin{bmatrix} \sin x_1 \\ x_2 \\ x_3 \\ x_4 \end{bmatrix} \quad (3.8.10)$$

$$\tilde{B} = \begin{bmatrix} 0 \\ T_1 \\ T_2 \\ 0 \end{bmatrix} \quad (3.8.11)$$

Note that equation (3.8.7) is a nonlinear system because $\dot{x} \neq \frac{d}{dt}\tilde{x}$. We choose to represent it in the form of (3.8.7) rather than $\dot{x} = f(x, u)$ because it makes it's near-linearity apparent (i.e., when $\sin x_1 \cong x_1$).

3.9 Thermal Model for the Motor

3.9.1 Introduction

When working at the limits of motor performance, motor temperature becomes a critical factor. The sustainable current depends on the allowable winding temperature T_{motor} usually less than $180\text{ }^{\circ}\text{C}$ and typically $130\text{ }^{\circ}\text{C}$, and on motor thermal resistance R_{th} which is the temperature rise in $^{\circ}\text{C}$ per dissipated watt due to ohmic heating [13]. High currents can also cause demagnetization of permanent magnet motors. But modern rare-earth permanent magnetic materials are not easily demagnetized i.e., motor currents are typically limited by thermal and not by magnetic considerations.

The power losses in the motor are dissipated as heat which causes the motor temperature to rise. Motor rotation, heat sinking and air flow over the motor will improve the heat transfer and will result in lower thermal impedance. Motor resistance, torque constant and back emf constant are functions of temperature. As the motor temperature increases, each of the three parameters will change in a manner which degrades motor performance and increases the power loss. Hence, prediction of motor temperature is important. In this section, we derive a thermal model to predict motor temperature.

3.9.2 Assumptions in Motor Thermal Model

In implementing the thermal model for biped motors the following assumptions are made.

- (1) Motor is treated as a single dimension lumped mass system.
- (2) Entire motor is made out of copper. We consider this a worst case assumption because it reduces the thermal time constant (Sub-section 3.9.4).
- (3) Even though the reduction unit and leg assembly attached to the motor provide some conduction path for heat dissipation, they have not been considered for this model.

3.9.3 Thermal Model Equations

With the above assumptions the transient conduction model [14] (single dimension) of the motor can be approximately represented by the differential equation given below.

$$\frac{dT_{motor}}{dt} = -\frac{1}{C_{th}R_{th}}T_{motor} + \frac{1}{C_{th}}i^2R + \frac{T_a}{C_{th}R_{th}} \quad (3.9.1)$$

Considering temperature as state-5 and expressing armature current as a function of control voltage, back emf and terminal resistance, equation (3.9.1) can be written in state-space form as given below.

$$\dot{x}_5 = -\frac{1}{C_{th}R_{th}}x_5 + \frac{1}{C_{th}} \left[\frac{u - K_b x_3 N}{R} \right]^2 R + \frac{1}{C_{th}R_{th}} T_a \quad (3.9.2)$$

Combining equations (3.8.7) and (3.9.2), the new state equation of the system can be expressed as given below.

$$\dot{x} = \tilde{A}\tilde{x} + \tilde{B}u + \tilde{C}(x, u) \quad (3.9.3)$$

Where

$$\dot{x} = \begin{bmatrix} \dot{x}_1 \\ \dot{x}_2 \\ \dot{x}_3 \\ \dot{x}_4 \\ \dot{x}_5 \end{bmatrix} \quad (3.9.4)$$

$$\tilde{A} = \begin{bmatrix} 0 & 1 & 0 & 0 & 0 \\ S_{11} & 0 & S_{12} & 0 & 0 \\ S_{21} & 0 & S_{22} & 0 & 0 \\ 0 & 0 & 1 & 0 & 0 \\ 0 & 0 & 0 & 0 & -\frac{1}{C_{th}R_{th}} \end{bmatrix} \quad (3.9.5)$$

$$\tilde{x} = \begin{bmatrix} \sin x_1 \\ x_2 \\ x_3 \\ x_4 \\ x_5 \end{bmatrix} \quad (3.9.6)$$

$$\tilde{B} = \begin{bmatrix} 0 \\ T_1 \\ T_2 \\ 0 \\ 0 \end{bmatrix} \quad (3.9.7)$$

$$\tilde{C}(x, u) = \begin{bmatrix} 0 \\ 0 \\ 0 \\ 0 \\ \frac{T_a}{C_{th}R_{th}} + \frac{(u - K_b x_3 N)^2}{C_{th}R} \end{bmatrix} \quad (3.9.8)$$

Equation (3.9.3) is the state-space representation of the entire model to be used for final simulations.

3.9.4 Practical issues of Thermal modelling

The thermal capacitance C_{th} which is used to establish the thermal model is defined [14] as given below.

$$C_{th} = \frac{\text{Change in heat stored}}{\text{Change in temperature}} \left(\frac{J}{^\circ C} \right)$$

The thermal capacitance can be expressed in terms of the specific heat of the material of the motor and motor mass [14] as given below.

$$C_{th} = C_p \text{motor Mass} \quad (3.9.9)$$

Where, C_p is the specific heat of the motor substance. Generally, motor manufacturers will not project the value of C_{th} for each individual motor. Motors will be made out of a combination of materials like copper, iron, steel etc. The material break up for individual motor components is very difficult to get unless we dismantle a representative motor and weigh individual components. Since the amount of various materials used will differ from motor to motor, disassembling representative motor and weighing individual components may not give an accurate estimate for other motors. Also, this is a tedious process. Hence, we have assumed that the entire motor will be made out of copper. The value of specific heat of copper will be used to calculate C_{th} for each individual motor which in turn will be used to predict motor temperature. The specific heat of copper [15] ($383 \frac{J}{kg \ ^\circ C}$) is low compared to that of steel ($486 \frac{J}{kg \ ^\circ C}$), iron ($420 \frac{J}{kg \ ^\circ C}$) and aluminium ($896 \frac{J}{kg \ ^\circ C}$) [15]. This assumption will decrease the thermal time constant ($-\frac{1}{C_{th}R_{th}}$) which makes the motor temperature to rise quickly to reach its maximum value. Hence, the assumption that "the entire motor is made out of copper" is a worst case assumption based on practical limitations.

3.10 Foot Force and Friction Equations

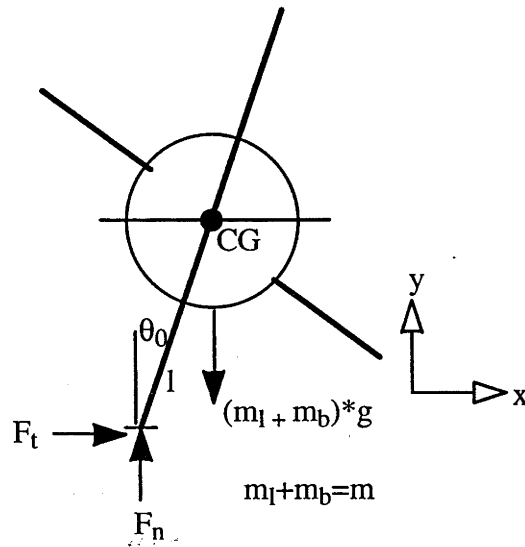


Figure 3-4: Foot Forces.

The dynamic equations derived in Section 3.4 are only valid if the support foot remains fixed to the ground surface. Lifting and slipping will be avoided if the following conditions are satisfied.

$$F_n > 0 \quad (3.10.1)$$

$$|F_t| < \mu F_n \quad (3.10.2)$$

Here μ represents the coefficient of static friction between the support foot and the ground surface, F_n and F_t are the normal and tangential foot force components which can be expressed as functions of mass center acceleration by Newton's 2nd law (Figure 3-4) as given below.

$$\begin{bmatrix} F_t \\ F_n \end{bmatrix} = m \begin{bmatrix} 1 & 0 \\ 0 & 1 \end{bmatrix} \begin{bmatrix} \ddot{x} \\ \ddot{y} + g \end{bmatrix} \quad (3.10.3)$$

where

$$x = l \sin \theta_0 \quad (3.10.4)$$

$$y = l \cos \theta_0 \quad (3.10.5)$$

Chapter 4

Formulation of the Design Optimization Problem

4.1 Introduction

This Chapter formalizes our design objectives stated in Chapter 2, Section 2.4 into a design optimization problem. This Chapter begins by presenting an optimization criteria developed for crossing large obstacles and concludes by presenting a summary of the design optimization problem. Also, major design constraints are discussed and established in this Chapter.

Section 4.2 develops an optimization criteria for crossing large obstacles. Section 4.3 presents relevant actuator constraints. Section 4.4 covers gear box constraints. Section 4.5 establishes foot force constraints and friction limits. Section 4.6 develops criteria for the biped's stability in the lateral plane. Section 4.7 discusses the materials envisaged for the biped components and their constraints. Section 4.8 develops design constraints for the body. Section 4.9 develops design constraints for the leg assemblies. Final section presents the summary of the design optimization problem.

4.2 Optimization Criteria

4.2.1 Introduction

The designer of legged robots has to solve an optimization problem. He or she considers a variety of criteria such as cost, reliability, manoeuvrability and aims to design a machine that is in some sense the best possible (McGhee 1976) [10]. Also, it should be noted

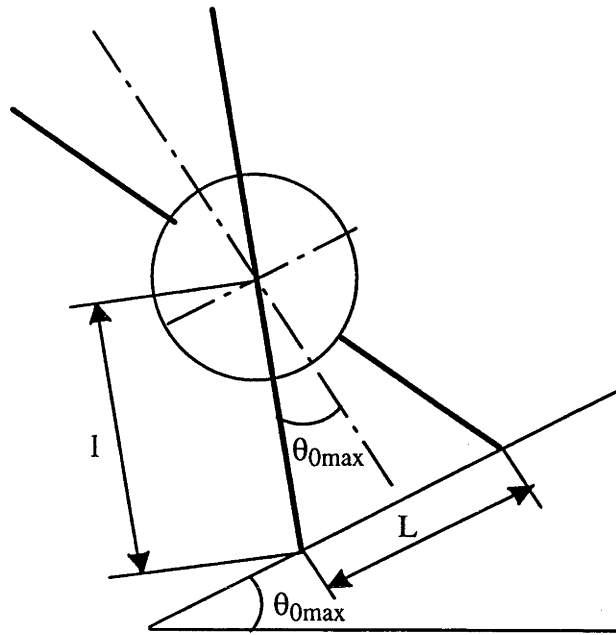


Figure 4-1: Maximum Slope that the Biped can Climb .

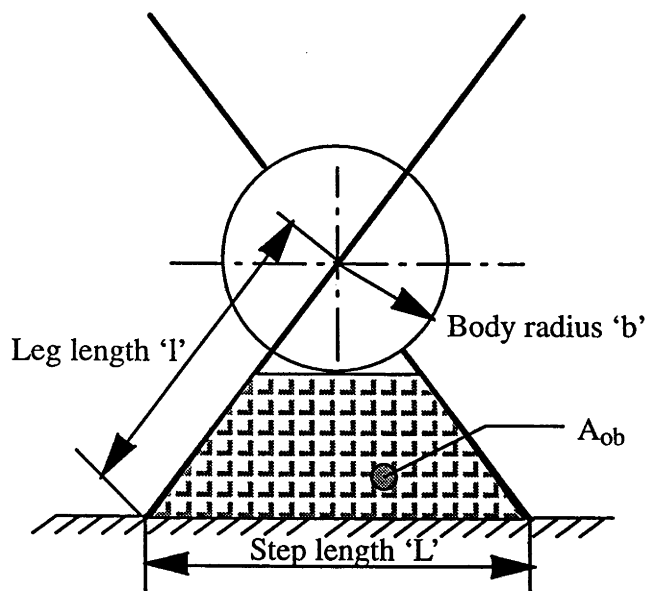


Figure 4-2: Measure of Ability to Cross Large Obstacles.

here that the legs and gaits of animals are the products of two very potent optimization processes- that of evolution by natural selection and of learning by experience [10].

Because legged vehicles are aimed at rough terrain locomotion, one of their most important attributes is their capacity to step over large obstacles. Therefore, we have chosen to optimize our biped design based on that criteria. For our biped, it turns out that this criteria also tends to maximize the biped's ability to climb steep slopes (Figure 4-1). Other legged vehicle designers have also used largest obstacle crossing criteria to optimize their design [2].

4.2.2 Largest Obstacle Crossing Criteria

Our objective is to design the biped to cross the largest obstacle possible relative to its dimension. We choose to quantify this ability using the dimensionless area $A_{ob}^* = \frac{A_{ob}}{l^2}$ where, A_{ob} is the area shown in Figure 4-2. Hence, our objective will be to design the biped to maximize the area A_{ob}^* that the biped can step over.

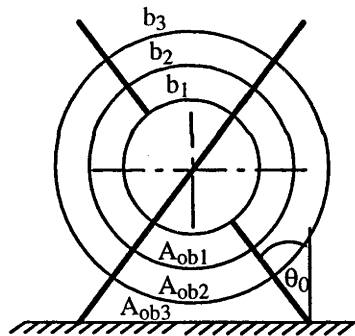


Figure 4-3: Variation of Area A_{ob} due to increase in the Body Radius.

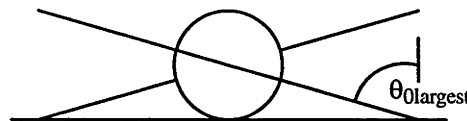
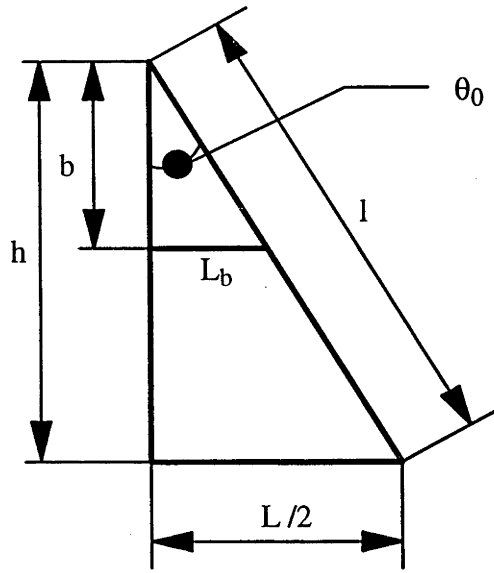


Figure 4-4: Area A_{ob} as $\theta_0 \rightarrow \theta_{0largest}$.

Figure 4-3 shows that for a given angle θ_0 , increase in body radius decreases the area A_{ob} . Figure 4-4 shows that for a given body radius, b_i , increasing θ_0 to its largest possible value $\theta_{0largest}$ will result in $A_{ob} = 0$. Thus body radius, b , and angle θ_0 contribute significantly to increase or decrease of area A_{ob} .

By geometry (Figure 4-5), area A_{ob} (Figure 4-2) enclosed between the legs and the floor below the body is as given below.

Figure 4-5: Relation between θ_0 and step length L .

$$A_{ob} = \frac{L}{2} \left(h - \frac{b^2}{h} \right) \quad (4.2.1)$$

Where

$$h = \sqrt{\ell^2 - \left(\frac{L}{2} \right)^2} \quad (4.2.2)$$

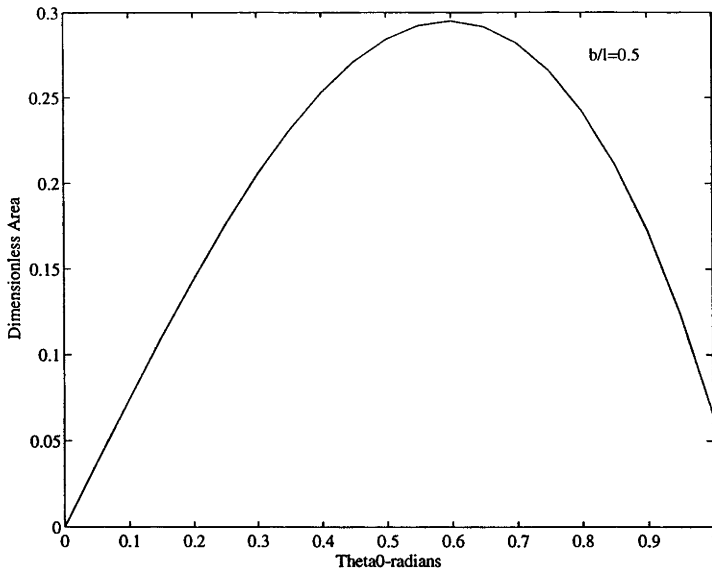
$$L = 2\ell \sin \theta_0 \quad (4.2.3)$$

Figure 4-6 plots area A_{ob} versus θ_0 ($0 \rightarrow \theta_{0largest}$) for a given $\frac{b}{\ell}$ ratio of 0.5 and for a unit leg length. This clearly indicates that area A_{ob} reaches a maximum for a certain value of θ_0 . The rest of this section is devoted to determining an analytic expression for this angle which we call $\theta_{0optimum}$.

The problem is to determine the value of θ_0 which maximizes the dimensionless area $A_{ob}^* = \frac{A_{ob}}{\ell^2}$ for any body radius b . This problem has been approached in two stages (1) finding out the unique step length L for each body radius b that maximizes the dimensionless area A_{ob}^* , (2) solve $\frac{L}{2} = \ell \sin \theta_0$ to determine the value $\theta_{0optimum}$ associated with that value of L . The dimensionless area is given by

$$A_{ob}^* = \frac{L}{2\ell^2} \left(h - \frac{b^2}{h} \right) \quad (4.2.4)$$

Equating the partial derivative with respect to L of equation (4.2.4) to zero and sim-

Figure 4-6: Area A_{ob} Vs θ_0 .

plifying, we get two roots for $\left(\frac{L}{\ell}\right)^2$

$$\left(\frac{L}{\ell}\right)^2 = 3 \pm \sqrt{1 + 8 \left(\frac{b}{\ell}\right)^2} \quad (4.2.5)$$

The smaller root is the one that maximizes A_{ob}^* . The other root is meaningless because it implies $\left(\frac{L}{\ell}\right)^2 > 4$ which is physically impossible.

To see this, consider $0 \leq \frac{b}{\ell} \leq 1$. Substituting lower and upper bounds of the ratio $\frac{b}{\ell}$ in the two roots of $\left(\frac{L}{\ell}\right)^2$, we get

$$4 < \left\{ 3 + \sqrt{1 + 8 \left(\frac{b}{\ell}\right)^2} \right\} < 6 \quad (4.2.6)$$

$$2 > \left\{ 3 - \sqrt{1 + 8 \left(\frac{b}{\ell}\right)^2} \right\} > 0 \quad (4.2.7)$$

The theoretical maximum limit on $\left(\frac{L}{\ell}\right)^2$ is 4 when $L = 2\ell$. Therefore, the smaller root used for obtaining limits (4.2.7) which respects the condition $\left(\frac{L}{\ell}\right)^2 < 4$ is the one which maximizes A_{ob}^* .

Hence, from the smaller root the unique step length L is given by

$$L = \ell \sqrt{3 - \sqrt{1 + 8 \left(\frac{b}{\ell}\right)^2}} \quad (4.2.8)$$

Once unique step length L has been derived, the optimum stance angle $\theta_{0optimum}$ can be

determined by geometry (Figure 4-5).

$$\theta_{0optimum} = \sin^{-1} \left(\frac{\left[\sqrt{3 - \sqrt{1 + 8 \left(\frac{b}{\ell} \right)^2}} \right]}{2} \right) \quad (4.2.9)$$

Note that the detailed derivation for the optimum stance angle is presented in Appendix B.

4.2.3 Optimization Strategy

Let θ_{0max} represent the maximum angle, θ_0 , from which the biped can recover to the balanced vertical position. Note that θ_{0max} will be determined by system dynamics, controls and actuator performance limits (Chapter 5).

Based on our criteria for large obstacle crossing, we feel that little will be gained if $\theta_{0max} > \theta_{0optimum}$. Therefore, we chose to design the biped such that $\theta_{0max} = \theta_{0optimum}$. This ensures that the biped with a given $\frac{b}{\ell}$ ratio does not waste it's dynamic potential rising from a very low angle that does not contribute much to it's ability to step over large obstacles. However, this constraint does not tell us which $\frac{b}{\ell}$ ratio is best.

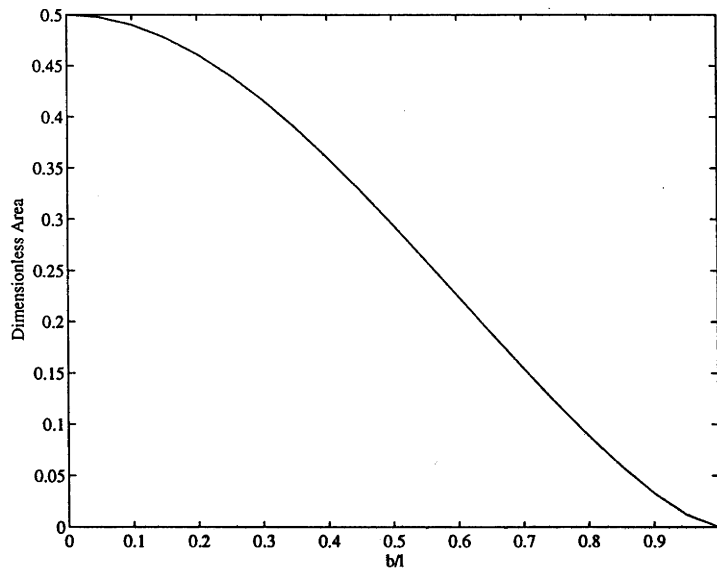


Figure 4-7: Dimensionless Area A_{ob}^* Vs $\frac{b}{\ell}$.

Choice of $\frac{b}{\ell}$ ratio is a compromise. If $\theta_{0optimum}$ can be achieved, then small $\frac{b}{\ell}$ ratios allow larger obstacles to be crossed as shown in the Figure 4-7. However, the biped's dynamic ability to rise from a low angle is increased with larger $\frac{b}{\ell}$ ratio (Chapter 3).

Therefore our optimization criteria is :

minimize $\frac{b}{l}$ subject to $\theta_{0max} = \theta_{0optimum}$ and practical design and actuator constraints to be discussed in the following sections.

4.3 Actuator Constraints

4.3.1 Introduction

We decided to use conventional DC motor or brushless DC motor (Chapter 2). Major drawback of the DC motors is that large currents are delivered to the rotor through mechanical commutation. At the brush and commutator, large sparks are created because of the high currents and voltages supplied to the rotor windings. These sparks are harmful, causing the brush to wear quickly. Such sparks also produce unwanted noise which is harmful to other electrical devices. The brush mechanism increases mechanical friction which degrades control performances [12]. However, brushless DC motors will not have these disadvantages. The advantages of brushless DC motors over conventional DC motors are as given below.

- (1) No brush commutation.
- (2) Low winding inductance.
- (3) Low mechanical time constant.
- (4) High torque to inertia ratio.
- (5) Very high thermal efficiency.

It should be noted that for comparable torque ranges of motors, the PITTMAN brushless DC series stators have inductances of the order of seven times less than those of conventional designs [16].

The main actuator constraints are it's (1) performance limits, (2) dimensions, (3) other parameters. These are dealt in detail in the following subsections.

4.3.2 Actuator Performance Limits

The three main actuator performance specifications that should not violate their limits in the course of operation are

- (1) Current
- (2) Voltage
- (3) Temperature.

The above factors depend on the nature of operation of the motors and other parameters like K_b, K_t, R_{th} which are specific to an actuator.

Motor Current and Voltage

Irrespective of the type of motor and its operation scheme, voltage and current cannot exceed their maximum limits pertaining to particular motor or group of motors. Hence, constraints on the motor voltage and current are as follows.

$$|v| < V_{max} \quad (4.3.1)$$

$$|i| < i_{max} \quad (4.3.2)$$

Because we have decided to use the motor voltage, u , as the control, voltage and current (recall Section 3.7) constraints can be rewritten as follows.

$$|u| < V_{max} \quad (4.3.3)$$

$$\left| \frac{u - K_b N x_3}{R} \right| < i_{max} \quad (4.3.4)$$

Constraints on Maximum Supply Voltage and Current

For conventional DC motors, the limit on the maximum supply voltage comes from the maximum peak current that a motor can withstand. Usually, for short term operations, maximum peak current for conventional DC motors is in the range of six times the continuous sustainable currents for small motors [17]. In case of brushless DC motors, restriction on maximum supply voltage and current comes from their power supply and amplifier circuits. For Maxon brushless DC motors it is ≈ 65 volts and 14 ampere current. Hence, constraints on the maximum supply voltage and the maximum supply current can be written as given below.

$$V_{max} = V_{supply\ max} \quad (4.3.5)$$

$$i_{max} = i_{supply\ max} \quad (4.3.6)$$

Motor Temperature

Power losses in the motor are dissipated as heat which causes the motor temperature to rise (Chapter-3). The temperature of the motor will be predicted as mentioned in Chapter-3. The typical permissible maximum temperature of the conventional DC and brushless DC motors is in the range of $125^\circ C$ to $155^\circ C$ [17] [16]. Considering respective motor

thermal resistances, the permissible motor temperature will be reached during continuous operation at 25 °C ambient which is known as “thermal limit” [17]. Irrespective of our operation scheme, it is important not to exceed this thermal limit. The connection between Joule loss and rotor temperature is given by thermal resistance $R_{th} = R_{th1} + R_{th2}$ where thermal resistance R_{th1} characterizes the heat transfer from the winding to the housing, while the thermal resistance R_{th2} characterizes the heat transfer from the housing to the ambient air. The heat transfer will be fast and efficient if these thermal resistances are as low as possible thus avoiding overheating of the motor. Constraints on the temperature of DC and brushless motors can be written as given below.

$$T_{motor} \triangleq x_5 \leq T_{motor \ max.} \text{ } ^\circ C \quad (4.3.7)$$

4.3.3 Actuator Dimensions

Important actuator dimensions are motor diameter and motor length. These dimensions will effect overall size of the biped. There are numerous DC and brushless DC motors in the market. Selecting a motor for our biped is a difficult task. However, it is possible to consider a group of actuators, design the biped for each motor in that set, and pick the best design.

There are no real constraints on the motor diameter and motor length, except that these actuator dimensions should provide a relatively small biped suitable for laboratory experimentation. It should be noted that larger the motor greater it’s mass and may result in a large, heavy biped. Also, torque capabilities of the motors will increase with increase in their mass which amounts to using larger motor. Hence, selecting a group of motors for our design optimization is a compromise between the torque capabilities of the motors and their mass and dimensions.

Since the biped motors will be selected from a particular set of actuators, it can be written as a constraint as given below.

$$motor \in \{ActuatorSet\} \quad (4.3.8)$$

For a motor selected from such a set, dimensions, motor diameter and motor length are constant. Hence, these dimensions are treated as constants in our problem. These dimensions will be used to establish design constraints on the leg length, ℓ , in Subsection 4.9.4.

4.3.4 Other Actuator Parameters

System dynamics represented by equation (3.9.3) depends on motor parameters like torque constant (K_t), back emf constant (K_b), terminal resistance (R), thermal capacitance ($C_{th} = C_p * motor\ Mass$), thermal resistance (R_{th}), ambient temperature (T_a), mass moment of inertia of the rotor (J_m) and motor mass (motor Mass). For a particular motor selected from a typical set (4.3.8), these parameters are constant.

4.4 Gear Box Constraints

4.4.1 Gear Box Properties

Usually, motor manufacturers will provide a few gear boxes to match each of the motors selected from a typical actuator set (4.3.8). The system dynamics (3.9.3) depends on (1) gear ratio, (2) efficiency, (3) mass of the gear box. The diameter and length of the gear box will influence the size of the biped. These parameters differ from gear box to gear box. Hence, they are discrete variables in our overall design problem to be chosen from the set of available properties. However, if the gear box is given then these properties are constant.

$$gear\ properties \in \{Gear\ Set(motor)\} \quad (4.4.1)$$

Where

$$gear\ properties = (N, \eta, gear\ Mass, gear\ Diameter, gear\ Length) \quad (4.4.2)$$

Since the gear box diameter and length also effect the size of the biped they will be used to establish constraint on leg length in Subsection 4.9.4.

4.4.2 Gear Box Speed Constraint

The recommended input speed of the reduction units to accompany these small DC motors are in the range of 4000 rpm to 6000 rpm [17]. If we adhere to this recommended input speeds for these reduction gears, none of the small DC motors and brushless DC motors can be operated above 4000 to 6000 rpm. It should be noted here that the no load speed of small DC and brushless DC motors at their nominal supply voltage is in the range of 10,000 to 16,000 rpm [17] which of course depends on V_{max} and K_b for a particular motor.

Stresses in the gears will be predominant due to high torques at low speeds. Very high speed results in noise, vibration, loss of lubrication and wear of bearings. The factors that

are predominant at high speeds reduce the expected life of the reduction units. However, for short term applications, we could operate reduction units at greater input speeds. Generally, manufacturers will not provide this value and it is left to the user to make his own judgment.

We have decided to design our biped based on an input speed of about 2 times that of recommended input speed for these class of reduction units. This is less than the achievable maximum speed of small DC motors by 3 to 4 times. Hence, we arrive at the constraint given below.

$$|x_3| \leq \frac{2M_{gis}}{N} \quad (4.4.3)$$

4.5 Foot Force Constraint and Friction Limits

4.5.1 Foot Force Constraint

Normal foot force component, F_n , must be greater than zero to avoid lifting and slipping (Section 3.10) i.e., $F_n > 0$. In terms of our state variables, this foot force constraint can be expressed as follows.

$$\left\{ m \left(-\dot{x}_2 \sin(x_1) - \dot{x}_2^2 \cos(x_1) \right) + mg \right\} > 0 \quad (4.5.1)$$

4.5.2 Friction Limits

The coefficient of friction between the foot and the ground surface should be sufficient to prevent any slipping. This coefficient of friction can be predicted by the relation (Section 3.10).

$$\frac{|F_t|}{F_n} \leq \mu \quad (4.5.2)$$

In terms of state variables, equation (4.5.2) can be written as given below.

$$\frac{|m (\dot{x}_2 \cos(x_1) - \dot{x}_2^2 \sin(x_1))|}{\left\{ m (-\dot{x}_2 \sin(x_1) - \dot{x}_2^2 \cos(x_1)) + mg \right\}} \leq \mu \quad (4.5.3)$$

Where μ is the coefficient of friction between the foot and the ground surface. It is envisaged that the biped walks on a rubber sheet spread on the ground whose coefficient of friction with solids is in the range of 1 - 4 [18]. See Chapter 8 for verification.

4.6 Stability in the Lateral Plane

Along the sagittal plane, the biped will be stable because (1) it will be controlled in the single-leg support balance, (2) vertical reaction force on the foot will always be main-

tained positive (Checked in Chapter 8), (3) coefficient of friction between the foot and ground surface will be maintained enough to prevent any slipping (Verified in Chapter 8). Adhering to above conditions will result in a stable biped if stability in lateral plane is addressed. However, stability in the lateral plane depends on the width of the biped/foot. It is already mentioned in our concept that these class of bipeds will be realized in three dimension by means of sufficiently wide feet (Chapter 2). This sub-section presents a simple constraint on the width of the biped which will be used to decide the width of the body and the foot in a later sub-section.

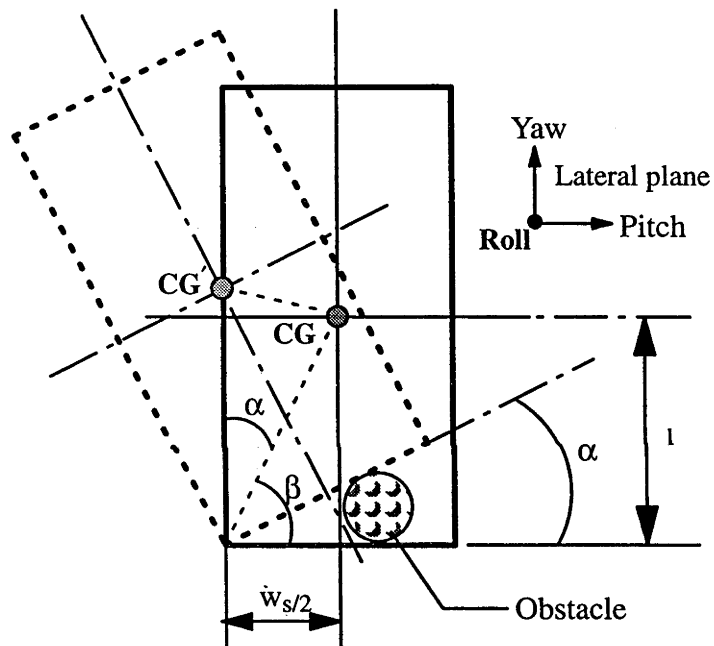


Figure 4-8: Stability in Lateral Plane.

If biped has sufficiently wide feet and by design it's CG is configuration-invariant, it should not tilt about the roll axis while walking on level surface or while climbing a slope. However, if it comes across an obstacle which will cause the biped to tilt about the roll axis, the width of the biped should be sufficient to prevent it from falling. For a given tilt angle α about the roll axis, if the CG falls outside the width of the biped then the biped will fall along the lateral plane. From Figure 4-8, the condition for CG to be within the stable width w_s of the biped is as follows.

$$\beta = 90 - \alpha \quad (4.6.1)$$

By geometry,

$$\beta = \arctan \frac{2\ell}{w_s} \quad (4.6.2)$$

Substituting (4.6.1) in (4.6.2) yields

$$w_s = \frac{2\ell}{\tan(90 - \alpha)} \quad (4.6.3)$$

For design optimization it was decided that we use $\alpha \leq 10^\circ$ i.e., biped will be stable while crossing an obstacle which causes it to tilt by an angle $\leq 10^\circ$ in the lateral plane.

4.7 Material Selection

This section presents discussion on the material selected for biped components and concludes by pointing out to some light weight alloys which can be used in future. Aluminium alloys have been selected for all the components in order to make the biped compact and light. Some of the properties of these alloys based on which they were selected [19] are listed below.

- (1) The density of aluminium alloys is about $2.7 \times 10^3 \frac{kg}{m^3}$ which is approximately one third to that of steel. Taking into account comparative strengths and sectional dimensions, an aluminium structure can weigh as little as one third to half of an equivalent structure in steel.
- (2) Easy to work with.
- (3) Readily available.
- (4) Clean appearance.
- (5) Resists corrosion.
- (6) Takes anodic coatings.
- (7) Conducts electricity and heat, non-magnetic, good thermal conductivity of the legs can be effectively used to transfer/dissipate motor heat.
- (8) The aluminium alloy tubes envisaged for legs and feet will absorb impact loads if any, while walking. The low modulus of elasticity gives aluminium extra ability to resist impact without deforming permanently.
- (9) Good structural strength.
- (10) Can be readily fabricated by most of the methods commonly used for other materials. Can be bent, sawn, drilled, sheared, punched and planed. The body of the biped has to be milled out from an aluminium alloy plate. Also, well suited to most joining methods including bolting, welding, rivetting

and adhesive bonding. The feet of the biped legs are to be formed by bending aluminium alloy tubes.

For the body, following aluminium alloys will be tried.

2024-T0.

2024-T42.

2024-T62.

2024-T72.

5083-H112.

The only restriction is the availability of these in higher thickness ranges of 0.075m - 0.1m. They have minimum yield strength of 97 MPa, 262 MPa, 344 MPa, 317 MPa and 159 MPa respectively. It should be noted that the non-heat treatable alloy 5083 (H112) is available upto a maximum thickness of 100mm and is also widely used in transportation equipment [19] [20]. The material constraint on the body can be written as given below.

$$SY_{body} \in \{SY_1, SY_2, SY_3, \dots\} \quad (4.7.1)$$

Where, SY_1, SY_2, \dots are the yield strengths of some of the commercially available aluminium alloy plates.

For legs, 6061-T6 standard aluminum alloy tubes which have minimum yield strength of 241 MPa has been considered. But the cross section of the legs has to be within the available standard outside diameter and corresponding thickness ranges of 6061-T6 tubes. This practical constraint on the leg cross section can be written as given below.

$$\text{Leg cross section} \in \{\text{Standard tubeset}\} \quad (4.7.2)$$

The aluminium alloys selected for the biped components have the ratings as shown in Table 4.7.1. They have a Young's modulus of 70 GPa and Poisson's ratio of 0.33. If cold workable magnesium alloy tubes are locally available, they can be considered for legs. This will further reduce the inertia of the legs about the hip axis. Other lightweight alloys like aluminium lithium, magnesium and magnesium lithium alloys were ruled out since they are expensive and are not easily available.

Table 4.7.1: Aluminum alloy Ratings.

Alloys	Corrosion Resistance	Machining	Weldability	Heat treatment
5083	A	C, B	C, A	No
6061	A	C	A, A	Yes
2024	D, D	B, B	D, C	Yes

4.8 Body Design Constraints

4.8.1 Introduction

This section presents simple stress, deflection, mass constraints and mass moment of inertia equations for the body. We have planned to implement design optimization and simulation using MATLAB [21] numeric computation and visualization software. Hence, constraints developed for design of the body are kept as simple as possible so that they can be easily implemented in MATLAB. To keep the design optimization of the body simple, we have assumed the shape of the body to be as shown in Figure 4-9 which comprises of a hub, disc and a rim. Also, Figure 4-9 shows the parameters of the body for this configuration.

Sub-section 4.8.2 presents the design objectives for the body. Sub-section 4.8.3 presents constraints on hub dimensions. Sub-section 4.8.4 develops constraints on body radius. Sub-section 4.8.5 establishes constraints on disc thickness. Sub-section 4.8.6 presents constraints on rim width and rim thickness. Sub-section 4.8.7 presents mass constraint equation for the body. Sub-section 4.8.8 presents equations for calculating mass moment of inertia of the body.

4.8.2 Design Objective

Following our general concept, the stance leg will be torqued from hip joint rather than at the ankle. The reaction torque on the stance leg will be more if the mass moment of inertia of the body about the hip axis is large for a given acceleration of the body (i.e., we want to effectively use the inertia of the body to torque the stance leg). Hence, the objective for body design is to maximize the mass moment of inertia of the body J_b about the hip axis meeting strength, stiffness and mass property constraints for a given body mass m_b and radius b .

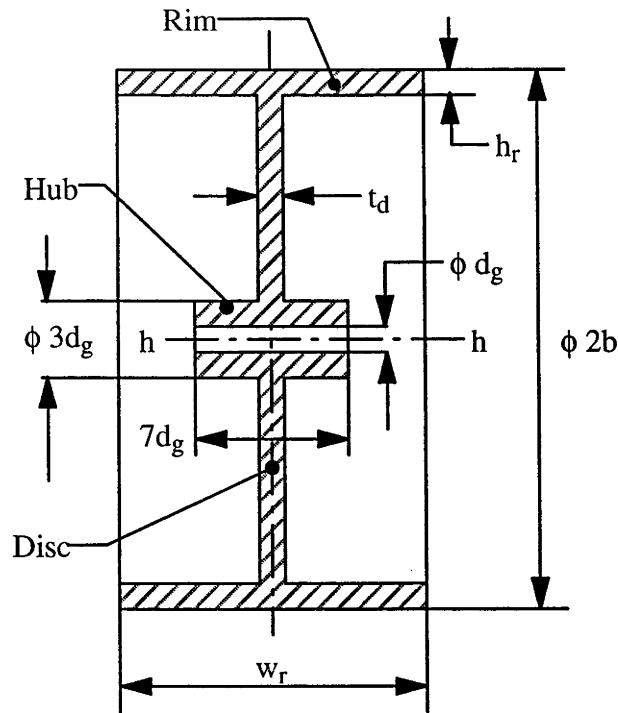


Figure 4-9: Design Parameters of the Body.

4.8.3 Hub Dimensions

Hub dimensions can be finalized based on the following simple criteria.

- (1) Inside diameter of the hub = Diameter of the reduction unit shaft d_g .
- (2) Outside diameter of the hub = $3d_g$. Hub outer diameter can be between $1.5d_g$ to $2d_g$ but $3d_g$ has been chosen to give sufficient tap depth for M3 Grub screws.
- (3) Length of the hub = $7d_g$, to accommodate full length of the two gear shafts with some clearance between them.

4.8.4 Constraints on the Body Radius b

Here, we consider two types of stresses that limit the body radius : stress in the rotating rim providing limit b_1 and stress in the rotating disc providing limit b_2 .

Limiting Speed of the Rim

Many rotating elements, such as flywheels and blowers can be simplified to a rotating ring to determine the stresses. When this is done, it is found that the same tangential and radial stresses exist as in the theory for thick-walled cylinders except that they are caused by inertial forces acting on all particles of the ring. The tangential and radial stresses so found are subjected to the following restrictions [22].

- (1) The outside radius of the rim b_1 is large compared to its thickness h_r i.e.,
 $b_1 \geq 10h_r$.
- (2) The thickness of the rim is constant.
- (3) The stresses are constant over thickness.

The tangential stress in the rotating ring [22] is given by

$$\sigma_t = \rho\omega^2 \left(\frac{3 + \nu}{8} \right) \left(r_i^2 + r_o^2 + \frac{r_i^2 r_o^2}{r^2} - \frac{1 + 3\nu}{3 + \nu} r^2 \right) \quad (4.8.1)$$

Where

ρ : is mass density of the material of the rim, $\frac{kg}{m^3}$.

r_i : inner radius, m.

r_o : outer radius, m.

r : radius where tangential stress is required, m.

ν : Poisson's ratio of the material.

ω : angular velocity, $\frac{rad}{sec}$

The rim of the body can be modelled as a thin ring which implies $r = r_o = r_i = b_1$.

Where, b_1 is the outer radius of the ring. With this assumption, equation (4.8.1) gets modified as given below.

$$\sigma_t = \rho\omega^2 b_1^2 \quad (4.8.2)$$

Generally, $\sigma_t \geq \sigma_r$. But, when tangential stress is equal to yield strength of the body material ($\sigma_t = SY_{body}$) at the outer radius b_1 , the rim will collapse [23]. Therefore, we replace σ_t with $\frac{SY_{body}}{N_{FS}}$ and solve (4.8.2) for b_1 which is a maximum limit on the body radius.

$$b_1 = \frac{N}{No\ Load\ Speed} \sqrt{\frac{SY_{body}}{N_{FS}\rho}} \quad (4.8.3)$$

Limiting Speed of the Disc

When a circular disc rotates about the axis of symmetry which is perpendicular to the disc, the inertia forces set up stresses which may become very large at high speeds. The stresses are distributed symmetrically with respect to the axis of rotation. It is assumed that the stresses do not vary over thickness of the disc. Neglecting the effect of the rim and the hub, the central portion of the body can be approximated (worst case) to a disc of outer radius b_2 as in Figure 4-10. The limiting speed of such a disc [23] is given by

$$\omega_{limiting} = \frac{1}{b_2} \sqrt{\frac{3SY_{body}}{\rho}} \quad (4.8.4)$$

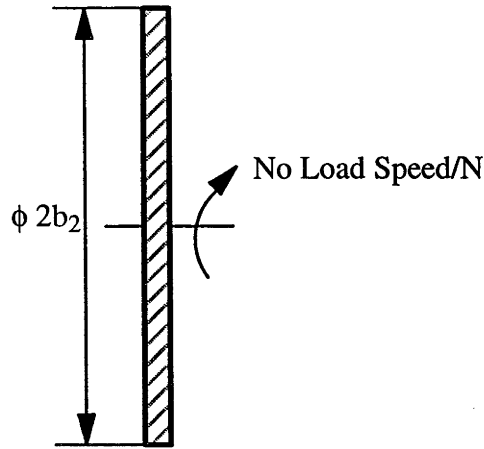


Figure 4-10: Limiting Speed of the Disc.

Considering that $\omega_{limiting} = \frac{No\ Load\ Speed}{N}$ and including a factor of safety N_{FS} , we solve (4.8.4) for b_2 which is another maximum limit on body radius.

$$b_2 = \frac{N}{No\ Load\ Speed} \sqrt{\frac{3SY_{body}}{N_{FS}\rho}} \quad (4.8.5)$$

In equations (4.8.3) and (4.8.5), the motor $No\ Load\ Speed = \frac{V_{max}}{K_b}$. Here, V_{max} , the maximum motor supply voltage and K_b are actuator parameters.

The two constraints on the radius of the body based on limiting speeds of the rim and disc can be expressed as given below.

$$b \leq \min(b_1, b_2) \quad (4.8.6)$$

4.8.5 Constraints on Disc Thickness t_d

In this sub-section, we consider four factors that may limit the disc thickness : shear stress due to torque, direct shear failure, failure due to bending and fabrication limitations.

Disc Thickness t_{d1} based on Shear Stress due to Torque

The worst torque is experienced by the disc when the body is suddenly held at it's outer radius b thus applying a reaction force F_r as shown in Figure 4-11 and is as given below.

$$F_r = \frac{N\text{Stall Torque}}{b} \quad (4.8.7)$$

Where, $\text{Stall Torque} = \frac{K_t V_{max} N}{R}$ is the maximum peak torque that the motor and reduction gear assembly can produce. The reduction ratio N is constant for a particular

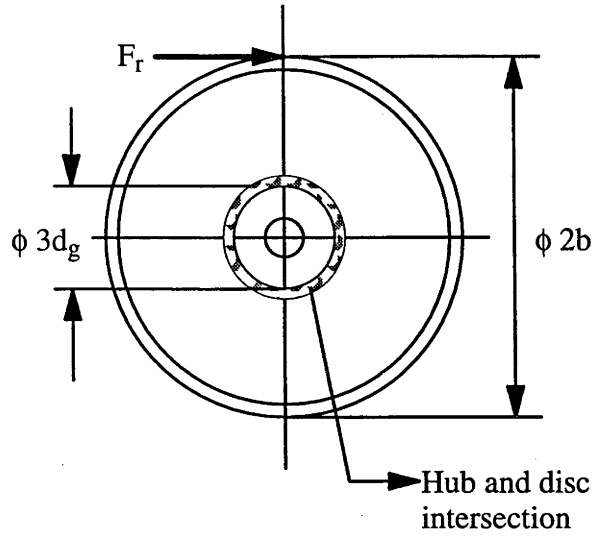


Figure 4-11: Braking Force on the Body.

reduction unit selected from the set (4.4.1). K_t and R are parameters of an actuator as already mentioned in Subsection 4.3.4. V_{max} is the maximum motor supply voltage. These parameters are constants for a particular actuator selected from the set (4.3.8). Hence, stall torque can be treated as a discrete variable in our problem. But, for a given motor and reduction unit it is constant.

Torque due to force F_r at the junction of the hub and disc is given by

$$T_{***} = F_r(b - 1.5d_g) \quad (4.8.8)$$

Substituting (4.8.7) in (4.8.8) yields

$$T_{***} = \frac{N \text{ Stall Torque}}{b}(b - 1.5d_g) \quad (4.8.9)$$

Corresponding reaction force at the junction of the hub and disc is given by

$$F_{r***} = \frac{N \text{ Stall Torque}}{b \cdot 1.5d_g}(b - 1.5d_g) \quad (4.8.10)$$

Since the disc is very thin, we can assume that the shear stress is constant over thickness. Shear stress in the disc at the junction of the hub and disc due to the reaction force F_{r***} is given by

$$S_{sy} = \frac{N \text{ Stall Torque}(b - 1.5d_g)}{b(1.5d_g)^2 2\pi t_{d1}} \quad (4.8.11)$$

Shear stress can be taken as

$$S_{sy} = 0.577SY_{body} \quad (4.8.12)$$

Substituting (4.8.12) in (4.8.11) and solving for t_{d1} , we get the first limit on the minimum disc thickness t_d as given below..

$$t_{d1} = \frac{N_{Stall} Torque (b - 1.5d_g) N_{FS}}{2\pi b (1.5d_g)^2 0.577 S Y_{body}} \quad (4.8.13)$$

Disc Thickness t_{d2} based on Direct Shear Failure

Considering the loading condition as shown in Figure 4-12, the intersection of the rim and disc is prone to direct shear failure. The second limit on the minimum disc thickness t_d based on direct shear stress at the junction of the rim and disc is given by (Figure 4-12)

$$t_{d2} = \frac{(m_b + m_a) g N_{FS}}{2\pi b 0.577 S Y_{body}} \quad (4.8.14)$$

Disc Thickness t_{d3} based on Plate Bending Theory

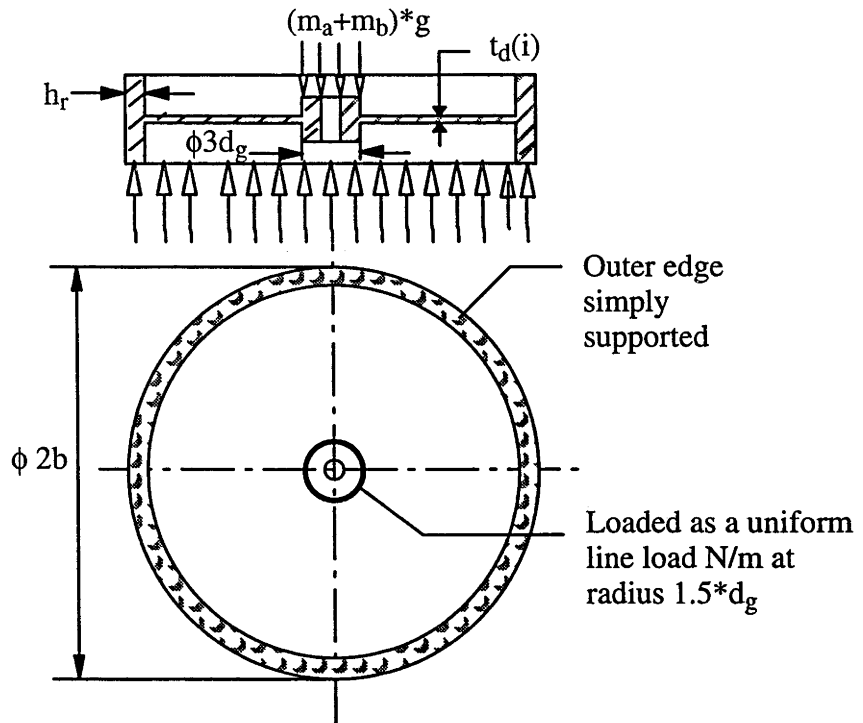


Figure 4-12: Body in Bending Mode.

The disc can be approximated to an annular plate simply supported along the outer edge (at radius b) and loaded as an uniform annular line load at inner radius $1.5d_g$ as shown in Figure 4-12. Such a loading condition will be encountered during assembly and handling. For an annular plate with above stated loading and support conditions, following points have to be considered [24].

$M_{r1.5d_g} = 0$, Unit radial bending moment $\frac{Nm}{m}$ of circumference at $1.5d_g$.

$M_{rb} = 0$, Unit radial bending moment $\frac{Nm}{m}$ of circumference at b.

$y_b = 0$, Vertical deflection of the plate at b.

$y_{max} = y_{1.5d_g}$, Maximum deflection occurs at $1.5d_g$.

$M_{max} = M_{t1.5d_g}$, Maximum unit bending moment is equal to unit tangential bending moment ($\frac{Nm}{m}$ of radius) at $1.5d_g$.

Maximum bending moment is given by

$$M_{t1.5d_g} = \Theta_{1.5d_g} \frac{D}{1.5d_g} (1 - \nu^2) + \nu M_{r1.5d_g} \quad (4.8.15)$$

Since $M_{r1.5d_g} = 0$, Maximum bending moment becomes

$$M_{t1.5d_g} = \Theta_{1.5d_g} \frac{D}{1.5d_g} (1 - \nu^2) \quad (4.8.16)$$

Where

D : Plate constant.

ν : Poisson's ratio of the material.

$\Theta_{1.5d_g}$: Slope of the plate measured from the horizontal at $1.5d_g$ and is given by

$$\Theta_{1.5d_g} = \frac{pb^2 L_9}{DC_7} \quad (4.8.17)$$

Here

L_9 : Loading constant dependent upon the ratio $\frac{b}{r}$, r = radial location of unit line loading and is $1.5d_g$ for loading at inner radius.

C_7 : Plate constant depending on the ratio $\frac{b}{1.5d_g}$

p : Unit load $\frac{N}{m}$ of the circumference and is given by

$$p = \frac{(m_b + m_a)g}{2\pi 1.5d_g} \quad (4.8.18)$$

Plate bending stress is given by

$$SY_{body} = \frac{6M_{t1.5d_g} N_{FS}}{t_{d3}^2} \quad (4.8.19)$$

Combining equations (4.8.16), (4.8.17), (4.8.18) and (4.8.19), the thickness of the plate based on plate bending theory [24] which is the third limit on the minimum disc thickness t_d is given by

$$t_{d3} = \sqrt{\left[\frac{3(m_b + m_a)gb^2(1 - \nu^2)N_{FS}L_9}{SY_{body}\pi(1.5d_g)^2C_7} \right]} \quad (4.8.20)$$

Where, the constants as explained earlier are given by

$$L_9 = \frac{1.5d_g}{b} \left[\frac{1+\nu}{2} \ln \left(\frac{b}{1.5d_g} \right) + \frac{1-\nu}{4} \left(1 - \left\{ \frac{1.5d_g}{b} \right\}^2 \right) \right] \quad (4.8.21)$$

$$C_7 = \frac{1}{2}(1-\nu^2) \left[\frac{b}{1.5d_g} - \frac{1.5d_g}{b} \right] \quad (4.8.22)$$

Disc Thickness t_{d4} based on Fabrication Limitations

Based on today's manufacturing capabilities and other limitations, the minimum thickness that can be machined without any significant warping and drastic local thickness reduction is 2mm to 2.5mm. Taking certain precautions during machining a minimum thickness of 2.4mm can be achieved for a body dimension of about $\phi 0.3m$. Also, it is dependent on tolerance and inspection requirements. Hence, based on practical fabrication limitations, the fourth limit on the minimum disc thickness t_d is set to be equal to t_{Fab} which we will consider to be 2.4 mm.

$$t_{d4} = t_{Fab} \quad (4.8.23)$$

The four disc thicknesses resulting from equations (4.8.13), (4.8.14), (4.8.20) and (4.8.23) can be combined into a single constraint on disc thickness (t_d).

$$t_d \geq \max(t_{d1}, t_{d2}, t_{d3}, t_{d4}) \quad (4.8.24)$$

4.8.6 Constraints on Rim Width w_r and Rim Thickness h_r

Constraint on rim width or body width comes from the width of the biped based on the lateral stability criteria as discussed earlier in Section 4.6. Taking lateral stability into consideration constraint on the width of the body can be written as given below.

$$w_r \leq w_s \quad (4.8.25)$$

The constraints on the rim thickness comes from the fabrication limitations and the configuration of the body itself. Following the same discussions presented earlier for arriving at the thickness t_{d4} , the constraint on the rim thickness due to fabrication limitations can be written as given below.

$$h_r \geq t_{Fab} \quad (4.8.26)$$

Also, another constraint on the rim thickness due to configuration of the body as shown in Figure 4-9 can be written as given below.

$$h_r < (b - 1.5d_g) \quad (4.8.27)$$

Constraints (4.8.26) and (4.8.27) can be written as given below.

$$t_{Fab} \leq h_r < (b - 1.5d_g) \quad (4.8.28)$$

4.8.7 Mass of the Body

The body is assumed to be made up of hub, disc and the rim as shown in Figure 4-9. The only constraint is that the body mass should be equal to sum of the individual masses of the hub, disc and the rim as given below.

$$m_b = m_{hub} + m_{disc} + m_{rim} \quad (4.8.29)$$

Where

$$m_{hub} = \frac{\pi}{4} [(3d_g)^2 - d_g^2] 7d_g\rho \quad (4.8.30)$$

$$m_{disc} = \frac{\pi}{4} [(2b)^2 - (3d_g)^2] t_d\rho \quad (4.8.31)$$

$$m_{rim} = \frac{\pi}{4} [(2b)^2 - (2b - 2h_r)^2] (w_r - t_d)\rho \quad (4.8.32)$$

4.8.8 Mass Moment of Inertia of the Body

The mass moment of inertia of the body [22] about the hip axis should be equal to sum of the individual mass moment of inertia of the hub, disc and the rim about the hip axis. Hence, mass moment of inertia constraint on the body is as given below.

$$J_b = J_{hub} + J_{disc} + J_{rim} \quad (4.8.33)$$

Where, Moment of inertia of the hub, disc and rim respectively about the hip axis are given by

$$J_{hub} = \frac{m_{hub}}{8} [(3d_g)^2 + d_g^2] \quad (4.8.34)$$

$$J_{disc} = \frac{m_{disc}}{8} [(2b)^2 + (3d_g)^2] \quad (4.8.35)$$

$$J_{rim} = \frac{m_{rim}}{8} [(2b)^2 + (2b - 2h_r)^2] \quad (4.8.36)$$

4.9 Design Constraints of the Leg Assemblies

4.9.1 Introduction

Configuration of the leg assembly assumed for the detailed design of the biped is as shown in Figure 4-13(a). As already mentioned in Chapter-2, biped consists of two such leg assemblies. Each leg assembly consists of a reduction unit, a motor, an encoder and two

L-shaped legs of tubular cross section as shown in Figure 4-13(a). One end of each of these legs is attached to reduction unit housing through a bracket and the other end is bent to form the foot. Figure 4-13(b) shows the simplified configuration of the leg assembly considered for the implementation of design optimization in MATLAB. In this simplified configuration of the leg assembly, leg is assumed to be made up of a vertical portion and two feet of tubular cross section.

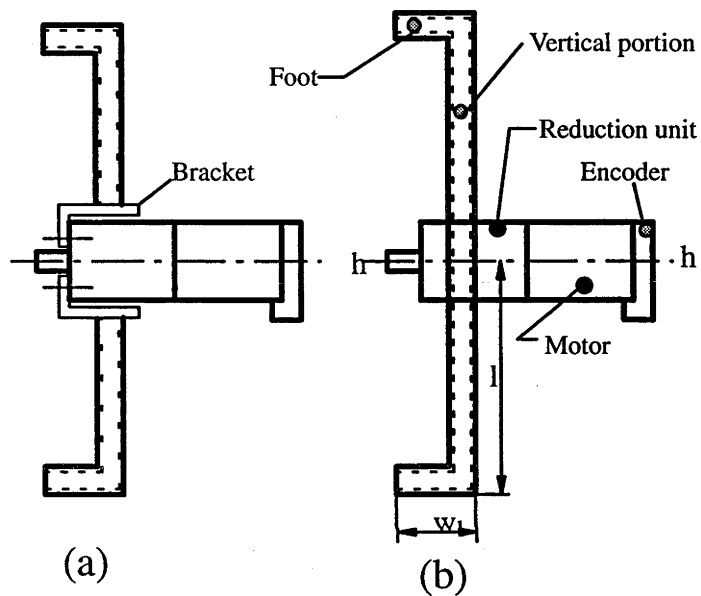


Figure 4-13: Leg Assembly.

Sub-section 4.9.2 presents the objectives and the assumptions made in arriving at design constraints on the leg assemblies. Sub-section 4.9.3 establishes the stress and the deflection criteria for the legs. Sub-section 4.9.4 develops a constraint for the leg length ℓ which will be responsible for overall size of the biped and also presents constraints on the width of the foot. Sub-section 4.9.5 presents equations for computing the mass of the leg assemblies. Sub-section 4.9.6 presents equations for calculating the mass moment of inertia of the leg assemblies.

4.9.2 Objectives and Assumptions

Objectives

The moment of inertia of the legs about the hip axis should be minimized for controllability of the leg [9]. Also, light legs reduce the disturbance during single-leg support phase

balance (Chapter 2). Hence, leg design objectives are

- (1) minimize mass moment of inertia of the legs about hip axis.
- (2) minimize mass of the legs.

Assumptions

- (1) Mass distribution of the motor and reduction unit is assumed to be uniform about the hip axis i.e., their product of inertia about $I_{yaw\ roll} = 0$ and $I_{roll\ pitch} = 0$.
- (2) Encoder mass and it's dimensions are included with the motor.
- (3) The allowable deflection per unit length of the leg $\frac{\Delta\ell}{\ell}$ in bending is assumed to be 0.01.

4.9.3 Leg Stress and Deflection Constraints

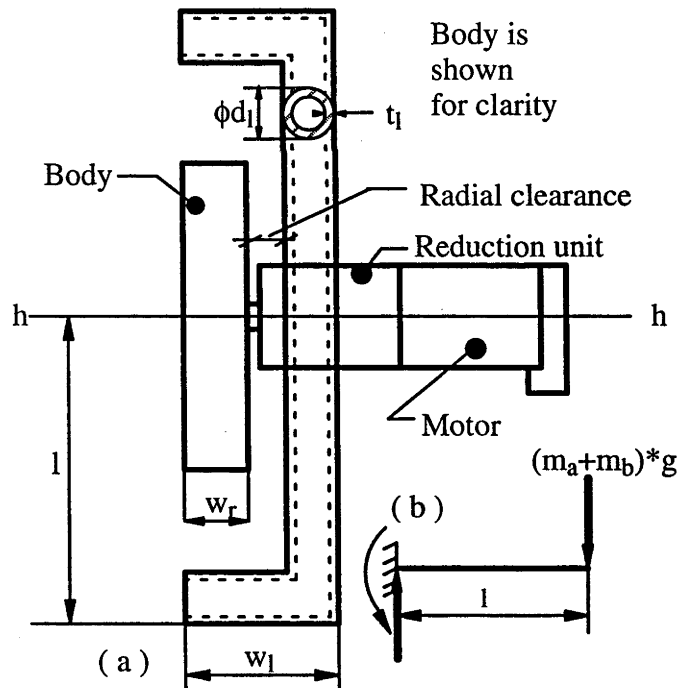


Figure 4-14: Design Parameters of the Leg.

The design parameters of the leg are as shown in Figure 4-14(a) where the body is included for clarity and to illustrate constraints on width of the foot. A simple model of the leg is as shown in Figure 4-14(b) which is a cantilever fixed at one end and loaded at the other end. This worst scenario is encountered when the biped is held horizontally by gripping one of it's feet. The constraints based on deflection and bending stress can be respectively

expressed by following equations.

$$\frac{64(m_b + m_a)g\ell^2}{3E\pi [d_\ell^4 - (d_\ell - 2t_\ell)^4]} \leq \frac{\Delta\ell}{\ell} \quad (4.9.1)$$

$$\frac{32(m_b + m_a)g\ell N_{FS}d_\ell}{\pi [d_\ell^4 - (d_\ell - 2t_\ell)^4]} \leq SY_{leg} \quad (4.9.2)$$

Where, d_ℓ and t_ℓ define the cross section of the legs (Figure 4-14). The constraint on the cross section of the legs which was established in Section 4.7 by equation (4.7.2) can be rewritten as given below.

$$[d_\ell, t_\ell] \in \{\text{Standard aluminium alloy tube set}\} \quad (4.9.3)$$

4.9.4 Constraint on the Leg Length ℓ and Width of the Foot w_ℓ

In order to meet our design objectives, we have to establish a constraint on leg length, ℓ , which makes some sense to overall size of the biped. It is possible to constrain overall size of the biped by making this criteria dependent on motor and reduction unit dimensions. We feel leg length criteria established in this manner may contribute in yielding a laboratory size biped.

Minimum leg length, ℓ_{min} , is set equal to maximum of either $2 \times D$ or W as given below.

$$\ell_{min} = \max(2D, W) \quad (4.9.4)$$

Where, D is the maximum of either motor diameter or reduction unit diameter and W is equal to twice the length of the motor plus length of the reduction unit as given below.

$$D = \max(\text{motor Diameter}, \text{gear Diameter}) \quad (4.9.5)$$

$$W = 2 \times (\text{motor Length} + \text{gear Length}) \quad (4.9.6)$$

Once ℓ_{min} is evaluated using equation (4.9.4), the constraint on leg length is that it should be greater than ℓ_{min} .

$$\ell \geq \ell_{min} \quad (4.9.7)$$

Constraint on the Width of the Foot

The constraint on width of the foot comes from the biped width based on stability criteria in the lateral plane as well as width of the body as given below.

$$w_\ell > w_s \quad (4.9.8)$$

Where, w_s is given by (4.6.3).

4.9.5 Mass of the Leg Assemblies

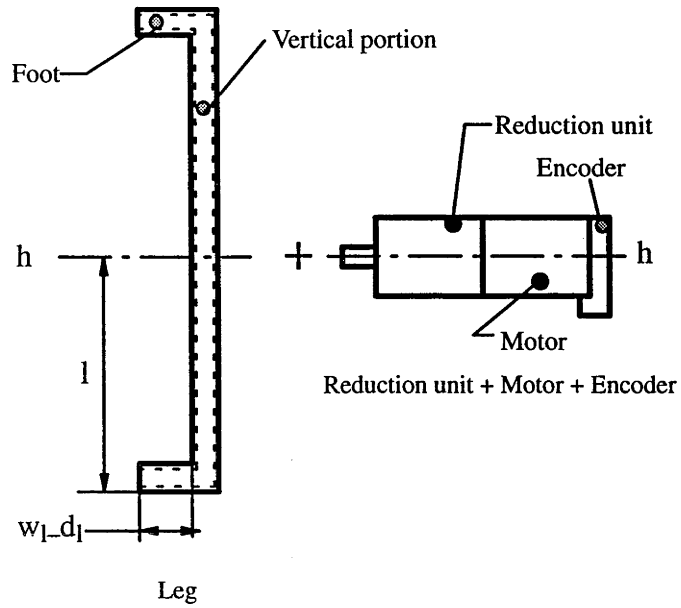


Figure 4-15: Biped Leg Assumed for Design Optimization.

As mentioned earlier, our biped broadly constitutes two leg assemblies and a body (Figure 2-8). Each leg assembly is made up of a motor, a reduction unit, an encoder and a leg as shown in Figure 4-15. Also, each leg consists of a vertical portion and two feet of tubular cross section. Hence, we can write constraint on mass of the leg assemblies as given below.

$$m_\ell = m_a + 2m_{\ell 1} + 2m_{\ell 2} \quad (4.9.9)$$

Where

$m_a = 2 \times (\text{motor Mass} + \text{gear Mass})$ is the mass of the actuators. Note that the mass of the encoder is included with motor mass.

$m_{\ell 1} = \frac{\pi}{4} [d_\ell^2 - (d_\ell - 2t_\ell)^2] 2l\rho$ is the mass of the vertical portion of a leg.

$m_{\ell 2} = \frac{\pi}{4} [d_\ell^2 - (d_\ell - 2t_\ell)^2] 2(w_\ell - d_\ell)\rho$ is the mass of the feet of each leg.

4.9.6 Mass Moment of Inertia of the Leg Assemblies

The constraint on the mass moment of inertia of leg assemblies about the hip axis can be expressed by the equation below.

$$J_\ell = 2(J_1 + J_2 + J_3 + J_4) \quad (4.9.10)$$

Where

$J_1 = \frac{m_\ell}{48} [3d_\ell^2 + 3(d_\ell - 2t_\ell)^2 + 4(2\ell)^2]$ is the moment of inertia of the vertical portion of the leg about the hip axis.

$J_2 = \frac{m_\ell t_\ell}{8} [d_\ell^2 + (d_\ell - 2t_\ell)^2] + m_\ell t_\ell \left(\ell - \frac{d_\ell}{2}\right)^2$ is the moment of inertia of the feet of each leg about hip axis.

$J_3 = \text{motor Mass} \frac{\text{motor Diameter}^2}{8}$ is the approximate moment of inertia of the motor about the hip axis. Note that dimensions and mass of the encoder is accounted with the motor.

$J_4 = \text{gear Mass} \frac{\text{gear Diameter}^2}{8}$ is the approximate moment of inertia of the reduction unit about the hip axis.

Effective Mass Moment of Inertia, J_0

The constraint on effective mass moment of inertia of the leg assemblies about the point of contact between the support leg and the ground is as given below.

$$J_0 = m\ell^2 + J_\ell \quad (4.9.11)$$

Where, J_ℓ is the mass moment of inertia of the leg assemblies about the hip axis as given by equation (4.9.10) and m is the mass of the biped as given below.

$$m = m_\ell + m_b \quad (4.9.12)$$

Here, m_ℓ is given by equation (4.9.9) and m_b is given by equation (4.8.29).

4.10 Summary of the Design Optimization Problem

Based on previous sections, our design optimization problem can be summarized as follows.

For a given *motor* $\in \{ActuatorSet\}$, (4.3.8) with *gear properties* $\in \{Gear Set(motor)\}$, (4.4.1), choose ℓ , b , and m_b to

$$\text{minimize } \frac{b}{\ell}$$

$$\text{subject to } \theta_{0max} = \theta_{0optimum} \triangleq \sin^{-1} \left(\frac{\left[\sqrt{3 - \sqrt{1 + 8\left(\frac{b}{\ell}\right)^2}} \right]}{2} \right)$$

Where

θ_{0max} is the largest dual-support value of θ_0 that allows recovery to a balanced single-leg equilibrium.

subject to :

Dynamics

$$\dot{x} = \tilde{A}\tilde{x} + \tilde{B}u + \tilde{C}(x, u) \quad (3.9.3)$$

Actuator Performance Limits

$$|u| < V_{max} \quad (4.3.3)$$

$$\left| \frac{u - K_b N x_3}{R} \right| < i_{max} \quad (4.3.4)$$

$$x_5 \leq T_{motor \ max} \quad (4.3.7)$$

Gear Box Input Speed Constraint

$$|x_3| \leq \frac{2M_{gis}}{N} \quad (4.4.3)$$

Foot Force Constraint & Friction Limit

$$\{m(-\ell x_2 \sin(x_1) - \ell x_2^2 \cos(x_1)) + mg\} > 0 \quad (4.5.1)$$

$$\frac{|m(\ell x_2 \cos(x_1) - \ell x_2^2 \sin(x_1))|}{\{m(-\ell x_2 \sin(x_1) - \ell x_2^2 \cos(x_1)) + mg\}} \leq \mu \quad (4.5.3)$$

Lateral Stability Criteria

$$w_\ell > w_s \quad (4.9.8)$$

Body Design Constraints

Choose h_r , w_r , t_d and SY_{body} to maximize J_b subject to :

$$SY_{body} \in \{SY_1, SY_2, SY_3, \dots\} \quad (4.7.1)$$

$$b \leq \min(b_1, b_2) \quad (4.8.6)$$

$$t_d \geq \max(t_{d1}, t_{d2}, t_{d3}, t_{d4}) \quad (4.8.24)$$

$$w_r \leq w_s \quad (4.8.25)$$

$$t_{Fab} \leq h_r < (b - 1.5d_g) \quad (4.8.28)$$

Leg Design Constraints

Choose d_ℓ , t_ℓ , w_ℓ to minimize J_ℓ subject to :

$$\frac{64(m_b+m_a)g\ell^2}{3E\pi[d_\ell^4-(d_\ell-2t_\ell)^4]} \leq \frac{\Delta\ell}{\ell} \quad (4.9.1)$$

$$\frac{32(m_b+m_a)g\ell N_{FS}d_\ell}{\pi[d_\ell^4-(d_\ell-2t_\ell)^4]} \leq SY_{leg} \quad (4.9.2)$$

$$\ell \geq \ell_{min} \quad (4.9.7)$$

$$[d_\ell, t_\ell] \in \{\text{Standard tube set}\} \quad (4.9.3)$$

$$\text{Note (Stability criteria } w_\ell > w_s \text{ also applies)} \quad (4.9.8)$$

Note : 1) Simple body and leg geometry have been assumed. Material properties are assumed to be given.

2) The system dynamics, foot force constraint & friction limits, body design constraints and leg design constraints are functions of mass properties as follows.

$$m_b = m_{hub} + m_{disc} + m_{rim} \quad (4.8.29)$$

$$J_b = J_{hub} + J_{disc} + J_{rim} \quad (4.8.33)$$

$$m_\ell = m_a + 2m_{\ell 1} + 2m_{\ell 2} \quad (4.9.9)$$

$$J_\ell = 2(J_1 + J_2 + J_3 + J_4) \quad (4.9.10)$$

$$m = m_\ell + m_b \quad (4.9.12)$$

$$J_0 = m\ell^2 + J_\ell \quad (4.9.11)$$

3) Controls have not been assumed.

Chapter 5

Solution to the Design Optimization Problem

5.1 Introduction

This chapter presents solution to the design optimization problem. Section 5.2 presents the intended motor operation scheme to achieve our objective. Section 5.3 starts with the assumptions made for obtaining maximum stance angle and then presents solution to the maximum stance angle θ_{0max} . Section 5.4 presents the overall solution procedure. Section 5.5 presents a procedure for verifying the optimized biped design by simulating its performance under control.

5.2 Motor Operation Scheme

DC motors offer very versatile operation schemes for the user. These operation methods depend on what we want to achieve. As mentioned earlier, our objective is to bring the biped from position OA to OB as shown in Figure 2-7 and balance in position OB. To achieve this, we intend to utilize the full potential of DC motors. DC motors can be operated in any of the four quadrants. Figure 5-1 gives a typical torque speed curve of a DC motor for four quadrant operation. It is possible to utilize a torque equal to $2 \times N \times Stall\ Torque$ for achieving our objective by the following motor operation scheme.

Starting from a stationary dual-leg support stance,

- (1) Supply $-V_{max}$, the maximum supply voltage to the motor terminals to accelerate the body in the direction shown in Figure 3-3 until the body speed

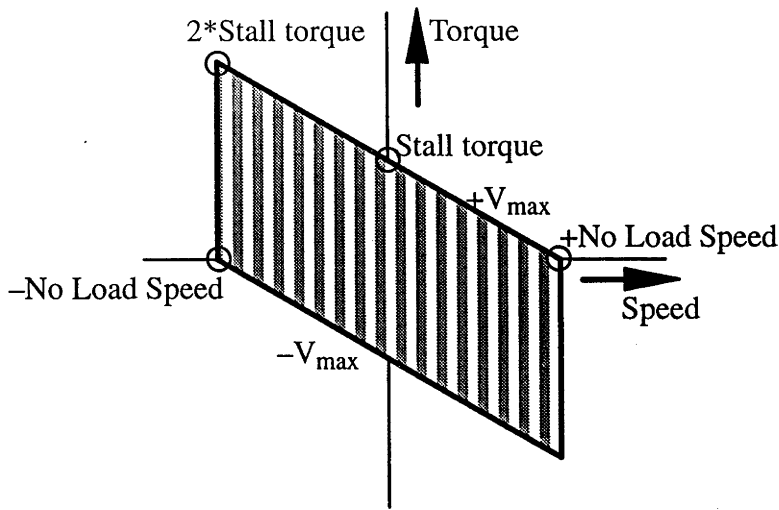


Figure 5-1: Torque Vs Speed Curve of a typical DC Motor.

reaches $-\frac{\text{No Load Speed}}{N} \triangleq -\frac{V_{max}}{K_b N}$,

(2) At this moment, change the polarity to be on the $+V_{max}$ curve thus utilizing a reaction torque of $2 \times N \times \text{Stall Torque}$ on the leg in the direction shown in Figure 3-3. Maximum torque will be applied to the hip causing the biped to rise. As the body decelerates and reverses direction of spin, the output torque will follow $+V_{max}$ curve of Figure 5-1.

Considering the actuator classification based on the direction of energy flow [9] we are using each motor as type 1 actuator. A type 1 actuator is the one that consumes energy during all work modes (positive, negative, isometric) and is the least efficient [9]. We use it nevertheless in order to avoid complicating our design with a brake or a scheme for regenerative braking.

It must be noted here that the achievable torque depends on the specified duty cycle and higher torques can be achieved for short durations than for long or continuous periods.

We feel that the above operation scheme will maximize the initial angle θ_0 that the biped is able to recover. This is because the scheme utilizes maximum control effort. As shown in the next section, this scheme also allows an analytical solution for that angle, θ_{0max} .

5.3 Maximum Stance Angle

This section presents a closed form solution for determining the maximum stance angle θ_{0max} . Sub-section 5.3.1 presents the assumptions made in obtaining this solution. Then Sub-section 5.3.2 derives an expression for computing θ_{0max} .

Because this solution is based on a linear model, it is approximate. Nevertheless, it is very accurate and avoids determining θ_{0max} by an iterative process which would slow down the design optimization algorithm.

5.3.1 Assumptions

Assumptions made in deriving a closed form solution to θ_{0max} are as given below.

- (1) Since $\sin x_1 \cong x_1$ for $x_1 \leq 30^\circ$, system dynamics will be linearized.
- (2) Since the body position (*state*, x_4) has no influence on any other state, it will be ignored.
- (3) Temperature of the rotor (*state*, x_5) has no influence on dynamic behaviour of the system. Hence it will be ignored.
- (4) Control u is limited by the simple constraint $|u| < V_{max}$.

Note that the states x_4 & x_5 will be considered for final simulations only, especially state-5 to ensure that the motor temperature specifications will not exceed. Also, refer to Section 3.8 and Figure 3-2 for state ($x_1..x_4$) definitions.

5.3.2 Solution to Maximum Stance Angle θ_{0max}

With the assumptions as stated in section 5.3.1 and by setting the control voltage u to the maximum supply voltage V_{max} , equation (3.9.3) reduces to

$$\dot{x} = Ax + BV_{max} \quad (5.3.1)$$

Where

$$\dot{x} = \begin{bmatrix} \dot{x}_1 \\ \dot{x}_2 \\ \dot{x}_3 \end{bmatrix} \quad (5.3.2)$$

$$A = \begin{bmatrix} 0 & 1 & 0 \\ S_{11} & 0 & S_{12} \\ S_{21} & 0 & S_{22} \end{bmatrix} \quad (5.3.3)$$

$$x = \begin{bmatrix} x_1 \\ x_2 \\ x_3 \end{bmatrix} \quad (5.3.4)$$

$$B = \begin{bmatrix} 0 \\ T_1 \\ T_2 \end{bmatrix} \quad (5.3.5)$$

Equation (5.3.1) is a linear differential equation of the first order which has particular and homogeneous solutions.

Particular Integral

The particular integral is given by

$$x_p = -A^{-1}BV_{max} \quad (5.3.6)$$

Let the matrix representation of (5.3.6) be

$$x_p = \begin{bmatrix} x_{p1} \\ x_{p2} \\ x_{p3} \end{bmatrix} \quad (5.3.7)$$

Homogeneous Solution

Let, λ_1 , λ_2 and λ_3 be the eigen values of A and

$$V_1 = \begin{bmatrix} V_{11} \\ V_{21} \\ V_{31} \end{bmatrix}, \quad V_2 = \begin{bmatrix} V_{12} \\ V_{22} \\ V_{32} \end{bmatrix}, \quad V_3 = \begin{bmatrix} V_{13} \\ V_{23} \\ V_{33} \end{bmatrix} \quad (5.3.8)$$

eigen vectors of matrix-A.

Then homogeneous solution is given by

$$x_h = C_1V_1e^{\lambda_1t} + C_2V_2e^{\lambda_2t} + C_3V_3e^{\lambda_3t} \quad (5.3.9)$$

Where, C_1 , C_2 and C_3 are constants.

Based on physical intuition, we assume two eigen values will be negative and one will be positive (unstable) i.e., let $\lambda_1 < 0$, $\lambda_2 < 0$ and $\lambda_3 > 0$. The eigen value $\lambda_3 > 0$ corresponds to unstable dynamics associated with the unstable equilibrium position of the inverted pendulum model. Because we are looking for a stable solution, we set $C_3 = 0$

thus eliminating the part of the solution which is responsible for instability. This means that the initial angle θ_0 will be such that the step input V_{max} will bring the pendulum exactly to the unstable equilibrium position. Substituting $C_3 = 0$ in equation (5.3.9) the stable solution to our linearized system (5.3.1) is as given below.

$$x(t) = C_1 V_1 e^{\lambda_1 t} + C_2 V_2 e^{\lambda_2 t} + x_p \quad (5.3.10)$$

We will be initiating walking from the stationary dual-leg support phase with our intended motor operation scheme. Hence, the conditions at the start of walking are $x_2(0) \triangleq \dot{\theta}_0(0) = 0$ and $x_3(0) \triangleq \dot{\theta}_1(0) = -\frac{V_{max}}{K_b N}$ and $t = 0$. Using these initial conditions, the equation (5.3.10) can be solved for constants C_1 and C_2 as given below.

$$\begin{bmatrix} C_1 \\ C_2 \end{bmatrix} = \begin{bmatrix} V_{21} & V_{22} \\ V_{31} & V_{32} \end{bmatrix}^{-1} \begin{bmatrix} -x_{p2} \\ -\frac{V_{max}}{K_b N} - x_{p3} \end{bmatrix} \quad (5.3.11)$$

The solution to $x_1(t)$ from equation (5.3.10) can be written as given below.

$$x_1(t) = C_1 V_{11} e^{\lambda_1 t} + C_2 V_{12} e^{\lambda_2 t} + x_{p1}. \quad (5.3.12)$$

In the stationary dual-leg support phase i.e., when $t = 0$, x_1 will be maximum. Hence, substituting $t = 0$ in equation (5.3.12) the solution to the maximum stance angle is as given below.

$$\theta_{0max} = C_1 V_{11} + C_2 V_{12} + x_{p1} \quad (5.3.13)$$

Where, C_1 and C_2 are calculated from equation (5.3.11).

5.4 Solution to Optimized Biped

This section sets out the procedure for solving the design optimization problem posed in Chapter 4. Sub-section 5.4.1 presents solution to body design. Sub-section 5.4.2 presents solution to design of leg assemblies.

STEP 1. For each motor and gear box combination determine an optimal biped design by the following procedure.

Choose ℓ , m_b and b to minimize the ratio

$$\frac{b}{\ell}$$

Where b is chosen to satisfy

$$\theta_{0opt}(b, \ell) = \theta_{0max}(b, m_b, \ell)$$

Here, θ_{0opt} is given by (4.2.9) and $\theta_{0max}(b, m_b, \ell)$ is a complicated function that is evaluated by the following procedure :

- a. Design Body and Legs to satisfy constraints (4.7.1), (4.8.6), (4.8.24), (4.8.25), (4.8.28), (4.9.1), (4.9.2), (4.9.7), (4.9.3) and (4.9.8).
(The procedure for this is described in Subsections 5.4.1 and 5.4.2)
- b. Form linear model (5.3.1)
- c. Compute θ_{0max} using the procedure described in Subsection 5.3.2.

From results of step 1

STEP 2. Choose the motor and gear box combination that results in the lowest $\frac{b}{\ell}$ ratio.

STEP 3. Verify that an accurate nonlinear simulation of the resulting biped behaves as expected under linear regulator control and respects constraints (4.3.3), (4.3.4), (4.3.7), (4.4.3), (4.5.1) and (4.5.3). Controller design and simulations are covered in Section 5.5.

The following algorithm shows how step 1 optimization was actually implemented.

Determine ℓ_{opt} from

$$\min_{\ell} \frac{b}{\ell}(\ell, m_{bopt}, b_{opt})$$

Where, $m_{b_{opt}}$ is determined from

$$\min_{m_b} \frac{b}{\ell}(\ell, m_b, b_{opt})$$

Where, b_{opt} is determined from

$$\min_b |\theta_{0_{opt}}(b, \ell) - \theta_{0_{max}}(b, m_b, \ell)|$$

Note that ℓ_{opt} turned out to be the smallest ℓ i.e., $\ell_{opt} = \ell_{min}$.

5.4.1 Solution to Body Design

The aim of this solution is to select body design parameters (Figure 4-9) h_r , w_r , t_d and yield strength of the material of the body SY_{body} for given variables ℓ , b and m_b to maximize J_b subject to satisfying constraints (4.7.1), (4.8.6), (4.8.24), (4.8.25) and (4.8.28). This solution procedure is as given below.

1. Select minimum yield strength of the aluminium alloy to be used for the body from set (4.7.1) which satisfies constraint (4.8.6).

2. In order to maximize J_b , the mass should be distributed away from the hip axis which implies that the disc thickness should be as small as possible. Hence, constraint (4.8.24) can be expressed as an equality constraint as given below.

$$t_d = \max(t_{d1}, t_{d2}, t_{d3}, t_{d4}) \quad (5.4.1)$$

The disc thickness can be finalized by using the equation (5.4.1).

3. Again, for the same reason as mentioned in step 2, we set width of the rim equal to width of the biped based on the criteria (4.8.25) as given below.

$$w_r = w_s \quad (5.4.2)$$

4. Calculate mass of the hub and disc using equations (4.8.30) and (4.8.31) respectively.

5. For the configuration of the body shown in Figure 4-9, mass of the hub plus mass of the disc should always be less than m_b . If this is true, we go through the following steps. Otherwise, we go to step 6.

a. Compute the mass of the rim by solving the equation (4.8.29) for m_{rim} .

$$m_{rim} = m_b - m_{hub} - m_{disc} \quad (5.4.3)$$

b. Compute rim thickness h_r by substituting (5.4.3) in equation (4.8.32) and solve for h_r as given below.

$$h_r = b \pm \sqrt{b^2 - \frac{(m_b - m_{disc} - m_{hub})}{\pi\rho(w_r - t_d)}} \quad (5.4.4)$$

The larger root is meaningless because it implies $h_r > b$ which is physically impossible for the assumed configuration of the body. Hence, h_r can be computed using smaller root as given below.

$$h_r = b - \sqrt{b^2 - \frac{(m_b - m_{disc} - m_{hub})}{\pi\rho(w_r - t_d)}} \quad (5.4.5)$$

c. If h_r computed by equation (5.4.5) satisfies constraint (4.8.28) then compute mass moment of inertia of the body by using equation (4.8.33).

d. If the rim thickness h_r computed by equation (5.4.5) does not satisfy constraint (4.8.28), we set h_r as given below.

$$h_r = t_{Fab} \quad (5.4.6)$$

Now, compute w_r by substituting (5.4.6) in equation (4.8.32) and solving for rim width w_r as given below.

$$w_r = t_d + \frac{(m_b - m_{disc} - m_{hub})}{\pi\rho(2bt_{Fab} - t_{Fab}^2)} \quad (5.4.7)$$

Then, compute mass moment of inertia of the body by equation (4.8.33).

6. Note that this step is only for the special case when $m_{disc} + m_{hub} > m_b$. If the computed mass of the hub and the disc in step 4 are such that their sum is greater than m_b , it implies the fact that there is not enough mass to configure the body as shown in Figure 4-9. This condition is a special case and we may have to configure the body as shown in Figure 5-2. The mass of the body for this special case is as given below.

$$m_b = m_{hub} + m_{disc} \quad (5.4.8)$$

We solve equation (5.4.8) for the mass of the disc as given below.

$$m_{disc} = m_b - m_{hub} \quad (5.4.9)$$

This special configuration of the body sets the body radius b which can be obtained by substituting (5.4.9) in equation (4.8.31) and solving for b as shown below.

$$b = \sqrt{\frac{(m_b - m_{hub})}{\pi t_d \rho} + \frac{9}{4} d_g^2} \quad (5.4.10)$$

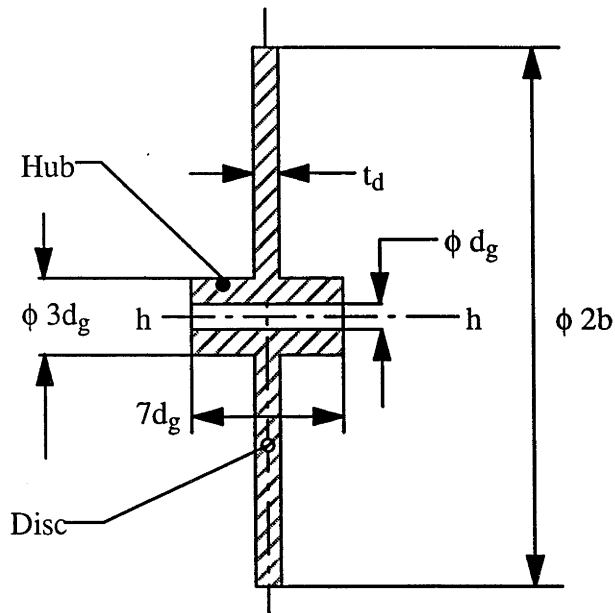


Figure 5-2: Configuration of the Body without Rim.

The mass moment of inertia of the body for this special case is as given below.

$$J_b = J_{hub} + J_{disc} \quad (5.4.11)$$

Where, J_{hub} and J_{disc} are given respectively by equations (4.8.34) and (4.8.35).

5.4.2 Solution to Design of Leg Assemblies

Aim of this solution is to select the cross section of the legs $[d_\ell, t_\ell]$ and width of the foot w_ℓ (Figure 4-14) for given ℓ , m_b and b to minimize J_ℓ subject to constraints (4.9.1), (4.9.2), (4.9.3) and (4.9.8). This solution procedure is as given below.

1. Select minimum outside diameter of the legs d_ℓ and corresponding minimum cross section thickness t_ℓ from standard aluminium alloy tube set (4.9.3) to satisfy constraints (4.9.1) and (4.9.2).
2. Select minimum width of the foot w_ℓ to satisfy constraint (4.9.8) as given below.

A clearance of 3mm is assumed between the body and the leg as shown in Figure 4-14. If, width of the rim is equal to w_s , then width of the foot will be set equal to $w_r + d_\ell + 3mm$. In case $w_r < w_s$, the width of the foot will be selected such that it is always greater than or equal to w_s maintaining a

minimum gap of 3mm between the body and the leg. Also, for the configuration of the body without rim the width of the foot will be set equal to w_s .

Choosing the cross section of the legs and the width of the foot as explained in steps 1 and 2 respectively will minimize J_ℓ .

3. Compute mass of the leg assemblies by equation (4.9.9).
4. Evaluate mass moment of inertia of leg assemblies by constraint (4.9.10).
5. Compute total mass of the biped by equation (4.9.12).
6. Finally, arrive at the effective mass moment of inertia J_0 by equation (4.9.11).

Note that the leg length ℓ selected should respect the constraint (4.9.7).

5.5 Verification by Simulation

As a final step, it is essential to check whether the biped behaves as expected and also respects constraints (4.3.3), (4.3.4), (4.3.7), (4.4.3), (4.5.1) and (4.5.3) under an appropriate control. Sub-section 5.5.1 presents a procedure for designing a linear regulator controller. Sub-section 5.5.2 presents a procedure for accurate nonlinear simulation of the biped under linear regulator control.

5.5.1 Controller Design

We have assumed linear quadratic regulator control to simulate the behaviour of our biped. In this section, we present a method of determining the feedback gain matrix. This determination of state feedback gain matrix K_r is based on our linear model (5.3.1) where,

- x = state vector (n-vector),
- u = control vector (r-vector),
- A = $n \times n$ constant matrix,
- B = $n \times r$ Constant matrix.

While designing control systems, it is important that we choose the control $u(t)$ such that the given performance index is minimized. It can be proved that a quadratic performance index such as

$$J = \int_0^{\infty} L(y, u) dt \quad (5.5.1)$$

Where, $L(y, u)$ is a quadratic function of y & u (y is a linear function of x and u) and will yield linear control law i.e., $u(t) = -K_r x(t)$, where K_r is $r \times n$ matrix. Therefore, the design of optimal regulator systems based on such quadratic performance indexes boils down to determination of elements of the matrix K_r [14].

Let, x_1 , x_2 and motor current be outputs of the system. Motor current has been considered as an output because it is a function of state x_3 and control u . Hence, these outputs can be written as given below.

$$y_1 = x_1 \quad (5.5.2)$$

$$y_2 = x_2 \quad (5.5.3)$$

$$y_3 = -\frac{K_b N}{R} x_3 + \frac{1}{R} u \quad (5.5.4)$$

The state-space representation of the outputs of the system is

$$\begin{bmatrix} y_1 \\ y_2 \\ y_3 \end{bmatrix} = \begin{bmatrix} 1 & 0 & 0 \\ 0 & 1 & 0 \\ 0 & 0 & -\frac{K_b N}{R} \end{bmatrix} \begin{bmatrix} x_1 \\ x_2 \\ x_3 \end{bmatrix} + \begin{bmatrix} 0 \\ 0 \\ \frac{1}{R} \end{bmatrix} u \quad (5.5.5)$$

which can be rewritten as given below.

$$y = Cx + Du \quad (5.5.6)$$

The MATLAB function to calculate feedback gain matrix K_r is as given below.

$$[K_r] = lqry(A, B, C, D, Q, z) \quad (5.5.7)$$

such that, the feedback law $u = -K_r x$ minimizes the cost function

$$J = \int (y^T Q y + u^T z u) dt \quad (5.5.8)$$

subject to the constraint equations (5.3.1) and (5.5.6). Here, Q decides penalty on the output and z decides penalty on the control. For our problem, we choose Q and z as follows.

$$Q = \begin{bmatrix} \frac{1}{\theta_{max}^2} & 0 & 0 \\ 0 & \frac{1}{\omega_{Gyro}^2} & \\ 0 & 0 & \frac{1}{i_{max}^2} \end{bmatrix} \quad (5.5.9)$$

$$z = \begin{bmatrix} 1 \\ V_{max}^2 \end{bmatrix} \quad (5.5.10)$$

Here, θ_{0max} is the maximum stance angle obtained from the solution presented in Section 5.3.2, $\pm\omega_{Gyro}$ is the maximum angular velocity that the rate gyro can measure (Chapter 7), i_{max} is the maximum supply current to the motor and V_{max} is the maximum supply voltage to the motor. We feel that the choice of Q and z based on practical limitations of the system will continuously drive all the states towards their desired values with minimum control effort or minimum output errors.

5.5.2 Simulation

Once the feedback gain matrix K_r is computed, we apply linear control $u = -K_r x$ to the nonlinear plant as shown in Figure 5-3. Where, $\dot{x} = f(x, u)$ is the nonlinear plant which is given by equation (3.9.3) and $K_{r-} = [K_r, 0, 0]$ is the feedback gain matrix for the complete system. Also, the control u based on current state and feedback gain matrix K_{r-} , will be set to respect the constraints on voltage (4.3.3) and current (4.3.4) through the following saturation algorithm.

$$u_{sat} = f(u)$$

where

$$u = -K_r x$$

$$\text{if, } |u| > V_{max}, \text{ then } u_{sat} = \text{sign}(u)V_{max}.$$

$$\text{Then, } i = \frac{u - K_b N x_3}{R}$$

$$\text{if, } |i| > i_{max}, \text{ then } i = \text{sign}(i)i_{max}$$

$$u_{sat} = Ri + K_b N x_3.$$

Runge Kutta numerical integration method is used to simulate our system. The time for this continuous system simulation was set from $0 \rightarrow T_{sim}$. Where, T_{sim} is the total simulation time which we have set at 2 seconds. Note that for a pendulum of length 0.25m, period of oscillation is about one second. However, total simulation time of 2 seconds will be verified after simulation (Chapter 8). Initial values of all the five states i.e., when time $t = 0$ are as follows.

$$x_1(0) = 0.99\theta_{0max} \triangleq \theta_0(0)$$

$$x_2(0) = 0 \triangleq \dot{\theta}_0(0)$$

$$x_3(0) = -\frac{V_{max}}{K_b N} \triangleq \theta_1(0)$$

$$x_4(0) = \frac{\pi}{2} \triangleq \theta_1(0)$$

$$x_5(0) = 25 \triangleq T_{motor}(0)$$

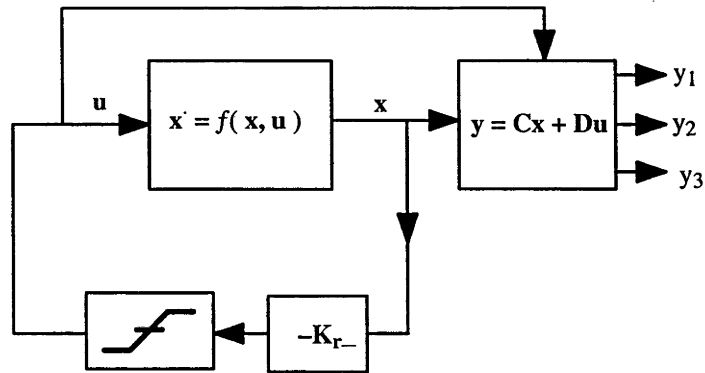


Figure 5-3: Representation of State Feedback Control

Where, θ_{0max} is given by equation (5.3.13) and is our estimate of the largest dual-leg support value of θ_0 that allows recovery to a balanced single-leg equilibrium. The initial angular velocity $x_2(0)$ of the stance leg is zero because we will be initiating walking from the stationary dual-leg support phase. The initial angular speed of the body $x_3(0)$ is set at $-\frac{V_{max}}{K_b N}$ according to our intended motor operation scheme presented in Section 5.2. The initial position of the body $x_4(0)$ which has no influence on dynamics has been set at $\frac{\pi}{2}$. The initial temperature of the motor $x_5(0)$ has been set at 25°C ambient [17].

We have observed that recovery of our system to a balanced vertical position is very sensitive to $x_1(0)$, the initial stance angle. For this reason, we normally set $x_1(0)$ to a value that is slightly less than our estimate (e.g., $x_1(0) = 0.99\theta_{0max}$). A few designs were unable to recover with this initial value of stance angle. In such cases, we tried different multiplication factors in the range of 0.8 to 0.99 for θ_{0max} . One could easily finalize on a particular value of $x_1(0)$ by repeating the simulations for a few different values of $x_1(0)$ and picking a value which results in a stable transition from the dual-leg support phase to a balanced vertical position.

Chapter 6

Results

The solution procedure to obtain optimized biped presented in Chapter 5, Section 5.4 was implemented in MATLAB. This chapter presents results obtained from this MATLAB routine (appendix C) for various motors. It begins by presenting broad criteria for selecting few actuator sets to try in our design optimization routine. Section 6.2 will present various results and finally point out the most optimized biped obtained so far.

6.1 Actuator Set Selection

Numerous traditional electromagnetic actuators, specially DC motors and brushless DC motors are available in the market. To select a few actuator sets out of them for our application is a difficult task. Hence, an attempt is made in this section to present some important characteristics of motors which are relevant to achieve our objective. These characteristics will enable us to select few actuator sets from various manufacturer catalogues to try in our algorithm. We followed the same approach as in [13] for analyzing the DC motor parameters in terms of motor “muscle” and motor constant. This section begins by presenting the motor “muscle” which we feel is important to our application. Sub-section 6.1.2 discusses the motor constant and combined motor parameter. Sub-section 6.1.3 stresses the importance of stall torque. The final sub-section presents the criteria for selecting actuator sets.

6.1.1 Motor Muscle

The most important motor specifications that one has to look for in selecting DC motors for robotic applications are the $\frac{Power}{Mass}$ ratio and $\frac{Torque}{Mass}$ ratio.

High $\frac{Power}{Mass}$ ratio is a general requirement for all robots [13]. The $\frac{Power}{Mass}$ ratio is an indicator of the total system limit (motor plus accompanying amplifier) [13]. The $\frac{Torque}{Mass}$ ratio plays a vital role in direct drive robotic applications.

6.1.2 Motor Constant and Combined Motor Parameter

Motor Constant

The ratio $\frac{Torque}{Mass}$ depends on the torque produced by the motor. In SI units $K_t = K_b$, hence the motor torque equation (3.5.5) can be written as given below.

$$\tau_m = \frac{K_t u}{R} - K_m^2 \dot{\theta}_m \quad (6.1.1)$$

Where

$$K_m = \frac{K_t}{\sqrt{R}} \quad (6.1.2)$$

K_m is defined as the motor constant. As long as the conductor area in the slot is the same, the motor constant K_m is virtually independent of motor speed, input current and of how the motor is wound (number of turns) [13]. It can be shown that continuous motor torque is given by

$$\tau_{cont} = K_m \sqrt{P_{loss cont}} \quad (6.1.3)$$

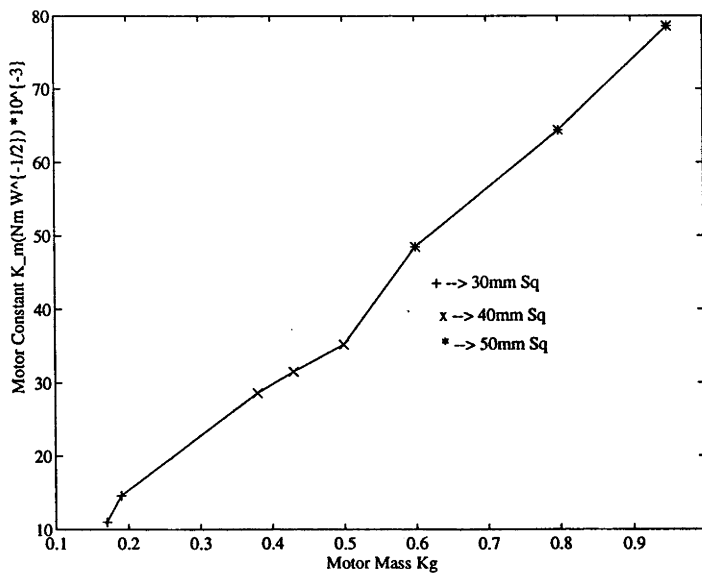


Figure 6-1: Motor Constant K_m Vs Motor Mass.

The motor constant $K_m \left(\frac{Nm}{\sqrt{W}} \right)$ implies a fundamental fact about motors that it is necessary to dissipate power in windings to produce torque (refer Equation 6.1.3). The higher the constant, the larger the exerted torque becomes and lower the power consumed. Figure 6-1 plots K_m versus mass for a range of PITTMAN brushless DC motors. It is evident that K_m rises approximately linearly with motor mass with a cross sectional dimensional dependence [13]. Figure 6-1 clearly indicates that greater torque can be achieved at the expense of motor dimension and mass.

Combined Motor Parameter

The dissipated power causes heat which must be transferred away to prevent overheating. This is determined by the thermal/mechanical design of the motor. This ability to transfer heat is indicated by $\frac{1}{R_{th}}$ (thermal conductance) which indicates how many dissipated watts are produced per $^{\circ}C$ temperature rise. Motor constant indicates how much torque is produced per dissipated watt. Hence, motor constant K_m and $\frac{1}{R_{th}}$ can be combined as $\frac{K_m}{R_{th}} \left(\frac{Nm}{\sqrt{^{\circ}C}} \right)$ to provide a single parameter that indicates the amount of torque that can be continuously sustained for a given winding temperature.

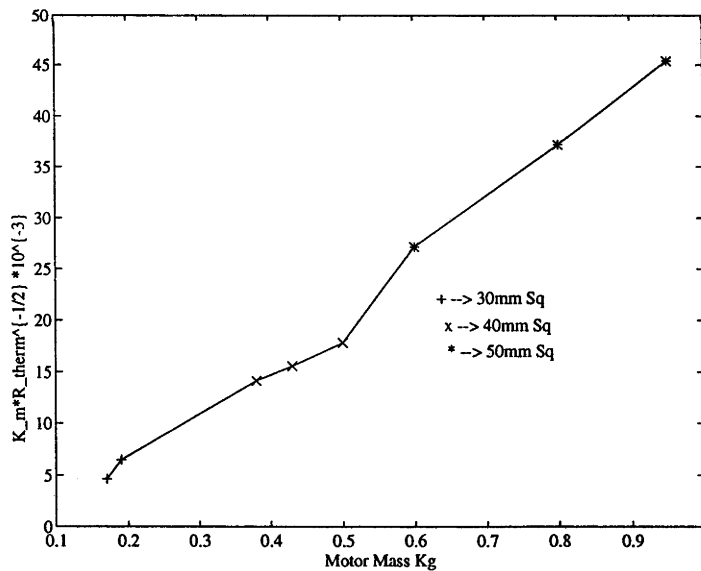


Figure 6-2: Combined Parameter $\frac{K_m}{R_{th}}$ Vs Motor Mass.

Figure 6-2 shows the variation of this combined parameter with respect to motor mass for PITTMAN brushless DC motors. When compared in this manner, seemingly disparate motor designs often end up with the same torque capability [13].

6.1.3 Stall Torque

Stall torque is another important parameter which will be useful in producing greater torques for short durations. Stall torque is a function of motor torque constant, terminal resistance and supply voltage and is as given below.

$$\tau_{peak\ stall} = \frac{K_t}{R} V_{max} \quad (6.1.4)$$

6.1.4 Criteria For Selecting Actuator Sets

This section summarizes the criteria for selecting motors to form an actuator set from various manufacturer catalogues. These criteria were formulated keeping our objectives in view and based on the discussions presented in previous sections. They are presented below in an order of importance.

- (1) In order to keep the biped small, mass of the motor should be between 0.1 kg to 0.5 kg.
- (2) Availability of appropriate reduction units with versatile reduction ratios and encoders.
- (3) Availability of relevant motor, gear, encoder and amplifier specifications.
- (4) Compare motor constant K_m of various motors having the same mass and select the one with largest K_m .
- (5) Generally, manufacturers specify various windings for each motor. Compare torque constant K_t among various windings and select the winding with largest value of K_t .

It was observed that the motors compared in this way also had greater values of combined motor parameter $\frac{K_m}{R_{th}}$ as well as peak stall torque $\tau_{peak\ stall}$.

6.2 Optimization Results

After studying about 25 manufacturer catalogues of DC and brushless DC motors, the selection boiled down to MAXON and PITTMAN motors. Others were rejected because of (1) unsuitable size, $\frac{torque}{mass}$ and $\frac{power}{mass}$ ratios, (2) non-availability of motor specifications, suitable reduction units and actuators in the mass range of 0.1 to 0.5 kg, (3) reduction

units with eccentric shafts. Important criteria for motor selection as discussed in Section 6.1 was also considered in evaluating them.

Sub-section 6.2.1 gives the specifications of the best biped obtained out of 19 Maxon DC motors. Sub-section 6.2.2 gives parameters of the best biped obtained out of 10 Pittman brushless DC motors. Sub-section 6.2.3 presents the characteristics of the best biped design obtained out of six Maxon brushless DC motors. Sub-section 6.2.4 compares specifications presented in Sections 6.2.1 - 6.2.3 and points out the most optimized biped obtained so far which will be considered for further detailed design.

6.2.1 Biped Design with Maxon DC Motors

Out of 19 Maxon motors [17] tried in simulations, the best design was achieved by Maxon_990 motor with a gear ratio of 33.2. The specifications of this motor is attached as Appendix D. It has resulted in a $\frac{b}{\ell}$ ratio of 0.7128. Figure 6-3 gives the plots of $\frac{b_{opt}}{\ell}$ versus gear set number for each of these motors. Each line in Figure 6-3 represents a particular motor from a set of 19 Maxon DC motors. Each of these motors can have a gear ratio selected from a set size of 7 (Appendix D) resulting in 7 different values of $\frac{b_{opt}}{\ell}$. For each and every motor, straight lines are drawn through points of intersection of $\frac{b_{opt}}{\ell}$ and the corresponding gear ratio set number. The resulting biped has a leg length (0.2028 m) to stride (0.175 m) ratio of 1.16. Also, this biped can rise itself to vertical balance position from an angle of 25.6°. The design parameters of the biped with this DC motor is listed in Table 6.2.1.

Table 6.2.1: Biped Design Parameters-Motor: Maxon_990, N: 33.2.

V_{max}	19.4, Volts	b	0.1446, m	h_r	0.0024, m	t_ℓ	$9.1 * 10^{-4}$, m
i_{max}	3.7, Ampere	w_r	0.04, m	w_ℓ	0.072, m	m_b	0.657, kg
ℓ	0.2028, m	t_d	0.0024, m	d_ℓ	0.0095, m	m_a	0.438, kg
m_ℓ	0.5083, kg	J_ℓ	0.0014, kgm^2	m	1.166, kg	J_b	0.0089, kgm^2

6.2.2 Biped Design with Pittman Brushless DC Motors

Out of 10 Pittman [16] brushless DC motors tried in simulations, Pittman_3112.43 (Winding No. 4, 3 Phase) motor with a reduction ratio of 24 gave the best design. The specifications of this actuator is given as Appendix E. The voltage and current meet their

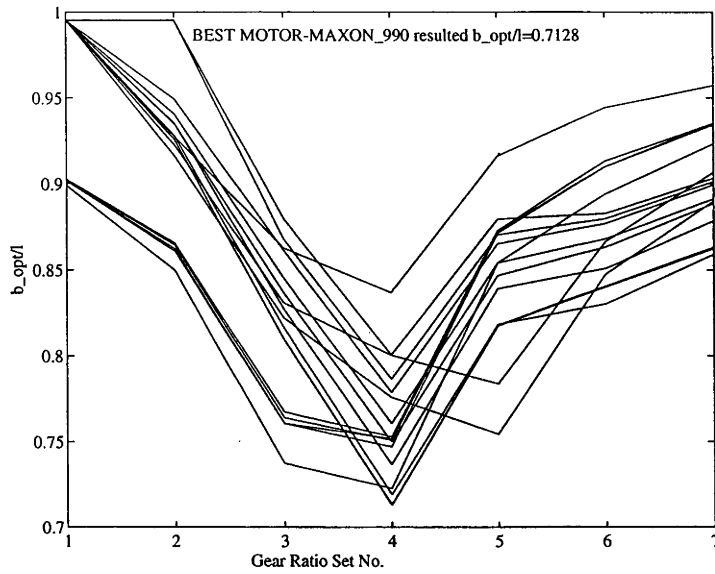


Figure 6-3: BOLOpt. for 19 Maxon DC Motors.

amplifier and power electronics limitations of 0-7 Ampere and 0-70 V dc supply to the motor [16]. This actuator and reduction gear combination gives a $\frac{b}{\ell}$ ratio of 0.5729. Figure 6-4 gives plots of $\frac{b_{opt}}{\ell}$ versus gear set number for each of these motors. Each line in Figure 6-4 represents a particular motor from a set of 10 Pittman Brushless DC motors. Each of these motors can have a gear ratio selected from a set size of 10 (Appendix E) resulting in 10 different values of $\frac{b_{opt}}{\ell}$. For each and every motor, straight lines are drawn through points of intersection of $\frac{b_{opt}}{\ell}$ and the corresponding gear ratio set number. The resulting biped has a leg length (0.2188 m) to stride (0.23 m) ratio of 0.95. Also, this biped can rise itself to vertical balance position from an angle of 31.6°. Table 6.2.2 gives the design parameters of the biped for this actuator.

Table 6.2.2: Biped Design Parameters-Motor: Pittman_3112_43, N: 24.

V_{max}	37.5, Volts	b	0.1253, m	h_r	0.0056, m	t_ℓ	$1 * 10^{-3}$, m
i_{max}	7, Ampere	w_r	0.0776, m	w_ℓ	0.092, m	m_b	1.2534, kg
ℓ	0.2188, m	t_d	0.0024, m	d_ℓ	0.012, m	m_a	1.01, kg
m_ℓ	1.122, kg	J_ℓ	0.003, kgm^2	m	2.3761, kg	J_b	0.0157, kgm^2

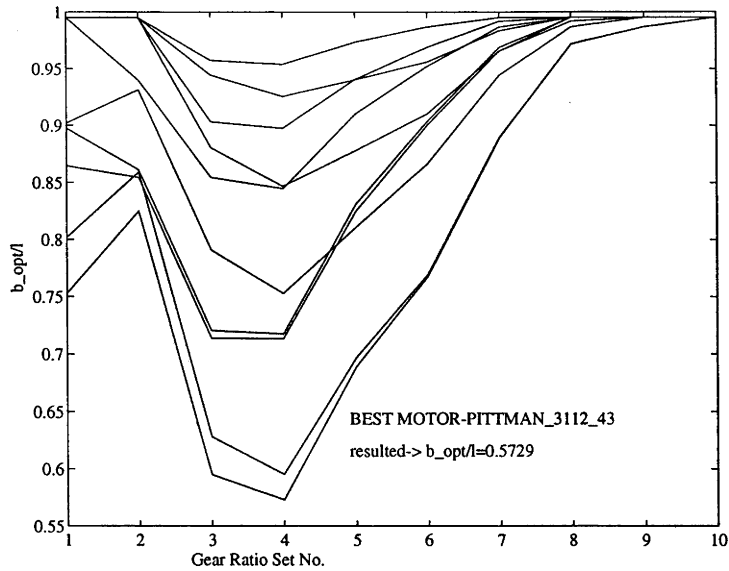


Figure 6-4: BOLOpt. for 10 Pittman Brushless DC Motors.

6.2.3 Biped Design with Maxon Brushless EC Motors

Six of these were tried in simulations. Results indicate that the best design is given by Maxon_136 motor with a reduction ratio of 19.2. The characteristics of this motor is given as Appendix F. Figure 6-5 gives plots of $\frac{b_{opt}}{\ell}$ versus gear set number for each of these motors. Each line in Figure 6-5 represents a particular motor from a set of 6 Maxon Brushless EC motors. Each of these motors can have a gear ratio selected from a set size of 8 (Appendix F) resulting in 8 different values of $\frac{b_{opt}}{\ell}$. For each and every motor, straight lines are drawn through points of intersection of $\frac{b_{opt}}{\ell}$ and the corresponding gear ratio set number. Table 6.2.3 gives the design variables. This design gives the lowest $\frac{b}{\ell}$ ratio (0.544) and the greatest step length of 0.249. The resulting biped has a leg length (0.2302 m) to stride (0.246) ratio of 0.93. Also, this biped can rise itself to vertical balance position from an angle of 32.4° . This biped can also climb a slope of 32.4° .

Table 6.2.3: Biped Design Parameters-Motor: Maxon_136, N: 19.2.

V_{max}	29, Volts	b	0.1252, m	h_r	0.0042, m	t_ℓ	$1 * 10^{-3}$, m
i_{max}	10, Ampere	w_r	0.0818, m	w_ℓ	0.0968, m	m_b	1.0339, kg
ℓ	0.2302, m	t_d	0.0024, m	d_ℓ	0.012, m	m_a	0.8, kg
m_ℓ	0.9176, kg	J_ℓ	0.0032, kgm^2	m	1.9515, kg	J_b	0.013, kgm^2

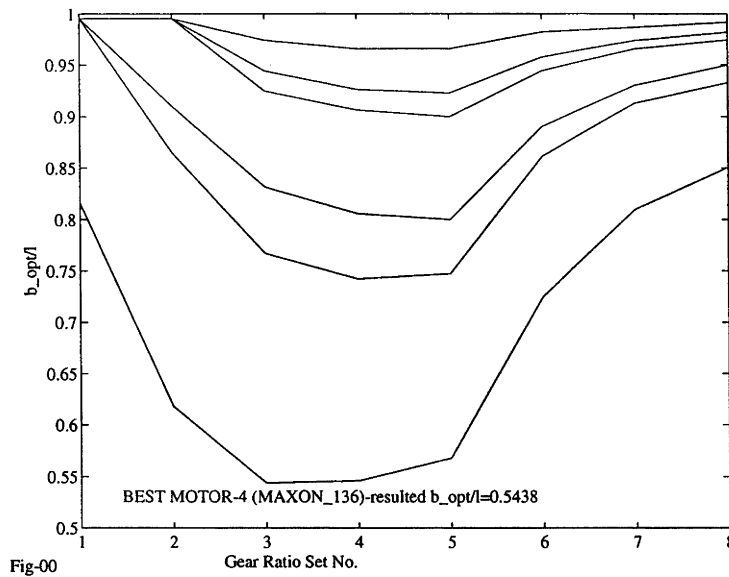


Figure 6-5: BOLOpt. for 6 Maxon Brushless EC Motors.

6.2.4 Biped Considered for the Detailed Design

Comparing specifications presented in Tables 6.2.1 - 6.2.3, the biped resulted from Maxon_136 brushless DC motor with a gear ratio of 19.2 will be able to cross larger obstacles and can take larger strides than bipeds using other motors. This is because of its lower $\frac{b}{l}$ ratio and greater θ_{0max} compared to corresponding results of Maxon DC and Pittman brushless DC motors. Furthermore, this has resulted in lower biped mass when compared to the biped mass resulting from the Pittman brushless DC motor. Therefore, this motor and reduction unit has resulted in the most optimized biped. The parameters of this biped (Table 6.2.3) are considered for further detailed design and verification. We refer to this biped as the **best biped** in later chapters.

Note : Simulation results obtained corresponding to the optimized biped parameters presented in Table 6.2.3 satisfies constraint (4.3.3), (4.3.4), (4.3.7), (4.4.3), (4.5.1) and (4.5.3). Also, this biped behaves as expected under linear quadratic regulator control. However, we choose to present these results in Chapter 8 after completing detailed design of the best biped.

Chapter 7

Specifications of the Best Biped

7.1 Introduction

This chapter presents specifications of components as well as overall specifications of the best biped after completing detailed design. The best motor and the associated gear box parameters corresponding to the best gear ratio were used in this detailed design. Also, design parameters of the best biped presented in Table 6.2.3 were used for detailed design. Sections 7.2 and 7.3 present the specifications of commercially available components and custom made components respectively. Section 7.4 presents the cost estimate for the best biped. Section 7.5 presents overall specifications of the best biped.

7.2 Commercially-available Components

Commercially available components of our best biped are given in Table 7.2.1. This section presents specifications of these components. Sub-sections 7.2.1, 7.2.2 and 7.2.3 present the specifications of the best motor, the motor control unit and the encoder respectively. Sub-section 7.2.4 gives the specifications of the best reduction unit. Sub-section 7.2.8 present the specifications of the rate gyro. Sub-section 7.2.9 present the specifications of the tilt sensor and the tilt sensor signal conditioner.

7.2.1 Motor

As concluded in Chapter 6, Section 6.2, the best biped resulted from a brushless DC motor Maxon, EC - 032 - 060 - 36 - EAB200B [17] which was designated as Maxon_136 in our algorithm. Electronically commuted maxon EC motors are high quality DC motors using Neodymium (NdFe) magnets. In contrast to maxon DC motors, the iron-less

Table 7.2.1: Commercially available components

Components	Quantity
Motors	2
Reduction Units	2
Encoders	2
Motor Control Units	2
Rate Gyros	2
Electrolytic Tilt Sensors	2
Tilt Sensor Signal Conditioner	2

Table 7.2.2: Specifications of the Best Motor Part-A.

Assigned power rating	W	40
Nominal Voltage	Volt	48
No load speed	rpm	11400
Stall torque	mNm	330
Speed/torque gradient	rpm/mNm	34.8
No load current	mA	61.6
Terminal resistance phase to phase	Ohm	5.8
Max. permissible speed	rpm	17000
Max. continuous current at 5000 rpm	A	0.928
Permissible continuous power loss	W	7.8
Max. efficiency	%	83.6
Torque constant	mNm/A	39.9

winding is stationary whereas the permanent magnet rotates in the field of three-phase electronically commuted field. Rotor position sensing is accomplished using three magnetic sensors [17]. Specifications of this motor are given in tables 7.2.2 and 7.2.3.

Table 7.2.3: Specifications of the Best Motor Part-B.

Speed constant	rpm/V	239
Mechanical time constant	ms	11
Rotor inertia	gcm^2	30
Terminal inductance (Phase to Phase)	mH	0.96
Thermal resistance housing - ambient	K/W	10.3
Thermal resistance rotor - housing	K/W	2.5
Weight of the motor	g	210
Length of the motor	mm	60
Diameter of the motor	mm	$\phi 32$
Max. permissible winding temperature	$^{\circ}C$	+125
Ambient temperature	$^{\circ}C$	-20/+125

7.2.2 Motor Control Unit

As mentioned in Chapter 2, these motor control units are kept off-board. Two Maxon MMC-SC070 motor control units are required to commutate and to control two of the biped motors independently. The Maxon electronic commutation control MMC-SC070 is a PWM servo amplifier. It enables rotor angle dependant, sinusoidal motor currents and the control of speed and torque of Maxon EC motors. Some important specifications of this control unit are given in Table 7.2.4. However, refer [17] for complete specifications.

7.2.3 Encoder

As mentioned in Chapter 2, accurate digital encoders have to be attached to respective motor shafts to detect the position of the body with respect to stance leg. Each of the biped motors is integrated with a digital encoder Maxon, HP HEDS 5500 which works on photoelectric principle. A LED emits light through the indexed code wheel, which is rigidly mounted on the motor shaft. The receiver (phototransistor) converts the light/dark pulses

Table 7.2.4: Specifications of the Motor Controller.

Supply voltage	VDC	24 to 70
	V AC	18
Maximum Current	A	14
Output Current Continuous	A	8
Weight	g	900
Temperature		
Storage	°C	-40..85
Operation	°C	-10..+70

into corresponding electrical signals which are subsequently conditioned and amplified in the associated miniature electronic system. The encoder output can be used to find the direction of rotation, position and to count number of rotations. Some of the important specifications of this encoder are presented in Table 7.2.5. Refer to [17] for complete specifications.

Table 7.2.5: Specifications of the Encoder.

Supply voltage	$5V \pm 10\%$
Rise time	200ns
Fall time	50ns
Number of channels	2
Counts per turn	500
Operating Temperature	-20 to + 100 °C
MI of code wheel	$\leq 0.6gm^2$
Max. acceleration	250 000 rad/s ²
Max. output current per channel	5mA
Phase shift	$90^\circ \pm 45^\circ$
Dimensions	41mm * 30mm * 18.3mm
weight	20g

7.2.4 Planetary Gearhead

As concluded in Chapter 6 and in Subsection 6.2.4, the best motor Maxon_136 along with the best planetary gear box with a reduction ratio of 19.2 resulted in the best biped. This gear ratio will be obtained in two stages [17]. These planetary gearheads are particularly suitable for the transmission of high torque and are equipped with ball bearings. Maxon product number for this gearhead is 2932.702 - 0019.0 - 000 [17]. Specifications of this gearhead is given in Tables 7.2.6 & 7.2.7

Table 7.2.6: Specifications of the Planetary Gearhead Part-A.

Planetary gearhead	straight teeth
Bearing at output	ball bearing
Radial play, 5mm from flange	max. 0.08mm
Max. permissible axial load	120N
Max. permissible force for press fits	120N
Average backlash no load/stage	< 0.9°
Recommended input speed	<4000 rpm

Table 7.2.7: Specifications of the Planetary Gearhead Part-B.

Recommended temperature	-20/+80 °C
No. of Stages	2
Efficiency	0.6
Max. radial load	140N at 12 mm
Weight	170g
Dimensions	L = 36.1mm & D = ϕ 32mm
Shaft diameter	$d_g = \phi$ 5.5mm

7.2.5 Output Resolution

Effective resolution of leg angle can be determined by using reduction gear and encoder specifications. The resolution can be computed by the following equation.

$$\Delta\theta_0 = \frac{360}{(\text{Counts per turn}) * N} \quad (7.2.1)$$

Since the gear ratio is 19.2 and encoder measures 500 counts per turn, the effective resolution of the leg angle is 0.0375° .

7.2.6 Rate Gyro

We will be using two rate gyros (Chapter 2) mounted one on each leg assembly to measure the position of the stance leg. We have envisaged to use Gyrostars manufactured by Murata, Manufacturing, Co., LTD., Japan [25] for this purpose. These Gyrostars measure angular velocity $\dot{\theta}_0$. Orientation θ_0 can be calculated by integration of angular velocity over time. The output of the device is a voltage proportional to the angular velocity relative to a reference. Thus Gyrostar mounted on each of the leg assembly bracket as shown in Dwg. 1019310011 measures the state x_2 ($\dot{\theta}_0$) which will be integrated over time to yield x_1 (θ_0).

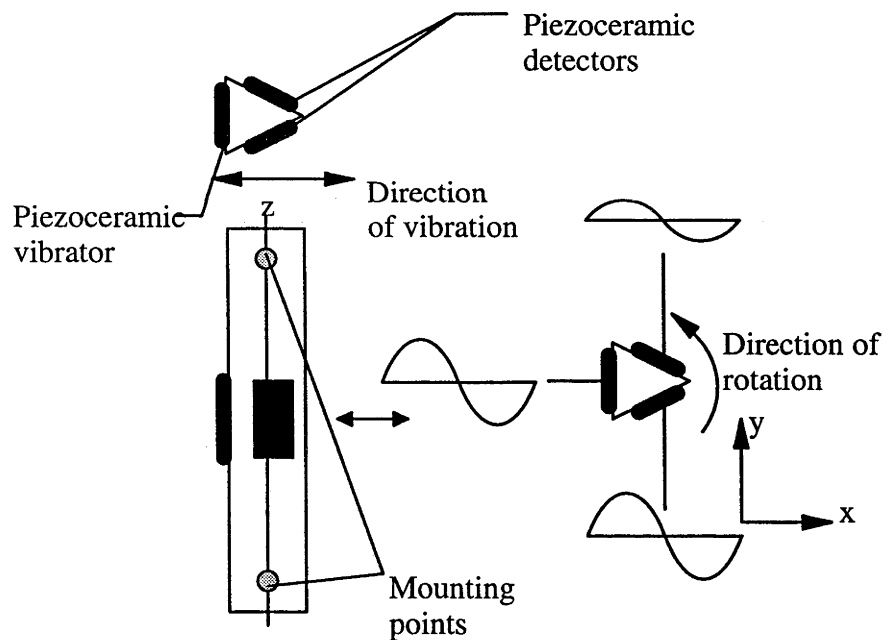


Figure 7-1: Gyrostar.

Inside this device is a triangular metal prism fixed at two points. This prism is forced to vibrate by the piezoelectric ceramic at 7KHz [26]. With no rotation around Z axis, each of the other two piezoelectric ceramics detect a large equal signal. When the prism is turned, it gets twisted such that the detectors receive different signals. This signal difference is examined by internal analogue circuits and brought out as a voltage proportional to angular velocity. Table 7.2.8 gives the specifications of ENC-05S [25] Gyrostar finalized for design.

Table 7.2.8: Specifications of the Gyrostar.

Supply voltage	5.0VDC, 2.5VDC (Vref.)
Supply Current	7mA
Maximum angular velocity	± 90 Deg/sec
Scale factor	0.8mV/Deg/sec $\pm 20\%$
Output	$V_0 = V_{ref} \pm 500$ mV at angular velocity = 0 $V_0 \pm 72$ mV DC $\pm 20\%$ at max. angular velocity
Linearity	within $\pm 5\%$
Scale factor offset	within +10% -20% at working tempr. range
Working tempr. range	-10° to +60°C
Dimensions	20mm*13mm*7mm
Weight	3.5g

This model was selected because it is more compact, light in weight and less expensive compared to the other model ENV - 05S. Some tests and compensation schemes have to be done for the successful use of this device. However, Gerharweib and his team [26] have done some tests on the model ENV - 05S. Their conclusions are as follows.

- (1) Noise due to it's own vibration at 7KHz can be suppressed.
- (2) Over time, self heating induces error in "offset drift".
- (3) Device is highly linear. At 21°C, deviations are $< 0.05^\circ$ /sec from ideal line.
- (4) Scale factor is 22 mV / ° /sec $\pm 0.15\%$ and offset is 0.5° /sec/ °C.

Scale factor results in a proportional error in the angle which has to be compensated during integration. The offset error leads to continuous drift due to integration over time which is a problem [26]. These points have to be critically examined for the model ENC-05S, such that they should not degrade the control performance. The biped comes to rest from time to time (dual support phase). This gives the actual offset of the angle which can be used for compensating "offset error". Also, the device should be maintained at constant temperature.

Since time constant of these rate gyros are small compared to tilt sensors we have planned to use rate gyros for single-leg support balance. Also, we have envisaged to use bubble inclinometers to estimate the ground slope and to correct for drift error in the rate

gyros.

7.2.7 Electrolytic Tilt Sensor

Each leg assembly carries a bubble inclinometer as shown in the large Drawing 1019310011 attached to this report. When they are connected in an appropriate electrical circuit they provide an output voltage proportional to the tilt angle and a phase indicative of tilt direction. It consists of a tubular glass envelope partially filled with an electrolytic fluid which contacts metal electrodes. When sensors are connected properly and levelled, an equal impedance to the common electrode will exist and digital voltmeter will indicate minimum (null) output. Tilting the level will cause an unbalanced impedance to common electrode and the output voltage will increase. This voltage is the useable output of the sensor and is proportional to the tilt angle. Spectron vertical sensing electrolytic potentiometer L-211U with housing 557A [27] is a single axis unit providing linear voltage output when the unit is tilted about the horizontal axis. The main advantage of these sensors is that they need not be mounted on feet. Some of the important characteristics [27] of the sensor Spectron L-211U are given in Table 7.2.9. However, for complete specifications refer [27].

Table 7.2.9: Specifications of the Electrolytic Tilt Sensor.

Tilt angle range (Deg)	± 60
Output (mV/Deg/Volt excitation)	$7.2 \pm 20\%$
Total null (mV at 3V 400Hz)	2
Repeatability at any angle	0.03 Deg.
Null repeatability	0.03
Linearity, Full scale (% of full sale)	5
Time constant (Seconds)	$0.1 \pm 25\%$
Excitation voltage (Volts AC)	0.5 to 5 (20 to 20,000Hz)
Operating tempr. range	-40° to $+80^\circ\text{C}$
Dimensions	14mm*13mm*13mm
Weight	2g

Tilt Sensor Signal Conditioner

Tilt sensor signal conditioner is required for (1) temperature compensation, (2) output gain adjustment for desired voltage, (3) sensor offset correction, (4) symmetry adjustment, (5) to develop the required AC sensor excitation. We have envisaged to use signal conditioning module SA40012 manufactured by [27]. Some of the important specifications of this signal conditioner is given in Table 7.2.10.

Table 7.2.10: Tilt Sensor Signal Conditioner Specifications.

Power requirement	5 V DC to 15 V DC
Supply Current	0.5 mA at 5 V DC; 0.9 mA at 15 V DC
Sensor Excitation	380 mV pp Square Wave
Input Impedance	5 Megaohms.
Output Signals	$50 \text{ mV} < V_{\text{out}} < V_{\text{DD}} - 1.5 \text{ V DC}$
Time Constant	30 ms
Offset Adjustment	$\pm 45 \text{ mV DC}$
Output Ripples	0.35% of Output Voltage
Temperature Coefficient	0.20% / °C at 1 V Output
Temperature Coefficient	100 Microvolt / °C at Null
Operating tempr. range	-25° to +70°C
Resistor Gain Adjustment	RG 10k \rightarrow ∞

7.3 Custom-manufactured Components

Detailed design was completed for the best biped taking all the necessary parameters presented in Table 6.2.3. The Biped Walking Machine Assembly is as shown in Drawing-1019310011 attached to this report. Table 7.3.1 lists the custom-manufactured components and gives reference to drawings which are attached to this thesis. From these drawings, it is clear that there are some deviations in the implementation of the body and the leg to that considered for the design optimization. The major deviations are (1) the hub of the body is replaced by a simple lightweight coupling which can be bolted to the disc (ref. Dwg. 1019310011), (2) A 'C' shaped bracket has been introduced as shown in the Drawing 1019310015 of leg assembly. These modifications were necessary to meet the assembly,

manufacturing and cost aspects. The mass properties obtained from CAD modelling after detailed design of our best biped is given in Table 7.3.2. Deviations are not significant when these mass properties were compared with that obtained from simulations (Table 6.2.3). However, simulations will be updated with these more realistic mass properties for final verifications covered in Chapter 8.

Table 7.3.1: Custom-manufactured Components.

Components	Aluminium alloy	Drawing No.	QTY.
Body	2024-T62 or 5083-H112	1019310012	1
Coupling	2014-T6	1019310013	1
Bracket	2014-T6	1019310014	2
Leg	6061-T6	1019310015	4
Leg Assembly	- NA -	1019310016	2

Table 7.3.2: Biped Mass Properties from CAD Model.

m_b	m_ℓ	m
1.0884, kg	0.979, kg	2.0742, kg
J_b	J_ℓ	J_o
0.0135, kgm^2	0.00287, kgm^2	0.11278, kgm^2

7.4 Cost Estimate

Table 7.4.1 presents the cost of all commercially available components for our biped. Also, it presents material and fabrication costs of all the custom made components of the biped which also includes cost for assembling the biped.

Table 7.4.1: Cost Estimate.

Item	Quantity	Cost (Aus. \$)	Remarks
Motor	2	679.00	STD
Motor Controller	2	4118.00	STD
Reduction Gear	2	647.00	STD
Encoder	2	374.00	STD
Gyrostar	2	540.00	STD
Tilt sensor	2	876.00	STD
Tilt sensor signal conditioner	2	177.00	STD
Material, Fabrication & Assembly of biped	1	2620.00	PRO PARTS PTY LTD Quotation No: 94033
Total		10031.00	

7.5 Overall Specifications of the Best Biped

This section presents the overall specifications of our best biped.

Biped Specifications

Mass	2.0742, kg
Overall Dimensions (Dual-leg support phase)	0.25m × 0.39m × 0.277m
Overall Dimensions (Single-leg support phase)	0.25m × 0.46m × 0.277m
Leg length to stride ratio	0.93
Maximum Slope that it can Climb	32.4°
Maximum Size of the Obstacle that it can Cross	0.07, m tall and 0.14, m long
Leg length	0.2302, m
Radius of the Body	0.1252, m
Mass of the Body	1.0884, kg
Mass of the Leg Assemblies	0.979, kg
Moment of Inertia of the Body	0.0135, kgm^2
Moment of Inertia of the Leg Assemblies	0.00287, kgm^2

Effective Moment of Inertia (J_0)	0.11278, kgm^2
Supply voltage to Motors	29 V DC 10 Amp
Supply voltage to Encoders	5 V \pm 10%
Supply voltage to Gyrostars	5 V DC, 2.5 V DC (Vref) 7 mA.
Supply voltage to Tilt Sensors	5 V AC Peak to Peak, Square wave 1 KHz

Chapter 8

Verification of the Final Design through Simulation

8.1 Introduction

This chapter presents the final simulation results. The parameters of the best biped presented in Table 6.2.3 were updated using the mass properties presented in Table 7.3.2. Then the simulation procedure defined in Chapter 5 Section 5.5 was applied to obtain the results presented in this chapter. Section 8.2 presents simulation results which verify that the biped behaves as expected and satisfies all constraints. Section 8.3 verifies that the thermal model is valid.

8.2 Behaviour of the Best Biped Under Control

Stance Leg Angle Versus Time

Figure 8-1 shows plot of stance leg angle θ_0 versus time. This plot indicates that the biped moves from OA to OB (Figure 2-7) and balances in vertical position from an initial angle of $0.99\theta_{0max}$ (32.4°) as expected. Steady state value of $\theta_0 = 0$ has been reached with a settling time of around 2 seconds without any oscillations and significant overshoot. The initial stance angle $x_1(0) = 32.4^\circ$ respects the maximum angle limit of the tilt sensor as given in Table 7.2.9. Note that the electrical time constant of the motors envisaged for the biped is 0.17ms (Tables 7.2.2 & 7.2.3) which is faster than the settling time of 2 seconds. This substantiates our assumption of neglecting low inductance and damping values of the DC motor in developing a mathematical model for the single-leg support phase (recall

discussions in Section 3.3).

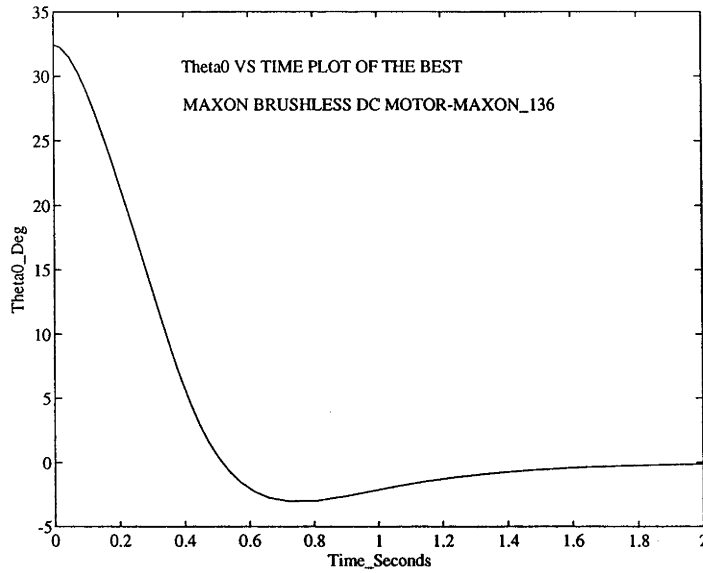


Figure 8-1: θ_0 Vs. Time.

Rate of Stance Leg Versus Time

Figure 8-2 shows plot of $\dot{\theta}_0$ versus time. This plot indicates that $\dot{\theta}_0$ becomes zero with a settling time of 2 seconds before reaching a maximum value of about $-1.5, \frac{\text{rad}}{\text{sec}}$. Also, maximum angular velocity reached by stance leg does not violate Gyrostar limits given in Table 7.2.8.

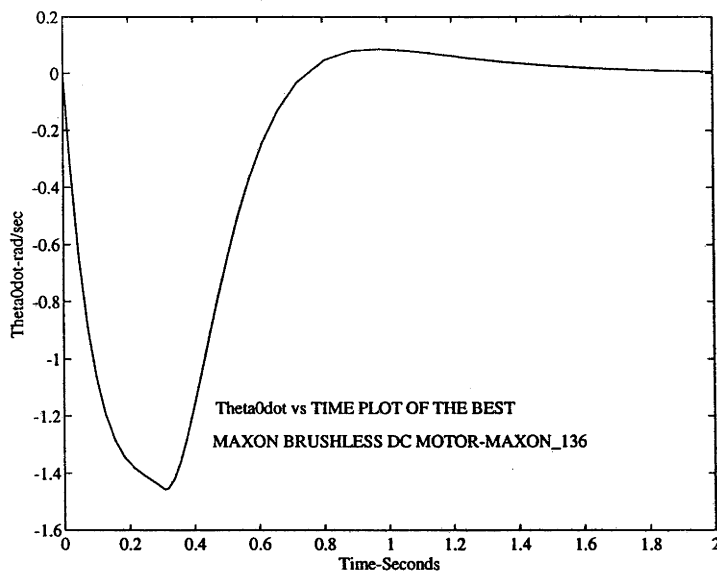


Figure 8-2: $\dot{\theta}_0$ Vs. Time.

Body Spin Rate and Body Position Versus Time

Figure 8-3 shows plot of $\dot{\theta}_1$ versus time. This plot indicates that the body spin rate reaches a steady state value of zero with a settling time of 2 seconds. Also, the maximum angular velocity reached by the body respects the gear box input speed limitations as discussed in Sub-section 4.4.2. Refer Table 7.2.6 for the recommended input speed of the gear box.

Figure 8-4 plots the position of the body versus time.

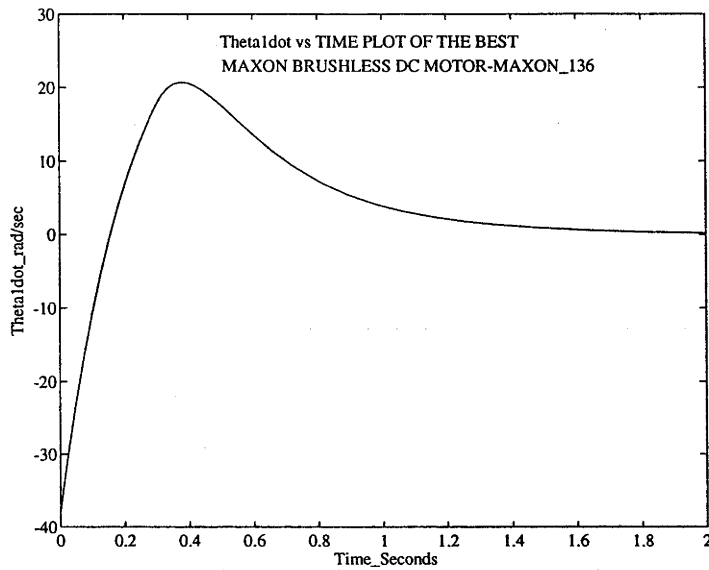


Figure 8-3: $\dot{\theta}_1$ Vs. Time.

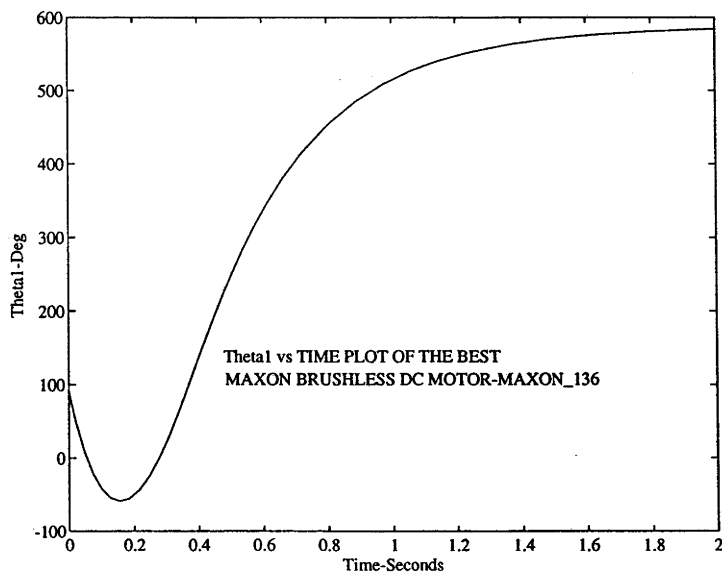


Figure 8-4: θ_1 Vs. Time.

Normal Foot Force F_n and Coefficient of Friction μ Versus Time

Figures 8-5 show the plot of normal reaction force F_n between the ground and foot versus time (recall discussions presented in Section 4.5). This plot indicates that the foot force constraint (4.5.1) is respected at all times and the foot stays in contact with the ground. Figure 8-6 shows variation of coefficient of friction between the ground and foot versus time. As discussed in Subsection 4.5.2 the biped walks on a rubber sheet spread on the ground whose coefficient of friction with solids is in the range of 1 - 4 [18]. Plot 8-6 indicates that that the biped will not slip if the coefficient of friction between the ground surface and the support foot is maintained greater than 0.3. Since μ will be maintained in the range of 1 to 4, the constraint (4.5.3) has been respected with a factor of safety of 3 - 13.

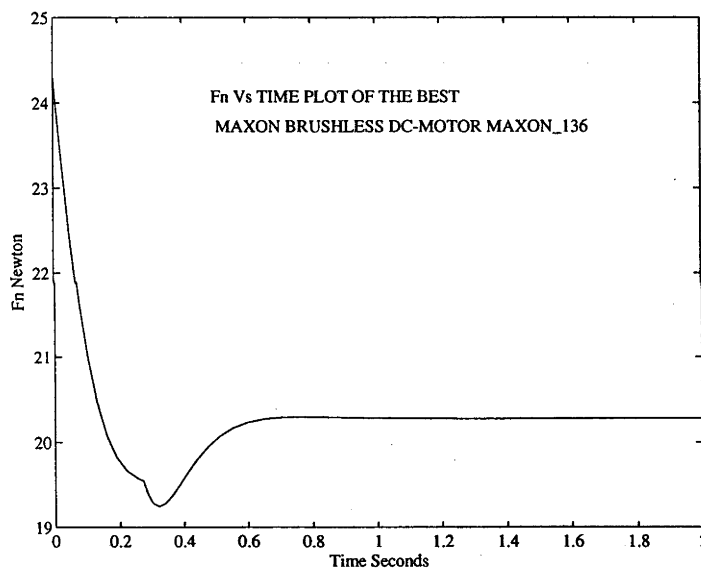


Figure 8-5: Normal Force Vs. Time.

Control Voltage, Back emf and Current Versus Time

Figures 8-7 and 8-8 show variation of control voltage u and current versus time respectively. Plot 8-7 shows that the constraint (4.3.3) on control voltage u has been respected with saturation. Maximum supply voltage of 29 volts was used for this motor as given in Table 6.2.3. Also, control u reaches a steady state value of zero in a settling time of about 2 seconds. Plot 8-8 indicates that the motor maximum current constraint (4.3.4) has been respected. Maximum supply current for this motor is < 14 amps as given in Table 7.2.4. The motor current reaches zero value with a settling time of 2 seconds without any

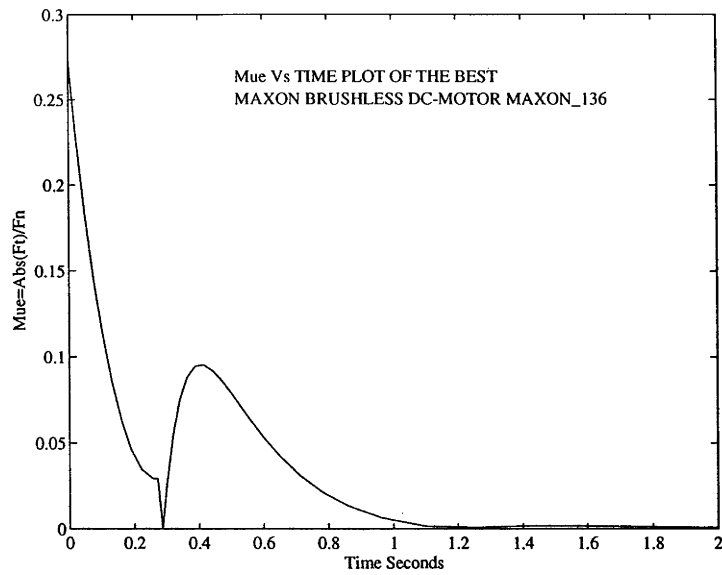


Figure 8-6: Coefficient of Friction Vs. Time.

significant rise. Figure 8-9 shows variation of back emf versus time.

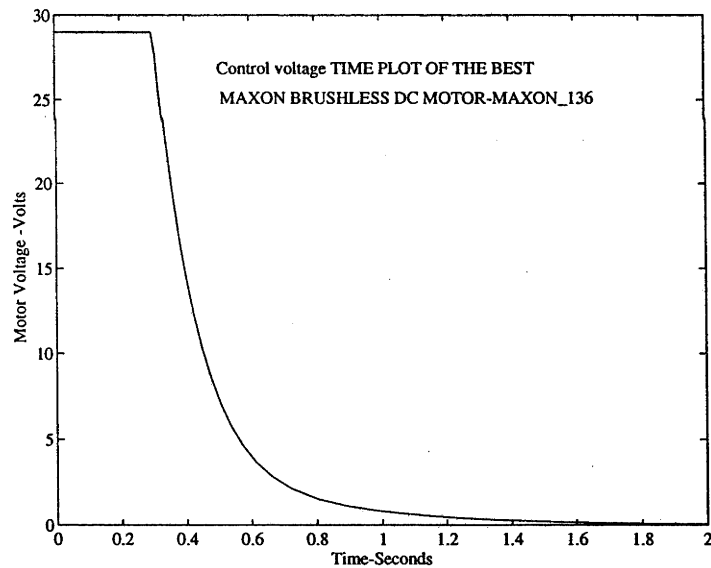


Figure 8-7: Control u Vs. Time.

Motor Temperature Versus Time

Figure 8-10 shows the variation of temperature over time which indicates that motor temperature rise is not significant compared to maximum winding temperature of $+125^{\circ}\text{C}$ (Table 7.2.3). Hence, it respects the constraint (4.3.7).

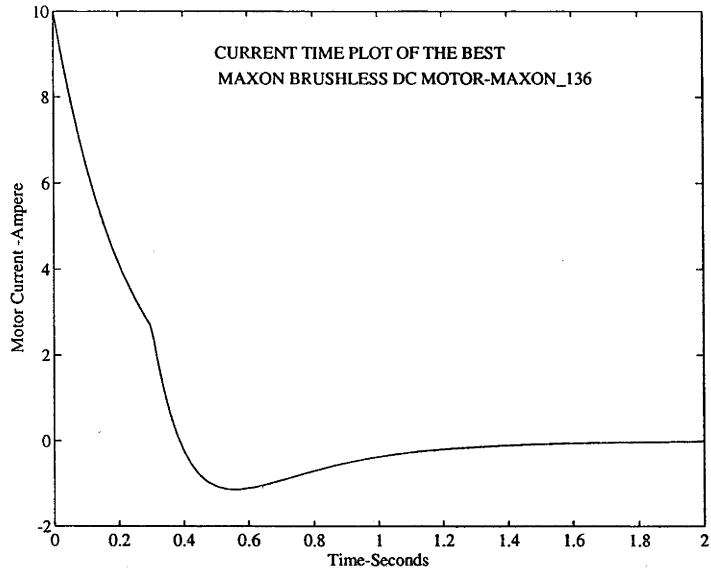


Figure 8-8: Current Vs. Time.

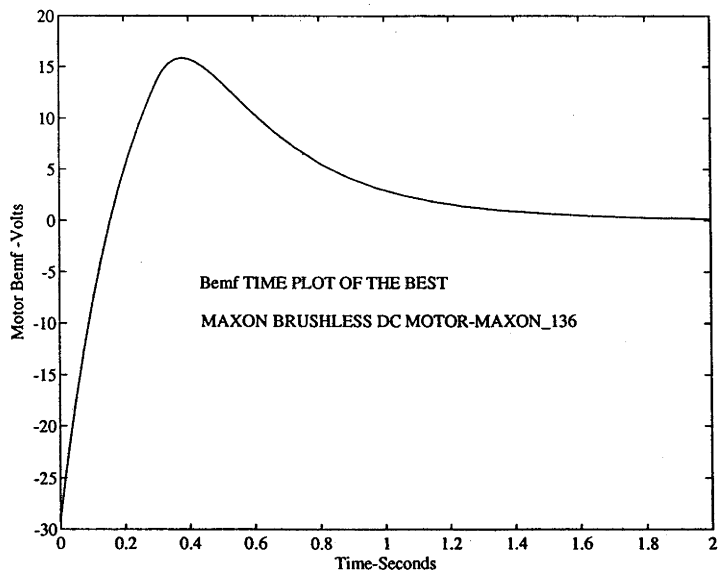


Figure 8-9: Back emf Vs. Time.

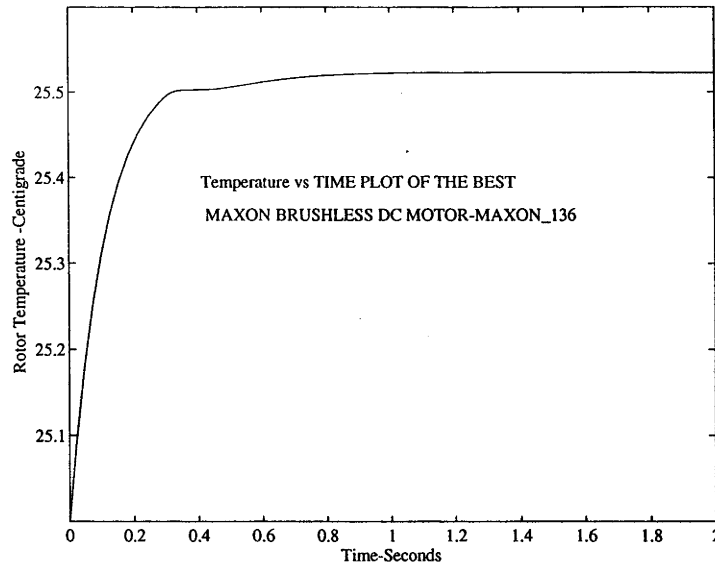


Figure 8-10: Temperature of the Motor Vs. Time.

8.3 Verification of the Motor Thermal Model

This section verifies that the behaviour of our thermal motor model is consistent with the manufacturer catalogue data. In particular, it shows that our model gives the same steady-state temperature rise for the permissible continuous power loss.

If i^2R be the permissible continuous power loss for the best motor selected, then Equation (3.9.1) can be written as given below.

$$\frac{dT_{motor}}{dt} + PT_{motor} = Q \quad (8.3.1)$$

Equation (8.3.1) is a first order linear differential equation. Where,

$$P = \frac{1}{C_{th}R_{th}} \quad (8.3.2)$$

$$Q = \frac{T_a}{C_{th}R_{th}} + \frac{i^2R}{C_{th}} \quad (8.3.3)$$

Solution to equation (8.3.1) is as given below.

$$T_{motor} = \frac{Q}{P} + \left[T_a - \frac{Q}{P} \right] e^{-Pt} \quad (8.3.4)$$

As the time $t \rightarrow \infty$, the permissible maximum winding temperature that will be reached during continuous operation at $25^\circ C$ ambient is given by

$$T_{motor \ max} = \frac{Q}{P} \quad (8.3.5)$$

For the best motor from Tables 7.2.2 & 7.2.3, we have the following values.

$$i^2R = 7.8, C_{th} \triangleq C_p \text{motor Mass} = 80.43, R_{th} = 12.8, T_a = 25. \quad (8.3.6)$$

Substituting (8.3.6) in (8.3.2) & (8.3.3) and then using equation (8.3.5) the maximum motor temperature comes to $125^\circ C$ which corresponds to the value given by the manufacturer (Table 7.2.3).

Since the leg assembly is attached to reduction unit housing which in turn is fixed to motor housing, legs act as good thermal dissipating fins. This conduction path will be more effective in case of brushless DC motors where the fixed stators are the main heat source coming in direct contact with the reduction gear housing. Also, black anodizing of leg assemblies, reduction gear & motor housings will increase thermal dissipation.

Chapter 9

Conclusion

Detailed design of a biped was achieved as a result of the work presented in this thesis. This design is ready for fabrication and assembly and subsequent implementation of control algorithms for dynamic walking. The design realized is first of its kind. A thorough effort was made to consider all theoretical and practical aspects and used good engineering design practice. An unique biped design was achieved because of our integrated approach to system modelling, design optimization and computer simulation.

Major design phases which we followed were :

Mathematical modelling.

Development of appropriate optimization criteria.

Mathematical establishment of all the major design constraints.

Formulation of a constrained optimization problem.

Solving the constrained optimization problem by numerical computation.

Verification of results.

The biped design was optimized with respect to a single control task. This control task was to raise the biped from a stationary dual-leg support phase to balance in a single-leg support condition. Keeping this control task in mind, the single-leg support phase was modelled and governing equations were derived in Chapter 3.

In Chapter 4, Section 4.2, optimization criteria to maximize the size of the obstacle that the biped can step over in raising itself from a stationary dual-leg support phase to balance in a single-leg support condition was developed. In the same chapter, all major design constraints (Section 4.3 - 4.9) were mathematically established. Finally, considering optimization criteria and all design constraints a constrained optimization problem was formulated. This is put in a standard mathematical framework in Section 4.10. This

proved to be a vital step in our biped design.

In Chapter 5, Section 5.4, the procedure for solving our constrained optimization problem was developed. Note that the solution makes use of an innovative analytical result derived in Section 5.3 of this thesis which predicts the maximum step size (angle) based on a linearized model. Also, an accurate non-linear simulation of the resulting biped under linear regulator theory is developed to verify accuracy of the final solution.

The algorithm named “OptAllscript” for solving our constrained optimization problem was implemented in MATLAB. The results obtained by solving this using numerical computation was presented in Chapter 6 and verified in Chapter 8. Note that constraints (4.3.7), (4.4.3), (4.5.1) and (4.5.3) which could not be enforced by the solution algorithm have also been verified in Chapter 8.

The biped that we have achieved is light and compact and satisfies all constraints. The results indicate that the single-leg support phase can be controlled by linear regulator theory. It has a superior leg length (0.23 m) to stride (0.246 m) ratio of 0.93 and weighs 2.1 kg. It can climb relatively large slope of 32.4° and it can cross relatively large obstacles of size 0.07 m tall and 0.14 m long. Also, the cost of building this biped is around 10,000 Aus\$.

In summary, this investigation has lead to the complete design of a biped that meets all of the original objectives, providing a simple low cost laboratory system suitable for control investigations.

Chapter 10

Recommendations

Building the first of this generation of bipeds and carrying out some experiments may lead to new theories and techniques in design optimization and control theory for such machines to be built in coming years. In particular, building the biped that we have achieved and experimenting with it will be useful for the following :

- Verification of theories that this design was based on.

- Verification of adequacy of sensors.

- Investigation and experimentation into general walking control.

Also, building and experimenting with the current design may give new insight into practical walking vehicles of this class to be built in future.

The work presented in this thesis can be extended for the development of practical walking vehicles in future. The main issues that will be of importance in extending these bipeds into more practical walking vehicles are as follows :

- Introduction of turning capabilities.

- Incorporating onboard power and control units.

- Introduction of terrain sensing capabilities.

Introducing knee and foot joints may give turning capabilities for these class of bipeds. However, it should be noted here that it complicates the entire system design.

Further improvements in brushless DC motors ($\frac{power}{mass}$, $\frac{torque}{mass}$) and reduction gears, availability of compact motor control units and compact direct drive motors will be useful to give onboard power capabilities to these class of bipeds. Also, work in areas of improved and efficient energy utilization/flow schemes such as regenerative braking or use of springs or use of flywheel etc. have to be done. These studies will be useful in realization of practical walking vehicle. Performance of these type of vehicles will improve in absence/reduced

gravity effects making them potential candidates for exploration of outer planets.

Finally, with the introduction of modern vision systems these walking vehicles will get capabilities for terrain sensing. However, it should be noted here that research in the area of vision systems is still ongoing and is a current topic in the field of robotics.

Bibliography

- [1] Kieffer, J., and Bale, R. : Walking Viability and Gait Synthesis for a Novel Class of Dynamically-Simple bipeds, *Informatica* 17(1993):145-155.
- [2] Waldron, K., J., Pery, A., McGhee, R., B.: Configuration Design of the Adaptive Suspension Vehicle, *Int. J. Robotics Research*, 3(2):37-47, 1984.
- [3] Raibert, M., H.: Introduction to Legged Locomotion, *Int. J. Robotics Research*, 3(2):2-3, 1984.
- [4] Furusho, J., and Sano. A.: Sensor-Based Control of a Nine-Link Biped, *Int. J. Robotics Research*, 9(2):83-98, 1990.
- [5] Yuan F. Zheng, Member, IEEE: *Acceleration Compensation for Biped Robots to Reject External Disturbances*, IEEE, 1989.
- [6] Raibert, M., H.: *Legged Robots that balance*, MIT press, 1986
- [7] Tad McGeer: *Powered Flight, Childs Play, Silly Wheels and Walking Machines*, IEEE, 1592-1597: 1989
- [8] Miura, H., and Shimoyama, I.: Dynamic Walk of a Biped, *Int. J. Robotics Research*, 3(2):60-74, 1984.
- [9] Hirose, S.: A Study of Design and Control of a Quadruped Walking Vehicle, *Int. J. Robotics Research*, 3(2):113-132, 1984.
- [10] Alexander, McN., R.: The Gaits of Bipedal and Quadrupedal Animals, *Int. J. Robotics Research*, 3(2):49-59, 1984.
- [11] McMahan, A., T.: Mechanics of Locomotion, *Int. J. Robotics Research*, 3(2):4-28, 1984.
- [12] Asada, H., Toumi, Y., K.: *Direct-Drive Robots Theory and Practice*, MIT press 1987.

- [13] Hollerbach, M., J., Hunter, W., I., Ballantyne, J.: *A Comparative Analysis of Actuator Technologies for Robotics*.
- [14] Ogata, K.: *Modern Control Engineering*, Second Edition, Prentice-Hall International, 1990.
- [15] Kreith, F., Black, Z., W. : *Basic Heat Transfer*, 1980, Harper & Row, Publishers, New York.
- [16] *elcom*, PITTMAN BRUSHLESS DC SERVOMOTORS, BULLETIN 4000, Revised March, 1989.
- [17] *Maxon Motor*, Drive Components with Selection Guide, 3-126, 1993/94 and Maxon Motor Control March 1994 edition.
- [18] Oberg, E., Jones, D., F., Horton, L., H.: *Machinery's Handbook*, 22nd edition, Industrial Press INC., NY 10157.
- [19] *Engineers HandBook Aluminium*, The Aluminium Development Council of Australia, second edition, 1986.
- [20] *Aluminium Standards and Data*, The Aluminium Development Council of Australia, 4th edition, 1986.
- [21] *MATLAB, High - Performance Numeric Computation and Visualization Software, User's Guide, For UNIX Workstations*, The MATH WORKS, Inc., August 1992.
- [22] Shigley, E., J., Mischke, R., C.: *Mechanical Engineering Design*, Fifth International Edition 1989, McGraw-Hill series.
- [23] *Design Data*, Compiled by Faculty of Mechanical Engineering, PSG College of Technology, Coimbotre, India, Reprinted: 1987.
- [24] Roark, J., R., Young, C., W.: *Formulas for Stress and Strain*, Fifth edition, McGraw-Hill publication, 1986, 14th printing.
- [25] Nakamura, T., Murata Manufacturing Co., Ltd.: *Vibration Gyroscope Employs Piezoelectric Vibrator*, JEE, September 1990.
- [26] Dipl.-Infrom. Weib, G., Prof. V. Puttkamer.: *Usage of a Vibrating Gyroscope for Orientation Estimation*, University of Kaiserslautern, Computer Science Department, D-67663 Kaiserslautern, Germany.

[27] *Spectron*, glass and electronics, inc., Electrolytic Tilt Sensors, 1-29.

Appendix A

Single-Leg Support Phase Equations

A.1 Introduction

This appendix derives equations (3.4.1) and (3.4.2) which are presented in Chapter 3, Section 3.4. Refer Figure 3-2 and Section ‘Nomenclature’ for the notations used in deriving these equations. Note that (1) the body (link-1) is mounted on the reduction unit shaft which in turn is connected to the motor. The reduction unit has a reduction ratio of N, (2) leg (link-0) is attached to the reduction unit housing, (3) recall that θ_m is the position of the rotor relative to stance leg.

A.2 Inverted Pendulum Model

As already mentioned in Chapter 3 we have followed Lagrange’s approach to derive single-leg support phase equations. Single-leg support phase equations are derived as given below.

Kinetic energy of the stance leg is

$$KE_0 = \frac{1}{2}m_\ell \dot{\theta}_0^2 \ell^2 + \frac{1}{2}J_\ell \dot{\theta}_0^2 \quad (\text{A.2.1})$$

Kinetic energy of the body is

$$KE_1 = \frac{1}{2}m_b \ell^2 \dot{\theta}_0^2 + \frac{1}{2}J_b (\dot{\theta}_0 + \dot{\theta}_1)^2 \quad (\text{A.2.2})$$

Kinetic energy of the rotor is

$$KE_m = \frac{1}{2}J_m (\dot{\theta}_0 + \dot{\theta}_m)^2 \quad (\text{A.2.3})$$

which can be rewritten as

$$KE_m = \frac{1}{2}J_m(\dot{\theta}_0 + N\dot{\theta}_1)^2 \quad (\text{A.2.4})$$

Total kinetic energy of the system can be obtained from the following steps.

$$KE = \frac{1}{2}m_\ell\dot{\theta}_0^2\ell^2 + \frac{1}{2}J_\ell\dot{\theta}_0^2 + \frac{1}{2}m_b\ell^2\dot{\theta}_0^2 + \frac{1}{2}J_b(\dot{\theta}_0 + \dot{\theta}_1)^2 + \frac{1}{2}J_m(\dot{\theta}_0 + N\dot{\theta}_1)^2 \quad (\text{A.2.5})$$

$$KE = \frac{1}{2}(m_\ell + m_b)\ell^2\dot{\theta}_0^2 + \frac{1}{2}J_\ell\dot{\theta}_0^2 + \frac{1}{2}J_b(\dot{\theta}_0 + \dot{\theta}_1)^2 + \frac{1}{2}J_m(\dot{\theta}_0 + N\dot{\theta}_1)^2 \quad (\text{A.2.6})$$

$$KE = \frac{1}{2}m\ell^2\dot{\theta}_0^2 + \frac{1}{2}J_\ell\dot{\theta}_0^2 + \frac{1}{2}J_b(\dot{\theta}_0 + \dot{\theta}_1)^2 + \frac{1}{2}J_m(\dot{\theta}_0 + N\dot{\theta}_1)^2 \quad (\text{A.2.7})$$

$$KE = \frac{1}{2}(m\ell^2 + J_\ell)\dot{\theta}_0^2 + \frac{1}{2}J_b(\dot{\theta}_0 + \dot{\theta}_1)^2 + \frac{1}{2}J_m(\dot{\theta}_0 + N\dot{\theta}_1)^2 \quad (\text{A.2.8})$$

$$KE = \frac{1}{2}J_0\dot{\theta}_0^2 + \frac{1}{2}J_b(\dot{\theta}_0 + \dot{\theta}_1)^2 + \frac{1}{2}J_m(\dot{\theta}_0 + N\dot{\theta}_1)^2 \quad (\text{A.2.9})$$

Potential energy of the system is as given below.

$$PE = mg\ell \cos \theta_0 \quad (\text{A.2.10})$$

Lagrangian L_g is given by

$$L_g = KE - PE \quad (\text{A.2.11})$$

Substituting (A.2.9) and (A.2.10) in (A.2.11), we have

$$L_g = \frac{1}{2}J_0\dot{\theta}_0^2 + \frac{1}{2}J_b(\dot{\theta}_0 + \dot{\theta}_1)^2 + \frac{1}{2}J_m(\dot{\theta}_0 + N\dot{\theta}_1)^2 - mg\ell \cos \theta_0 \quad (\text{A.2.12})$$

Torque at the contact of the foot and the ground i.e., at 'O' is given by

$$\tau_0 = \frac{d}{dt} \left[\frac{\delta L_g}{\delta \dot{\theta}_0} \right] - \frac{\delta L_g}{\delta \theta_0} \quad (\text{A.2.13})$$

Where

$$\frac{\delta L_g}{\delta \theta_0} = mg\ell \sin \theta_0 \quad (\text{A.2.14})$$

$$\frac{\delta L_g}{\delta \dot{\theta}_0} = J_0\dot{\theta}_0 + J_b(\dot{\theta}_0 + \dot{\theta}_1) + J_m(\dot{\theta}_0 + N\dot{\theta}_1) \quad (\text{A.2.15})$$

$$\frac{d}{dt} \left[\frac{\delta L_g}{\delta \dot{\theta}_0} \right] = J_0\ddot{\theta}_0 + J_b(\ddot{\theta}_0 + \ddot{\theta}_1) + J_m(\ddot{\theta}_0 + N\ddot{\theta}_1) \quad (\text{A.2.16})$$

Substituting (A.2.14) and (A.2.16) in (A.2.13), we have

$$\tau_0 = J_0\ddot{\theta}_0 + J_b(\ddot{\theta}_0 + \ddot{\theta}_1) + J_m(\ddot{\theta}_0 + N\ddot{\theta}_1) - mg\ell \sin \theta_0 \quad (\text{A.2.17})$$

which can be rewritten as given below.

$$\tau_0 = (J_0 + J_b + J_m)\ddot{\theta}_0 + (J_b + NJ_m)\ddot{\theta}_1 - mg\ell \sin \theta_0 \quad (\text{A.2.18})$$

Torque τ_1 is given by

$$\tau_1 = \frac{d}{dt} \left[\frac{\delta L_g}{\delta \dot{\theta}_1} \right] - \frac{\delta L_g}{\delta \theta_1} \quad (\text{A.2.19})$$

Where

$$\frac{\delta L_g}{\delta \theta_1} = 0 \quad (\text{A.2.20})$$

$$\frac{\delta L_g}{\delta \dot{\theta}_1} = J_b(\dot{\theta}_0 + \dot{\theta}_1) + NJ_m(\dot{\theta}_0 + N\dot{\theta}_1) \quad (\text{A.2.21})$$

$$\frac{d}{dt} \left[\frac{\delta L_g}{\delta \dot{\theta}_1} \right] = J_b(\ddot{\theta}_0 + \ddot{\theta}_1) + NJ_m(\ddot{\theta}_0 + N\ddot{\theta}_1) \quad (\text{A.2.22})$$

Substituting (A.2.20) and (A.2.22) in (A.2.19), we have

$$\tau_1 = J_b(\ddot{\theta}_0 + \ddot{\theta}_1) + NJ_m(\ddot{\theta}_0 + N\ddot{\theta}_1) \quad (\text{A.2.23})$$

which can be rewritten as given below.

$$\tau_1 = (J_b + NJ_m)\ddot{\theta}_0 + (J_b + N^2J_m)\ddot{\theta}_1 \quad (\text{A.2.24})$$

Appendix B

Optimum Step Angle $\theta_{0optimum}$

B.1 Introduction

This appendix presents complete derivation for the optimum stance angle which was discussed in Chapter 4, Section 4.2. Refer Figures 4-1 & 4-5 and Section 'Nomenclature' for the notations used in this derivation.

B.2 Unique Step Length

This section presents detailed derivation for unique step length L. The area A_{ob} enclosed between the legs and the floor below the body is as given below.

$$\frac{1}{2}A_{ob} = \frac{1}{2}\frac{L}{2}h - \frac{1}{2}L_b b \quad (\text{B.2.1})$$

Where, L_b is given by (Figure 4-5)

$$L_b = \frac{Lb}{2h} \quad (\text{B.2.2})$$

Substituting (B.2.2) in (B.2.1), we have

$$A_{ob} = \frac{Lh}{2} - b\frac{Lb}{2h} \quad (\text{B.2.3})$$

$$A_{ob} = \frac{L}{2} \left(h - \frac{b^2}{h} \right) \quad (\text{B.2.4})$$

To get dimensionless area, divide A_{ob} by leg length ℓ^2 which is given by

$$A_{ob}^* = \frac{L}{2\ell^2} \left(h - \frac{b^2}{h} \right) \quad (\text{B.2.5})$$

The unique step length L (recall discussions presented in Section 4.2) for each body radius b which maximizes the dimensionless area A_{ob}^* is derived by equating partial derivative of the equation (B.2.5) with respect to L to zero and simplifying as shown below.

$$\frac{\delta A_{ob}^*}{\delta L} = \frac{1}{2\ell^2} \left(h - \frac{b^2}{h} \right) + \frac{L}{2\ell^2} \left(1 + \frac{b^2}{h^2} \right) \frac{\delta h}{\delta L} \quad (\text{B.2.6})$$

Where

$$\frac{\delta h}{\delta L} = \frac{\delta}{\delta L} \left(\ell^2 - \frac{L^2}{4} \right)^{\frac{1}{2}} \quad (\text{B.2.7})$$

$$\frac{\delta h}{\delta L} = \frac{1}{2} \left(\ell^2 - \frac{L^2}{4} \right)^{\frac{1}{2}-1} \left(\frac{-2L}{4} \right) \quad (\text{B.2.8})$$

$$\frac{\delta h}{\delta L} = -\frac{L}{4} \frac{1}{\sqrt{\ell^2 - \left(\frac{L}{2} \right)^2}} \quad (\text{B.2.9})$$

$$\frac{\delta h}{\delta L} = -\frac{L}{4h} \quad (\text{B.2.10})$$

Substituting (B.2.10) in (B.2.6) and equating it to zero results in

$$\frac{1}{2\ell^2} \left(h - \frac{b^2}{h} \right) - \frac{L^2}{8\ell^2 h} \left(1 + \frac{b^2}{h^2} \right) = 0 \quad (\text{B.2.11})$$

$$h - \frac{b^2}{h} - \frac{L^2}{4h} \left(1 + \frac{b^2}{h^2} \right) = 0 \quad (\text{B.2.12})$$

$$h - \frac{b^2}{h} - \frac{L^2}{4h} - \frac{L^2 b^2}{4h^3} = 0 \quad (\text{B.2.13})$$

$$h^4 - b^2 h^2 - \left(\frac{L}{2} \right)^2 h^2 - \left(\frac{L}{2} \right)^2 b^2 = 0 \quad (\text{B.2.14})$$

$$h^4 - \left[b^2 + \left(\frac{L}{2} \right)^2 \right] h^2 - \left(\frac{L}{2} \right)^2 b^2 = 0 \quad (\text{B.2.15})$$

Substituting $h^2 = \ell^2 - \left(\frac{L}{2} \right)^2$ in (B.2.15), we have

$$\ell^4 - 2\ell^2 \left(\frac{L}{2} \right)^2 + \left(\frac{L}{2} \right)^4 - \left[b^2 + \left(\frac{L}{2} \right)^2 \right] \left[\ell^2 - \left(\frac{L}{2} \right)^2 \right] - \left(\frac{L}{2} \right)^2 b^2 = 0 \quad (\text{B.2.16})$$

$$\ell^4 - 2\ell^2 \left(\frac{L}{2} \right)^2 + \left(\frac{L}{2} \right)^4 - \left[b^2 \ell^2 - b^2 \left(\frac{L}{2} \right)^2 + \ell^2 \left(\frac{L}{2} \right)^2 - \left(\frac{L}{2} \right)^4 \right] - \left(\frac{L}{2} \right)^2 b^2 = 0 \quad (\text{B.2.17})$$

$$\ell^4 - 2\ell^2 \left(\frac{L}{2}\right)^2 + \left(\frac{L}{2}\right)^4 - b^2\ell^2 + b^2 \left(\frac{L}{2}\right)^2 - \ell^2 \left(\frac{L}{2}\right)^2 + \left(\frac{L}{2}\right)^4 - \left(\frac{L}{2}\right)^2 b^2 = 0 \quad (\text{B.2.18})$$

$$2 \left(\frac{L}{2}\right)^4 - 3\ell^2 \left(\frac{L}{2}\right)^2 + (\ell^4 - b^2\ell^2) = 0 \quad (\text{B.2.19})$$

$$\left(\frac{L}{2}\right)^2 = \frac{3\ell^2 \pm \sqrt{9\ell^4 - 8(\ell^4 - b^2\ell^2)}}{4} \quad (\text{B.2.20})$$

$$\left(\frac{L}{2}\right)^2 = \frac{3\ell^2 \pm \sqrt{9\ell^4 - 8\ell^2(\ell^2 - b^2)}}{4} \quad (\text{B.2.21})$$

$$\left(\frac{L}{2}\right)^2 = \frac{3\ell^2 \pm \sqrt{\ell^4 \left(9 - 8\frac{(\ell^2 - b^2)}{\ell^2}\right)}}{4} \quad (\text{B.2.22})$$

$$\left(\frac{L}{2}\right)^2 = \frac{3\ell^2 \pm \ell^2 \sqrt{1 + 8\frac{b^2}{\ell^2}}}{4} \quad (\text{B.2.23})$$

$$\left(\frac{L}{2}\right)^2 = \left[3 \pm \sqrt{1 + 8\frac{b^2}{\ell^2}}\right] \left(\frac{\ell}{2}\right)^2 \quad (\text{B.2.24})$$

$$\left(\frac{L}{\ell}\right)^2 = 3 \pm \sqrt{1 + 8\left(\frac{b}{\ell}\right)^2} \quad (\text{B.2.25})$$

As discussed in Chapter 4, Section 4.2, the smaller root is the one which maximizes dimensionless area A_{ob}^* . Hence, the unique step length L is as given below.

$$L = \ell \sqrt{3 - \sqrt{1 + 8\left(\frac{b}{\ell}\right)^2}} \quad (\text{B.2.26})$$

B.2.1 Optimum Stance Angle Corresponding to Unique Step Length

Once the unique step length L (B.2.26) has been established, we solve $\sin \theta_0 = \frac{L}{2\ell}$ to determine the value of $\theta_{0optimum}$ associated with this value of L as given below.

$$\theta_{0optimum} = \sin^{-1} \left(\frac{\left[\sqrt{3 - \sqrt{1 + 8\left(\frac{b}{\ell}\right)^2}} \right]}{2} \right) \quad (\text{B.2.27})$$

Appendix C

MATLAB ALGORITHM

C.1 Introduction

The design optimization and simulations performed throughout this thesis was carried out using MATLAB package. In this appendix, all the script files used will be presented. Note that we have tried to follow the notations given in Section ‘Nomenclature’ as far as possible.

C.2 Main Script File ‘OptAllscript’

Main script file ‘OptAllscript’ is the heart of the whole design optimization and simulation. Chart C-1 gives the flow chart of our main script file ‘OptAllscript’.

This script determines arrays MBopt(iN, iA), Bopt(iN, iA) and BOLOpt(iN, iA) for set of all actuators, assuming lolmin has been set. Then, it sorts BOLOpt to produce index of arrays iAbest(i), iNbest(i), $m_b_best(i)$ and $b_best(i)$ such that the n^{th} -best design is given by :

$iA = iAbest(n)$, n^{th} best motor.

$iN = iNbest(n)$, n^{th} best reduction ratio.

$m_b = m_b_best(n)$, n^{th} best mass of the body.

$b = b_best(n)$, n^{th} , best body radius.

$bol = bol_best(n)$, n^{th} best ratio of body radius b and leg length ℓ .

This script file is as given below.

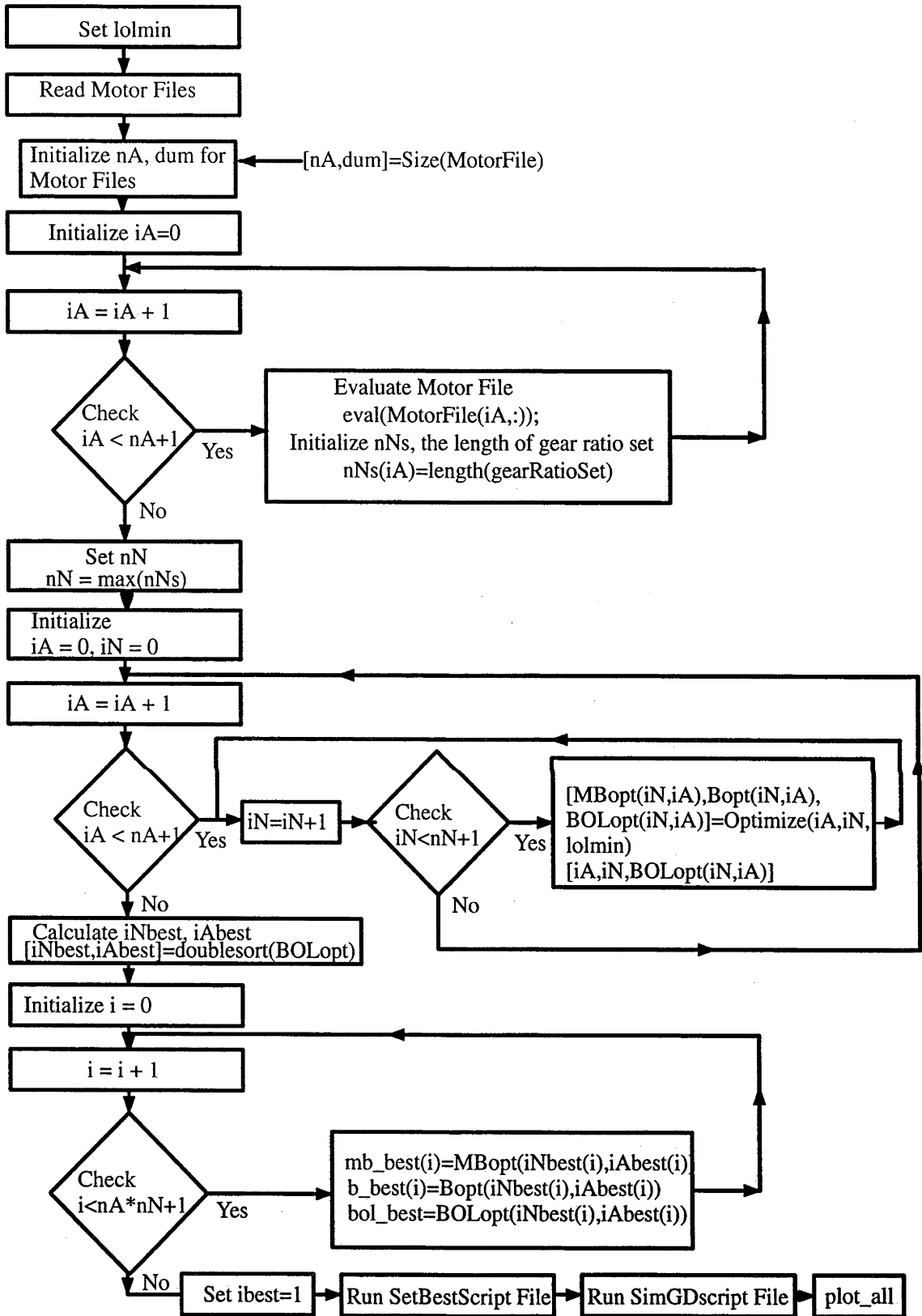


Figure C-1: Flow Chart of OptAllscript.

```

lolmin
MotorFiles;
[nA, dum] = size(MotorFile) ;
for iA = 1 : nA,
    eval(MotorFile(iA,:)) ;
    nNs(iA) = length(gear Ratio Set) ;
end
nN = max(nNs) ;

for iA = 1 : nA,
    for iN = 1 : nN,
        [MBopt(iN, iA), Bopt(iN, iA), BOLOpt(iN, iA)] = Optimize(iA, iN, lolmin) ;
        [iA, iN, BOLOpt(iN, iA)]
    end
end

[iNbest, iAbest] = doublesort(BOLOpt) ;

for i = 1 : (nA*nN),
    mb_best(i) = MBopt(iNbest(i), iAbest(i)) ;
    bbest(i) = Bopt(iNbest(i), iAbest(i)) ;
    bolbest(i) = BOLOpt(iNbest(i), iAbest(i)) ;
end
ibest = 1 ;
SetBestScript ;
SimGDscript ;
plot_all ;

```

C.2.1 MotorFiles

This is a version of MotorFiles.m that lists only the data for the MAXON DC motors and gearboxes. To use the data in the files listed below this file must be named 'MotorFiles.m'.

```
MotorFile = [ 'MAXON_949'; 'MAXON_948'; 'MAXON_990'; ] ;
```

Typical Motor Data File

Data for Maxon_990 with planetary gear set. Maxon_page-37. This is the individual motor data file to be named as MAXON_990.m.

```

R = 10.5; % Ohms
Kt = 0.0219 ; % Nm/Amp
Kb = 0.0219 ; % Volts/(rad/sec)
Jm = 5.5E - 7 ; % Kg*m2
Vmax = 19.37 ; % Volts
imax = 3.69 ; % Ampere
motor Mass = .092+.02 ; % Kg includes encoder mass
motor Diameter = .022 ; % m
motor Length = .048+.014 ; % m includes encoder length
Stall Torque = Kt*Vmax/R; % Nm
dg = 5/1000 ; % m gear shaft diameter
Cp = 383 ; % J/kg deg C Specific heat of copper.
Cth = Cp*motor Mass ; % Thermal capacitance of the motor J/deg C.
Rth = 14.1+3.6 ; % Thermal resistance of the motor deg C/J/sec.
Trotor = 125 ; % Maximum rotor temperature Deg C

gear Ratio Set = [ 1 4.33 18.75 33.2 81.2 143.8 199.3] ;
gear Eff. Set = [ 1 .85 .612 .612 .373 .373 .373] ;
gear Mass Set = 1/1000* [ 0 81 107 107 130 130 130] ; % Kg
gear Diameter Set = 1/1000*[ 0 26 26 26 26 26 26] ; % m
gear Length Set = 1/1000*[ 0 30.6 39.4 39.4 48.1 48.1 48.1] ; % m

```

C.2.2 Optimize

This is a function which determines optimum values for body mass and body radius based on minimizing $\frac{b}{l}$ and is as given below.

```

function [mb_opt, b_opt, bol_opt]=Optimize(iA, iN, lolmin)
global GLOBAL_DATA ;
b = 1 ;
mb = 1 ;

```

```

SetBipedScript ;
put_GLOBAL_DATA ;
mb_opt = fmin('find_bol_opt', .1*ma, 10*ma, [0, ma/100]) ;
bol_opt = find_bol_opt(mb_opt) ;
b_opt = bol_opt*ℓ ;

```

C.2.3 SetBipedScript

This script sets all biped design variables in the local workspace assuming that iA , iN , $lolmin$, b , m_b have been set. It also puts them in the global variable `GLOBAL_DATA`. This script is as given below.

```

global GLOBAL_DATA ;
gama = 1.57 ;
g = 9.81 ;
Tsim = 2 ;
α = 10*π/180 ;
NFS = 2 ;
SYleg = 241 *106 ;
ρ = 2.7*103 ;
E = 0.71*1011 ;
delol = .01; %( $\frac{\Delta \ell}{\ell}$ ).
MotorFiles ;
eval(MotorFile(iA,:)) ;
SetGearset ;
NoLoadSpeed =  $\frac{V_{max}}{K_b N}$  ;
ℓmin = Set_ℓmin(motor Diameter, motor Length, gear Diameter, gear Length) ;
ℓ = ℓmin*lolmin ;
d = ℓ ;
ma = 2*(motor Mass + gear Mass) ;
[ws] = Stability(α,ℓ) ;

[Jb, hr, wr, td, br] = BodyDesign(mb, b, ℓ, ma, N, NoLoadSpeed, Stall Torque, g,
dg, ws) ;

[mℓ, Jℓ, dℓ, tℓ, wℓ, J0] = LegDesign(ma, mb, ℓ, motor Diameter, gear Diameter,
motor Mass, gear Mass, wr, ws) ;

```

```
put_GLOBAL_DATA;
```

C.2.4 SetGearset

This file sets the gear-related parameters.

```
N = gearRatioSet(iN) ;
η (eff) = gear Eff. Set(iN) ;
gear Mass = gear Mass Set(iN) ;
gear Diameter = gear Diameter Set(iN) ;
gear Length = gear Length Set(iN) ;
```

C.2.5 Set_lmin

This function sets the minimum biped length based on simple design criteria considering motor and gearbox dimensions as shown below :

```
function lmin = Set_lmin(mD, mL, gD, gL)
D = max(mD, gD) ;
W = 2*(mL + gL) ;
lmin = max( 2*D, W ) ;
```

Where

mD : Diameter of the motor.

mL : Length of the motor.

gD : Diameter of the reduction unit.

gL : Length of the reduction unit.

C.2.6 Stability

This function calculates the width of the biped based on the stability criteria that the biped will not fall if it comes across an obstacle which causes the biped to tilt $\leq 10^\circ$ about roll axis.

```
function [w_s] = Stability(α, ℓ)
global GLOBAL_DATA ;
w_s =  $\frac{2\ell}{\tan(\frac{\pi}{2}-\alpha)}$  ;
```

C.2.7 BodyDesign

Based on realistic body design this function computes

Body radius b_r in m.

Width of the body w_r in m.

Thickness h_r of the rim in m.

Thickness t_d of the disc in m.

Moment of inertia of the body about hip axis $J_b \frac{kg}{m^2}$

function [J_b, h_r, w_r, t_d, b_r] = BodyDesign($m_b, b, \ell, m_a, N, NoLoadSpeed, Stall Torque,$
 g, d_g, w_s) ;

global GLOBAL_DATA ;

$N_{FS} = 2$;

$\rho = 2.7 * 10^3$;

$E = 0.675 * 10^{11}$;

$\nu = .33$;

$t_{Fab} = 2.4/1000$;

$SY_{body} = 10^6 * [97 \ 262 \ 310 \ 317 \ 337 \ 159]$;

Body radius based on the critical speed of the rim.

$iBN = size(SY_{body})$;

$ibN = iBN(1,2)$;

for $ibody1 = 1:ibN$;

$$b_1 = \frac{1}{NoLoadSpeed} \sqrt{\frac{SY_{body}(ibody1)}{N_{FS}\rho}}$$

if $b_1 \geq b$, break, end

end

$ibody1$;

Body radius based on the critical speed of the disc (approximate method)

for $ibody2 = 1:ibN$;

$$b_2 = \frac{1}{NoLoadSpeed} \sqrt{\frac{3SY_{body}(ibody2)}{N_{FS}\rho}}$$

if $b_2 \geq b$, break, end

end

$ibody2$;

% Setting radius of the rim and material of the body.

$bv = [b1 \ b2 \ b]$;


```

bmax = min(bv) ;
SYbody = SYbody(max(ibody1, ibody2)) ;
% Disc thickness based on shear stress due to torque
td1 = N*Stall Torque*NFS*(bmax-1.5*dg)/(2*bmax*π*.577*SYbody(ibN)*(1.5*dg)2);
% Disc thickness based on direct shear failure.
td2 = (ma + mb) * g * NFS/(2 * bmax * π * 0.577 * SYbody(ibN));
% Disc thickness based on plate bending theory.
L9 = 1.5 * dg/bmax * (.5 * (1 + ν) * ln(bmax/(1.5 * dg)) + (1 - ν)/4 * (1 - 1.52 * dg2/bmax2)) ;
C7 = 0.5 * (1 - ν2) * (bmax/(1.5 * dg) - 1.5 * dg/bmax) ;
td3 = sqrt(3 * (ma + mb) * NFS * g * bmax2 * L9 * (1 - ν2)/(π * 1.52 * dg2 * SYbody(ibN) * C7))

```

;

Finalized disc thickness is

```
tdv = [td1, td2, td3, tFab] ;
```

```
td = max(tdv) ;
```

% Mass property calculations & finalizing body dimensions

```
wr1 = ws ;
```

```
br = bmax ;
```

```
mhub = π/4 * ((3 * dg)2 - dg2) * 7 * dg * ρ ;
```

```
mdisc = π/4 * ((2 * br)2 - (3 * dg)2) * td * ρ ;
```

```
if mdisc + mhub < mb
```

```
    wr = wr1 ;
```

```
    hr = br - sqrt(br2 - (mb - mdisc - mhub)/π/ρ/(wr - td)) ;
```

```
    if hr > tFab & hr < (br - 1.5 * dg)
```

```
        wr = wr ;
```

```
        mrim = mb - mdisc - mhub ;
```

```
        mdisc = mdisc ;
```

```
        mhub = mhub ;
```

```
        Jdisc = mdisc/8 * ((2 * br)2 + (3 * dg)2) ;
```

```
        Jrim = mrim/8 * ((2 * br)2 + (2 * br - 2 * hr)2) ;
```

```
        Jhub = mhub/8 * ((3 * dg)2 + dg2) ;
```

```
        Jb = Jdisc + Jrim + Jhub ;
```

```
    else
```

```
        hr = tFab ;
```

```

     $w_r = t_d + (m_b - m_{disc} - m_{hub}) / (\pi * \rho * (2 * b_r * h_r - h_r^2)) ;$ 
     $m_{rim} = m_b - m_{disc} - m_{hub} ;$ 
     $m_{disc} = m_{disc} ;$ 
     $m_{hub} = m_{hub} ;$ 
     $J_{disc} = m_{disc} / 8 * ((2 * b_r)^2 + (3 * d_g)^2) ;$ 
     $J_{rim} = m_{rim} / 8 * ((2 * b_r)^2 + (2 * b_r - 2 * h_r)^2) ;$ 
     $J_{hub} = m_{hub} / 8 * ((3 * d_g)^2 + d_g^2) ;$ 
     $J_b = J_{disc} + J_{rim} + J_{hub} ;$ 
end

else

     $m_{disc} = m_b - m_{hub} ;$ 
     $b_r = \text{sqrt}(m_{disc} / (\pi * t_d * \rho) + 9 / 4 * d_g^2) ;$ 
     $m_{rim} = 0 ;$ 
     $h_r = 0 ;$ 
     $w_r = 0 ;$ 
     $J_{disc} = m_{disc} / 8 * ((2 * b_r)^2 + (3 * d_g)^2) ;$ 
     $J_{rim} = m_{rim} / 8 * ((2 * b_r)^2 + (2 * b_r - 2 * h_r)^2) ;$ 
     $J_{hub} = m_{hub} / 8 * ((3 * d_g)^2 + d_g^2) ;$ 
     $J_b = J_{disc} + J_{rim} + J_{hub} ;$ 

end

```

C.2.8 LegDesign

This function computes d_ℓ , t_ℓ , m_ℓ , J_ℓ and J_0 based on the realistic leg design criteria

```

[m $_\ell$ , J $_\ell$ , d $_\ell$ , t $_\ell$ , w $_\ell$ , J $_0$ ] = LegDesign(m $_a$ , m $_b$ ,  $\ell$ , motor Diameter, gear Diameter,
motor Mass, gear Mass, w $_r$ , w $_s$ ) ;

```

```

global GLOBAL_DATA ;

```

```

Data required for the leg design.

```

```

g = 9.81 ;

```

```

 $\alpha = 10 * \pi / 180 ;$ 

```

```

N $_{FS} = 2 ;$ 

```

```

SY $_{leg} = 241 * 10^6 ;$ 

```

```

 $\rho = 2.7 * 10^3 ;$ 

```

```
 $E = 0.71 * 10^{11} ;$ 
```

```
delol = .01 ;
```

```
Get Standard available aluminium alloy tube data.
```

```
Alalloytubes;
```

```
[nd, dumd] = size(Alalloytube) ;
```

```
for id= 1 : nd,
```

```
    eval(Alalloytube(id,:)) ;
```

```
    nds(id) = length(tubeDiaSet) ;
```

```
end
```

```
il = max(nds) ;
```

Calculates deflection per unit length and bending stress for first tube from the tube set.

```
 $Do = (tubeDiaSet(1,1)/1000)^4 ;$ 
```

```
 $Di = (tubeDiaSet(1,1)/1000 - 2 * tubeThicknessSet(1,1)/1000)^4 ;$ 
```

```
 $Delol = 64 * (m_a + m_b) * g * \ell^2 / (3 * E * \pi * (Do - Di)) ;$ 
```

```
C = tubeDiaSet(1,1)/1000 ;
```

```
 $St = 32 * (m_a + m_b) * g * \ell * N_{FS} * C / (\pi * (Do - Di)) ;$ 
```

```
% Picks best tube based on deflection & yield strength criteria.
```

```
if  $St \leq SY_{leg}$  &  $Delol \leq delol$ 
```

```
    cond = 1 ;
```

```
    ild = 1 ;
```

```
else
```

```
    for ild = 2 : il
```

```
         $Do = (tubeDiaSet(ild)/1000)^4 ;$ 
```

```
         $Di = (tubeDiaSet(ild)/1000 - 2 * tubeThicknessSet(ild)/1000)^4 ;$ 
```

```
         $Delol = 64 * (m_a + m_b) * g * \ell^2 / (3 * E * \pi * (Do - Di)) ;$ 
```

```
        C = tubeDiaSet(ild)/1000 ;
```

```
         $St = 32 * (m_a + m_b) * g * \ell * N_{FS} * C / (\pi * (Do - Di)) ;$ 
```

```
        if  $St < SY_{leg}$  &  $Delol < delol$ , break, end
```

```
    end
```

```
end
```

```
ild ;
```

Sets finalized design variables for the leg

$$d_l = \text{tubeDiaSet(ild)}/1000 ;$$

$$t_l = \text{tubeThicknessSet(ild)}/1000 ;$$

Calculation of width of the feet.

if $w_r > 0$ & $w_r == w_s$

$$w_l = w_r + d_l + 3/1000 ;$$

elseif $w_s > w_r + d_l + 3/1000$

$$w_l = w_s ;$$

else

$$fac = w_r + d_l + 3/1000 - w_s ;$$

$$w_l = w_s + fac ;$$

end

if $w_r == 0$

$$w_l = w_s ;$$

end

Calculates the Mass of the leg.

$$m_{\ell 1} = \pi/4 * (d_\ell^2 - (d_\ell - 2 * t_\ell)^2) * 2 * \ell * \rho ;$$

$$m_{\ell 2} = \pi/4 * (d_\ell^2 - (d_\ell - 2 * t_\ell)^2) * 2 * (w_\ell - d_\ell) * \rho ;$$

$$m_\ell = m_a + 2 * m_{\ell 1} + 2 * m_{\ell 2} ;$$

Calculation of Inertia of the leg about hip axis.

$$J_1 = m_{\ell 1}/48 * (3 * d_\ell^2 + 3 * (d_\ell - 2 * t_\ell)^2 + 4 * (2 * \ell)^2) ;$$

$$J_2 = m_{\ell 2}/8 * (d_\ell^2 + (d_\ell - 2 * t_\ell)^2) + m_{\ell 2} * (\ell - d_\ell/2)^2 ;$$

$$J_3 = \text{motor Mass} * (\text{motor Diameter})^2/8 ;$$

$$J_4 = \text{gear Mass} * (\text{gear Diameter})^2/8 ;$$

$$J_\ell = 2 * (J_1 + J_2 + J_3 + J_4) ;$$

Set leg dia. & leg thickness as global variable.

SetTubeset ;

Effective mass moment of inertia of the support leg about point of ground contact.

$$J_0 = (m_\ell + m_b) * \ell^2 + J_\ell ;$$

C.2.9 Alalloytubes

This is a version of Alalloytubes.m that lists only the data for the standard aluminium alloy tubes used for biped leg design. To use the data in the files listed below this file

must be named as Alalloytubes.m.

```
Alalloytube = ['Al6106-T6'];
```

C.2.10 Al6106-T6

Standard data on 6106 aluminium alloy tubes i.e., available standard diameter and thicknesses.

```
tubeDiaSet = [6.35 9.5 10 10 10 12 12 13 14 15 16 16 18 19 20 20 20 20 22.2];
```

```
tubeThicknessSet = [.91 .91 1 1.2 1.6 1 1.6 2 1.5 1.4 1.2 1.6 1.5 1.2 1.2 1.6 1.8 2 1.6];
```

C.2.11 SetTubeset

This file sets standard aluminium alloy tube related parameters.

```
 $d_l = \text{tubeDiaSet}(\text{ild})/1000 ;$ 
```

```
 $t_l = \text{tubeThicknessSet}(\text{ild})/1000 ;$ 
```

C.2.12 put_GLOBAL_DATA

This file stores the current design variables stored in a global array GLOBAL_DATA local.

Also see get_GLOBAL_DATA.

```
GLOBAL_DATA(1) =  $J_0$  ;
```

```
GLOBAL_DATA(2) =  $J_b$  ;
```

```
GLOBAL_DATA(3) =  $J_m$  ;
```

```
GLOBAL_DATA(4) = N ;
```

```
GLOBAL_DATA(5) =  $m_b$  ;
```

```
GLOBAL_DATA(6) =  $\ell$  ;
```

```
GLOBAL_DATA(7) =  $m_\ell$  ;
```

```
GLOBAL_DATA(8) = d ;
```

```
GLOBAL_DATA(9) = g ;
```

```
GLOBAL_DATA(10) =  $\gamma$  ;
```

```
GLOBAL_DATA(11) =  $\eta$  ;
```

```
GLOBAL_DATA(12) =  $K_t$  ;
```

```
GLOBAL_DATA(13) =  $K_b$  ;
```

```
GLOBAL_DATA(14) = R ;
```

```
GLOBAL_DATA(15) =  $V_{max}$  ;
```

```
GLOBAL_DATA(16) = NoLoadSpeed ;
```

```

GLOBAL_DATA(17) =  $J_\ell$  ;
GLOBAL_DATA(18) =  $m_a$  ;
GLOBAL_DATA(19) =  $T_{sim}$  ;
GLOBAL_DATA(20) =  $\alpha$  ;
GLOBAL_DATA(21) =  $N_{FS}$  ;
GLOBAL_DATA(22) =  $SY_{leg}$  ;
GLOBAL_DATA(23) =  $\rho$  ;
GLOBAL_DATA(24) =  $w_s$  ;
GLOBAL_DATA(25) = E;
GLOBAL_DATA(26) = delol;
GLOBAL_DATA(27) =  $d_\ell$  ;
GLOBAL_DATA(28) =  $t_\ell$  ;
GLOBAL_DATA(29) =  $w_\ell$  ;
GLOBAL_DATA(30) = motor Mass ;
GLOBAL_DATA(31) = gear Mass ;
GLOBAL_DATA(32) = motor Diameter ;
GLOBAL_DATA(33) = gear Diameter ;
GLOBAL_DATA(34) = Stall Torque ;
GLOBAL_DATA(35) =  $d_g$  ;
GLOBAL_DATA(36) =  $C_p$  ;
GLOBAL_DATA(37) =  $C_{th}$  ;
GLOBAL_DATA(38) =  $R_{th}$  ;
GLOBAL_DATA(39) = alpha_c ;
GLOBAL_DATA(40) =  $T_a$  ;
GLOBAL_DATA(41) =  $i_{max}$  ;

```

C.2.13 find_bol_opt

This function determines optimal $\frac{b}{\ell}$ ratio for a given body mass m_b .

```

function bol_opt = find_bol_opt( $m_b$ )
global GLOBAL_DATA ;
GLOBAL_DATA(5) =  $m_b$ ;
 $\ell$  = GLOBAL_DATA(6) ;
bol_opt = fmin('theta_minus_theta', 0,  $\ell$ , [0,  $\frac{\ell}{100}$ ]) ;
bol_opt =  $\frac{b_{opt}}{\ell}$  ;

```

C.2.14 theta_minus_theta

This function calculates $|\theta_{0max} - \theta_{0opt}|$ and is as given below.

```
function th_m_th = theta_minus_theta(b_arg)
global GLOBAL_DATA ;
get_GLOBAL_DATA ;
b = b_arg ;

[Jb, hr, wr, td, br] = BodyDesign(mb, b, ℓ, ma, N, NoLoadSpeed, Stall Torque, g,
                                     dg, ws) ;

[mℓ, Jℓ, dℓ, tℓ, wℓ, J0] = LegDesign2(ma, mb, ℓ, motor Diameter, gear Diameter,
                                             motor Mass, gear Mass, wr, ws) ;

[A,B] = LinearModel_Order3(J0, Jb, Jm, N, mb, ℓ, mℓ, d, g, γ, η, Kt, Kb, R) ;
%- estimate maximum initial displacement based on linear model,
Theta0max = MaxTheta0(Vmax, NoLoadSpeed, A, B) ;
%- compute optimal initial displacement based on criteria
Theta0opt = sin-1  $\left( \frac{\sqrt{3 - \sqrt{1 + 8\left(\frac{b}{\ell}\right)^2}}}{2} \right) ;$ 
th_m_th = abs(Theta0max - Theta0opt) ;
```

C.2.15 get_GLOBAL_DATA

This file makes the current design variables stored in a global array GLOBAL_DATA local.

Also, see put_GLOBAL_DATA.

```
J0 = GLOBAL_DATA(1) ;
Jb = GLOBAL_DATA(2) ;
Jm = GLOBAL_DATA(3) ;
N = GLOBAL_DATA(4) ;
mb = GLOBAL_DATA(5) ;
ℓ = GLOBAL_DATA(6) ;
mℓ = GLOBAL_DATA(7) ;
d = GLOBAL_DATA(8) ;
g = GLOBAL_DATA(9) ;
γ = GLOBAL_DATA(10) ;
```

```
 $\eta = \text{GLOBAL\_DATA}(11) ;$   
 $K_t = \text{GLOBAL\_DATA}(12) ;$   
 $K_b = \text{GLOBAL\_DATA}(13) ;$   
 $R = \text{GLOBAL\_DATA}(14) ;$   
 $V_{max} = \text{GLOBAL\_DATA}(15) ;$   
 $\text{NoLoadSpeed} = \text{GLOBAL\_DATA}(16) ;$   
 $J_\ell = \text{GLOBAL\_DATA}(17) ;$   
 $m_a = \text{GLOBAL\_DATA}(18) ;$   
 $T_{sim} = \text{GLOBAL\_DATA}(19) ;$   
 $\alpha = \text{GLOBAL\_DATA}(20) ;$   
 $N_{FS} = \text{GLOBAL\_DATA}(21) ;$   
 $SY_{leg} = \text{GLOBAL\_DATA}(22) ;$   
 $\rho = \text{GLOBAL\_DATA}(23) ;$   
 $w_s = \text{GLOBAL\_DATA}(24) ;$   
 $E = \text{GLOBAL\_DATA}(25) ;$   
 $delol = \text{GLOBAL\_DATA}(26) ;$   
 $d_\ell = \text{GLOBAL\_DATA}(27) ;$   
 $t_\ell = \text{GLOBAL\_DATA}(28) ;$   
 $w_\ell = \text{GLOBAL\_DATA}(29) ;$   
 $\text{motor Mass} = \text{GLOBAL\_DATA}(30) ;$   
 $\text{gear Mass} = \text{GLOBAL\_DATA}(31) ;$   
 $\text{motor Diameter} = \text{GLOBAL\_DATA}(32) ;$   
 $\text{gear Diameter} = \text{GLOBAL\_DATA}(33) ;$   
 $\text{Stall Torque} = \text{GLOBAL\_DATA}(34) ;$   
 $dg = \text{GLOBAL\_DATA}(35) ;$   
 $C_p = \text{GLOBAL\_DATA}(36) ;$   
 $C_{th} = \text{GLOBAL\_DATA}(37) ;$   
 $R_{th} = \text{GLOBAL\_DATA}(38) ;$   
 $\alpha_c = \text{GLOBAL\_DATA}(39) ;$   
 $T_\alpha = \text{GLOBAL\_DATA}(40) ;$   
 $i_{max} = \text{GLOBAL\_DATA}(41) ;$ 
```

C.2.16 LinearModel_Order3

This sets up the linear dynamic model of the single leg support phase of the biped.


```

[A,B] = LinearModel_Order3(J0, Jb, Jm, N, mb, l, ml, d, g, gamma, eta, Kt, Kb, R) ;
M = [J0 + Jb + Jm Jb + N * Jm; Jb + N * Jm Jb + N * N * Jm] ;
Ds = diag([(mb * l + ml * d) * g * sin(gamma) - eta * Kt * Kb * N * N/R]) ;
S = M(-1) * Ds ;
T = M(-1) * [0 eta * Kt * N/R]' ;
A = [ 0 1 0; S(1, 1) 0 S(1, 2); S(2, 1) 0 S(2, 2) ] ;
B = [ 0 T(1) T(2) ]' ;

```

C.2.17 MaxTheta0

This function estimates the maximum initial displacement (Theta0max) based on linear model, ideal initial conditions and constant maximum control effort.

```

function Theta0max = MaxTheta0(Vmax, NoLoadSpeed, A, B) ;
xp = -A(-1) * B * Vmax ;
[V,D] = eig(A) ;
lambda = diag(D) ;
[lamax,imax] = max(lambda) ;
[sortedlambda,sorti] = sort(lambda) ;
for j = 1 : 3 ; sortedV(:, j) = V(:, sorti(j)) ; end ;
Vc = [sortedV(2, 1) sortedV(2, 2); sortedV(3, 1) sortedV(3, 2)] ;
Xc = [ -xp(2) -NoLoadSpeed-xp(3) ]' ;
c = Vc(-1) * Xc ;
Theta0max = c(1)*sortedV(1, 1) + c(2)*sortedV(1, 2) + xp(1) ;

```

C.2.18 doublesort

This function returns the indexes of the elements of matrix A sorted in ascending order.

e.g.-min(A)= A(Msort(1), Nsort(1)).

```

function [Msort,Nsort] = doublesort(A)
[m,n] = size(A) ;

for i = 1 : m,
    for j = 1 : n,
        M(i, j) = i ;
        N(i, j) = j ;
    end
end

```

```

end
Avec = A(:) ;
Mvec = M(:) ;
Nvec = N(:) ;
[sortedAvec, Isort] = sort(Avec) ;

for i = 1 : length(Avec),
    Msort(i) = Mvec(Isort(i)) ;
    Nsort(i) = Nvec(Isort(i)) ;
end

```

C.2.19 SetBestScript

After obtaining MBopt(iN, iA), Bopt(iN, iA) and BOLOpt(iN, iA) from function “Optimize”, the function “doublesort” determines the indexes(iNbest, iAbest) by arranging the elements of matrix “BOLOpt” in an ascending order. Then the sort routine (1) sorts MBopt, Bopt, BOLOpt in an ascending order using indexes(iNbest, iAbest) for all the actuator and reduction unit combinations, (2) assigns them to m_b_best , b_best , bol_best respectively and (3) sets $ibest = 1$. Once the $ibest$ is set, the script “SetBestScript” sets the local environment upto the parameters of $ibest$. This script is as given below.

```

ibest
iA = iAbest(ibest);
iN = iNbest(ibest) ;
 $m_b = m_b\_best(ibest)$  ;
b = b.best(ibest) ;
SetBipedScript ;

```

C.2.20 SimGDscript

This script simulates the controlled single-leg support phase modelled as inverted pendulum based on the data in GLOBAL_DATA which is as given below.

```

global GLOBAL_DATA ;
global  $K_b$  R alpha.c  $C_{th}$   $R_{th}$  N i_max ;
get_GLOBAL_DATA;
[A,B] = LinearModel_Order3( $J_0$ ,  $J_b$ ,  $J_m$ , N,  $m_b$ ,  $\ell$ ,  $m_\ell$ ,  $d$ ,  $g$ ,  $\gamma$ ,  $\eta$ ,  $K_t$ ,  $K_b$ , R) ;
%– estimate maximum initial displacement based on linear model,

```

```

Theta0max = MaxTheta0(V_max, NoLoadSpeed, A, B) ;
%- compute optimal initial displacement based on criteria
Theta0opt = sin-1  $\left( \frac{\left[ \sqrt{3 - \sqrt{1 + 8\left(\frac{b}{l}\right)^2}} \right]}{2} \right)$  ;
th_m_th = abs(Theta0max - Theta0opt) ;
% LQR design with output weighting
% Set optimization weights and calculate feedback gains
Q = diag([1/Theta0max/Theta0max 1/1.6/1.6 1/i_max/i_max]') ;
z = 1/V_max/V_max ;
C = diag([1 1 -K_b*N/R]') ;
D = [0 0 1/R]';
[Kr, S] = lqry(A, B, C, D, Q, z) ;
% set global variables for closed-loop simulation function pend
global A_ B_ Kr_ Vmax_ i_max_
A_ = [A, [0 0 0]'; [0 0 1 0]] ;
B_ = [B', 0]';
Kr_ = [Kr, 0, 0] ;
Vmax_ = V_max ;
i_max_ = i_max ;
% integrate the ode's to simulate the closed-loop system
[t, x] = ode23('pend', 0, Tsim, [.99*Theta0max, 0, -NoLoadSpeed, pi/2, 25]') ;
%- Computation of motor control voltage, back emf & current for plotting.
u = uofx(x') ;
bemf = K_b*x(:,3)*N ;
amps = (u - bemf)/R ;
[F_n, F_t, mu] = Foot_forces(x, J_0, J_b, J_m, N, m_b, l, m_l, d, g, gamma, eta, K_t, K_b, R, u) ;

```

C.2.21 pend

This function which is named as 'Pend' sets the final state equation for simulation. This name also signifies the inverted pendulum model used for deriving the single-leg support phase dynamics.

```

function xdot = pend(t, x)
global A_ B_ K_b R alpha_c C_th R_th N ;

```

```

global GLOBAL_DATA ;
u = uofx(x) ;
x_nl = x ;
x_nl(1) = sin(x1) ;
Coeffth1 = -1/Cth/Rth ;
i = (u - Kb * N * xnl(3))/R ;
Coeffth2 = 1/Cth/Rth * 25 + 1/Cth * i2 * R ;
xdot = [A-, [0 0 0 0]'; [0 0 0 0 Coeffth]]*x_nl + [B-; 0] *u + [0 0 0 0 Coeffth2]' ;

```

C.2.22 uofx

This function is responsible for setting the control u based on the current state x and feedback gain K_r . Also, it models the control saturation based on maximum supply voltage and current. Name of this function 'uofx' ($u=f(x)$) signifies control 'u' as a function of current state 'x'.

```

function u = uofx(x)
global Kr- Vmax- Kb N R imax- ;
u = (-Kr*x)';

for I = 1 : length(u)
    if abs(u(I)) > Vmax-
        u(I) = sign(u(I))*Vmax- ;
    end
    x3 = x(3,I);
    it =  $\frac{u(I)-K_b*N*x_3}{R}$ ;
    if abs(it) > imax-
        it = sign(it)*imax- ;
        u(I) = R*it + Kb * N * x3 ;
    end
end
end

```

Where

$K_r = [K_r \ 0 \ 0]$, feedback gain matrix for the complete system.

$V_{max} = V_{max}$, Maximum supply voltage.

$i_{max} = i_{max}$, Maximum supply current.

Appendix D

Motor Data for Maxon_990

D.1 Introduction

This appendix presents the data for Maxon_990 DC motor (Chapter 6, Subsection 6.2.1) and associated gear properties. Note that this motor with a gear ratio of 33.2 was responsible for the biped design parameters presented in Table 6.2.1.

D.2 MAXON_990.m File Used in MATLAB Routine

```
R = 10.5; % Ohms
Kt = 0.0219; % Nm/Amp
Kb = 0.0219; % Volts/(rad/sec)
Jm = 5.5E - 7; % Kg*m2
Vmax = 19.37; % Volts
imax = 3.69; % Ampere
motor Mass = .092+.02; % Kg includes encoder mass
motor Diameter= .022; % m
motor Length = .048+.014; % m includes encoder length
Stall Torque = Kt*Vmax/R; % Nm
dg = 5/1000; % m gear shaft diameter
Cp = 383; % J/kg deg C Specific heat of copper.
Cth = Cp*motor Mass; % Thermal capacitance of the motor J/deg. C.
Rth = 14.1+3.6; % Thermal resistance of the motor deg C/J/sec.
Trotor = 125; % Maximum rotor temperature Deg. C.
gear Ratio Set = [ 1 4.33 18.75 33.2 81.2 143.8 199.3];
```

gear Eff. Set = [1 .85 .612 .612 .373 .373 .373];

gear Mass Set = 1/1000* [0 81 107 107 130 130 130]; % Kg

gear Diameter Set = 1/1000*[0 26 26 26 26 26 26]; % m

gear Length Set = 1/1000*[0 30.6 39.4 39.4 48.1 48.1 48.1]; % m

Appendix E

Motor Data for Pittman_3112_43

E.1 Introduction

This appendix presents the data for Pittman_3112.43 brushless DC motor (Chapter 6, Subsection 6.2.2) and associated gear properties. Note that this motor with a gear ratio of 24 was responsible for the biped design parameters presented in Table 6.2.2.

E.2 PITTMAN3112_43.m File Used in MATLAB Routine

```
R = 10.7; % Ohms
Kt = 0.0486; % Nm/Amp
Kb = 0.0486; % Volts/(rad/sec)
Jm = 1.52E - 6; % Kg*m2
Vmax = 37.5; % Volts
imax = 7; % Ampere
motor Mass = .19; % Kg includes encoder mass
motor Diameter= .043; % m
motor Length = .067; % m includes encoder length
Stall Torque = Kt*Vmax/R; % Nm
dg = 8/1000; % m gear shaft diameter
Cp = 383; % J/kg deg C Specific heat of copper.
Cth = Cp*motor Mass; % Thermal capacitance of the motor J/deg. C.
Rth = 5.1; % Thermal resistance of the motor deg C/J/sec.
Trotor = 155; % Maximum rotor temperature Deg. C.
gear Ratio Set = [ 1 4 17.33 24 75.11 144 325.47 864 1410.37 5184];
```

gear Eff. Set = [1 .80 .64 .64 .51 .51 .41 .41 .33 .33];
gear Mass Set = 1/1000* [0 258 315 315 371 371 427 427 483 483]; %Kg
gear Diameter Set = 1/1000*[0 56 56 56 56 56 56 56 56 56]; % m
gear Length Set = 1/1000*[0 34.8 42.4 42.4 50 50 57.7 57.7 65.3 65.3]; % m

Appendix F

Motor Data for Maxon_136

F.1 Introduction

This appendix presents the data for Maxon_136 DC motor (Chapter 6, Subsection 6.2.3) and associated gear properties. Note that this motor with a gear ratio of 19.2 was responsible for the biped design parameters presented in Table 6.2.3.

F.2 MAXON_136.m File Used in MATLAB Routine

```
R = 5.8; % Ohms
Kt = 0.0399; % Nm/Amp
Kb = 0.0399; % Volts/(rad/sec)
Jm = 30E - 7; % Kg*m2
Vmax = 29; % Volts
imax = 10; % Ampere
motor Mass = .210+.02; % Kg includes encoder mass
motor Diameter= .032; % m
motor Length = .06+.019; % m includes encoder length
Stall Torque = Kt*Vmax/R; % Nm
dg = 6/1000; % m gear shaft diameter
Cp = 383; % J/kg deg C Specific heat of copper.
Cth = Cp*motor Mass; % Thermal capacitance of the motor J/deg. C.
Rth = 12.8; % Thermal resistance of the motor deg C/J/sec.
Trotor = 125; % Maximum rotor temperature Deg. C.
gear Ratio Set = [ 1 5.2 19.2 27 35 100 181 236];
```

gear Eff. Set = [1 .80 .6 .6 .6 .42 .42 .42];

gear Mass Set = 1/1000* [0 130 170 170 170 215 215 215]; % Kg

gear Diameter Set = 1/1000*[0 32 32 32 32 32 32 32]; % m

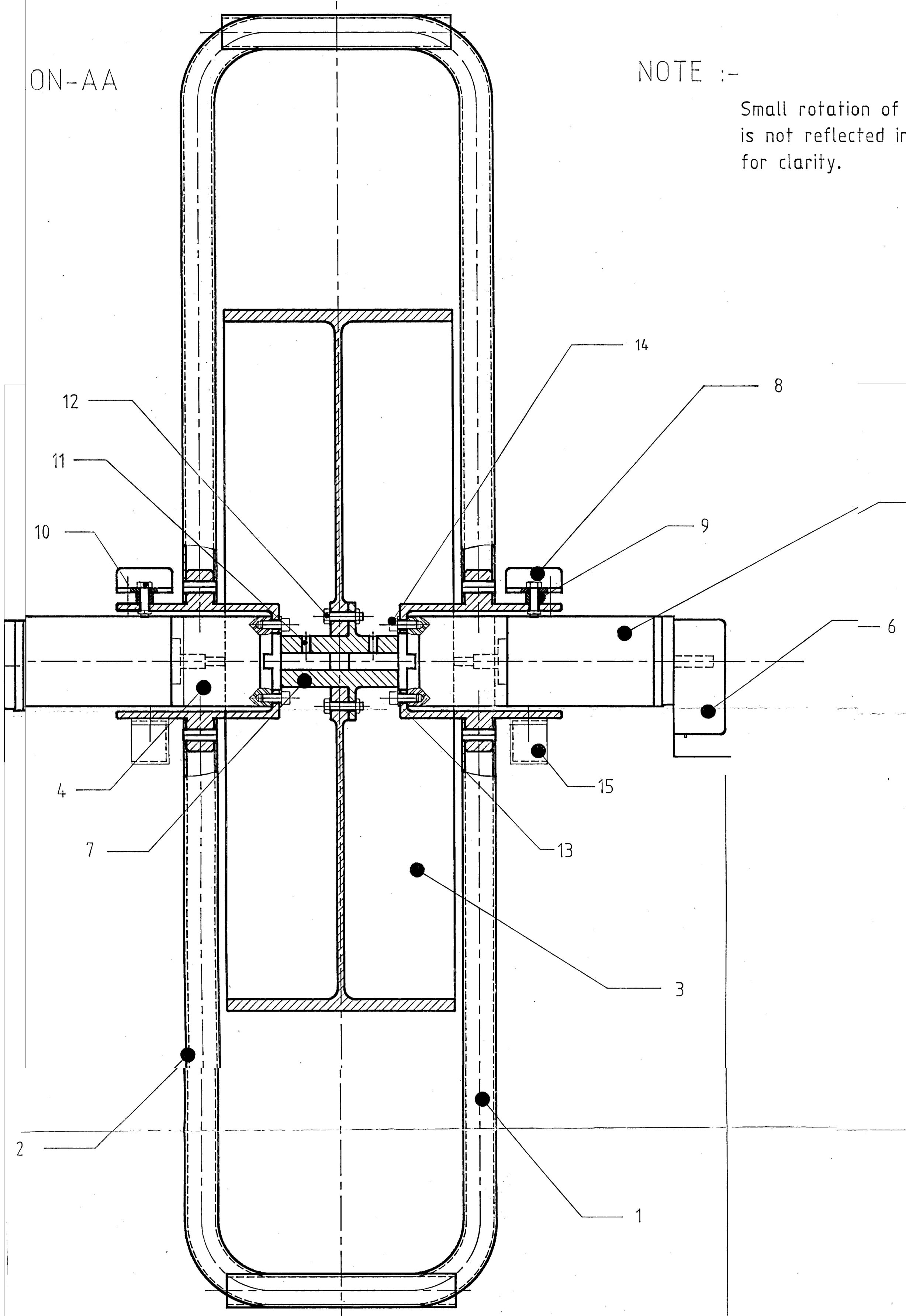
gear Length Set = 1/1000*[0 26.6 36.1 36.1 36.1 45.6 45.6 45.6]; % m

COMPUTER DRAWING - DRAWN TO AS1100		
Tolerances unless otherwise specified	DIMENSIONS	
Linear +/-	MILLIMETRES	
Angular +/-		
Surface Finishes are in micro metres Ra	Remove all burrs & sharp edges	

ON-AA

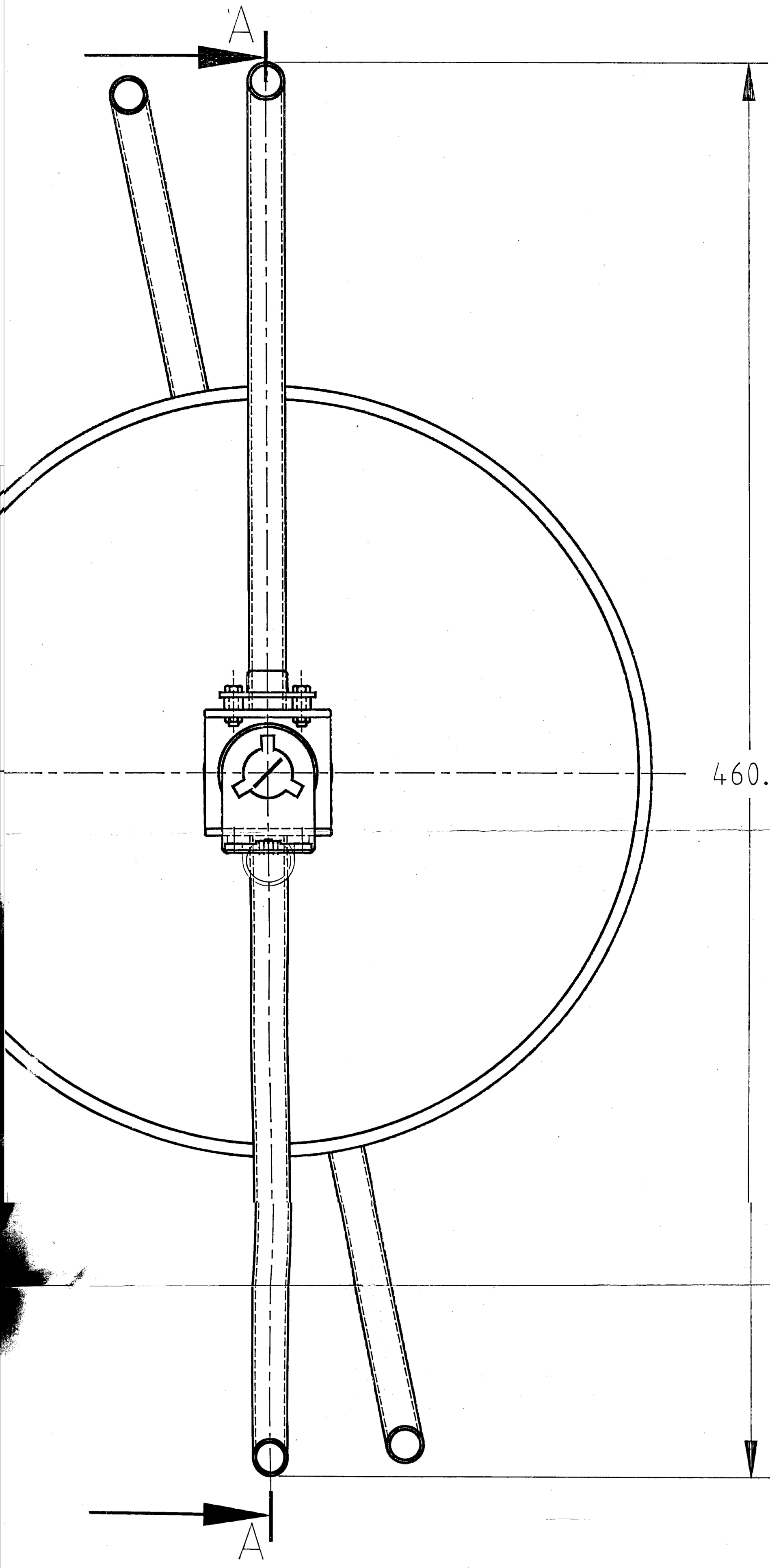
NOTE :-

Small rotation of the leg assy-1 is not reflected in the side view for clarity.



15	Spectron Tilt Sensor L211U+557A	2	STD
14	Hexagonal Socket Head Screw	8	STD -HTS 8.8 M3x.5x8mm long
13	Washer	16	STD M3
12	Hexagonal headed bolt & nut	6	STD M3x.5x14mm long
11	Grub Screw Slotted HD & Flat end	6	STD -HTS 8.8 M3x.5x6mm long
10	Hexagonal headed bolt & nut	2	STD -HTS 8.8 M3x.5x10mm long
9	Spacer	2	Al alloy
8	Gyrostar Assy	2	PCB+Std Murata-ENC-055
7	Coupling	1	Drg. No.: 1019310013
6	Digital Encoder	2	STD part- Maxon-34-09
5	EC Motor	2	STD part- Maxon-EC-032-060- -36-EAR20DB
4	Reduction Unit	2	STD part- Maxon-2932.702.0019. 0.000
3	Body	1	Drg. No.: 1019310012
2	Leg Assembly-2	1	Drg. No.: 1019310016
1	Leg Assembly-1	1	Drg. No.: 1019310015
NO.	PART NAME & REFERENCE	QTY	REMARKS

Drawn R BALE	Scale 1:1	DO NOT SCALE	Date NOV 16 1993
Title BIPED WALKING MACHINE ASSEMBLY			
Drawing No. 1019310011	Sheet 1 of 1		Sheet Size A1
THE AUSTRALIAN NATIONAL UNIVERSITY FACULTY OF ENGINEERING AND INFORMATION TECHNOLOGY DEPARTMENT OF ENGINEERING Canberra, ACT, 0200, ph 06-2493378, fax 06-2490506			



460.4

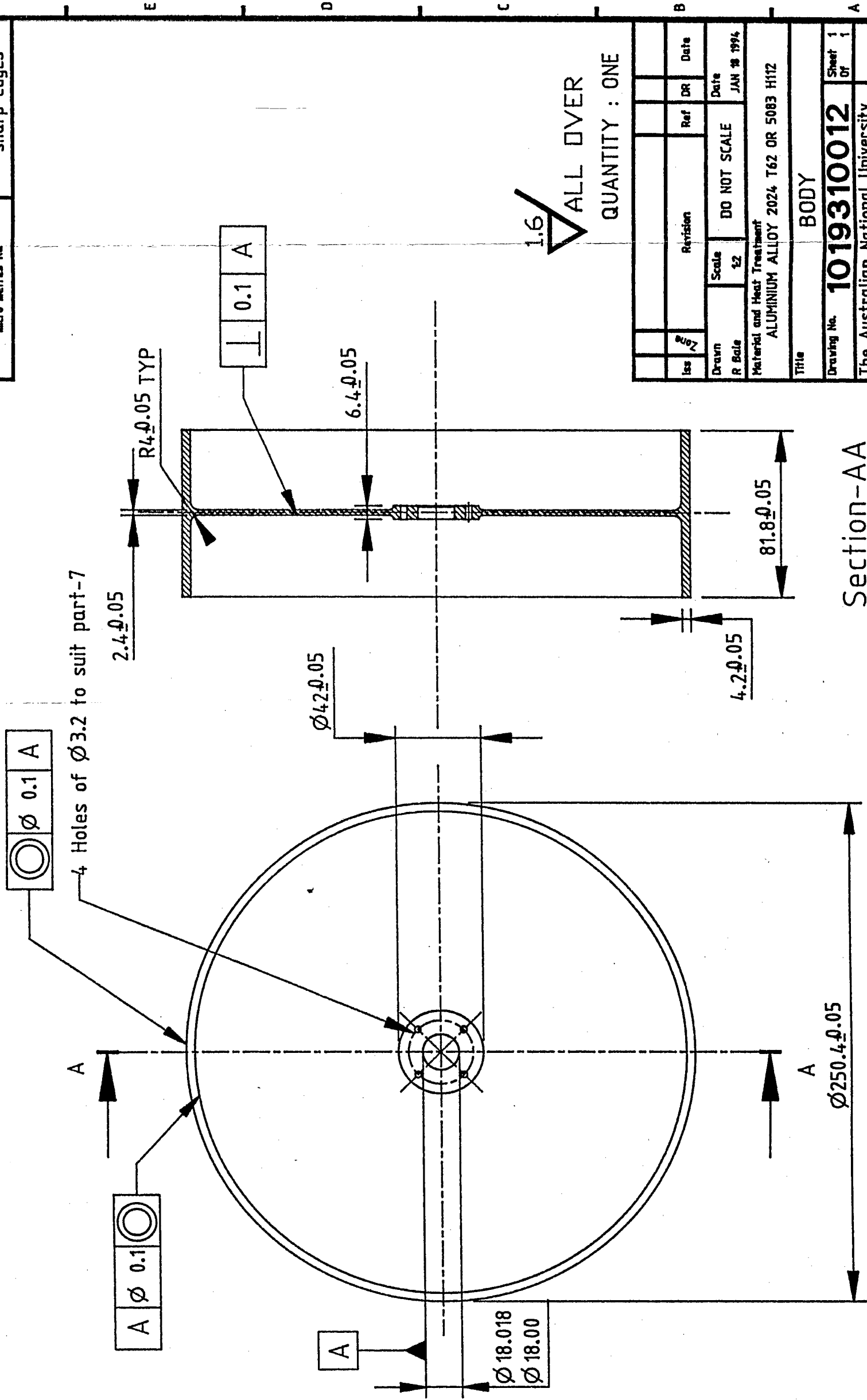
S

E

COMPUTER DRAWING - DRAWN TO AS1100

DIMENSIONS MILLIMETRES	
Remove all burrs & sharp edges	
Surface finishes are in micro metres Ra	

1 2 3 4 5 6 7 8



1.6 ALL OVER
 QUANTITY : ONE

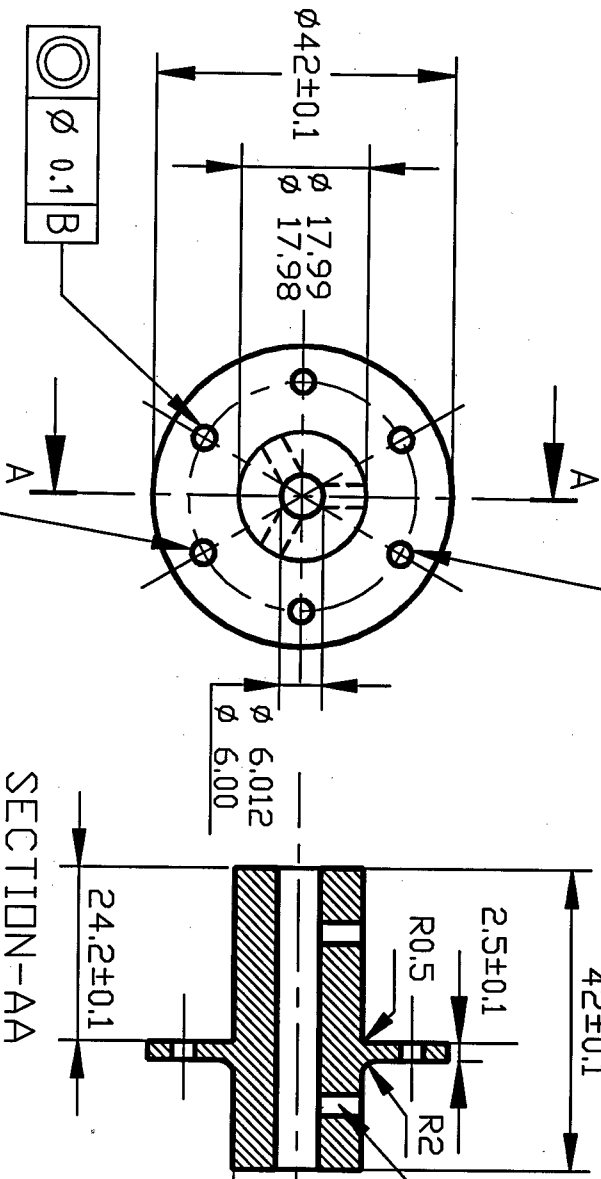
Iss	Zone	Revision	Ref	DR	Date
Drawn	Scale	DO NOT SCALE	Date	JAN 18 1994	
R	Bale	12	Material and Heat Treatment		
ALUMINIUM ALLOY 2024 T62 OR 5083 H112					
Title					
BODY					
Drawing No.	1019310012				Sheet 1
The Australian National University					Of 1
Faculty of Engineering and Information Technology					Sheet Size
Department of Engineering					A3
Canberra, ACT, 0200, ph 06-2493378, fax 06-2490506					

Section-AA

Drawing No. 1019310012

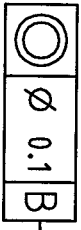
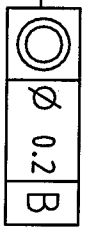
6 5 4 3 2 1

6 Equipped Holes
of ϕ 3.2 on 32mm
PCD



COMPUTER DRAWING - DRAWN TO AS1100	
DIMENSIONS MILLIMETRES	
Surface Finishes are in micro metres Ra	Remove all burrs & sharp edges

SECTION-AA

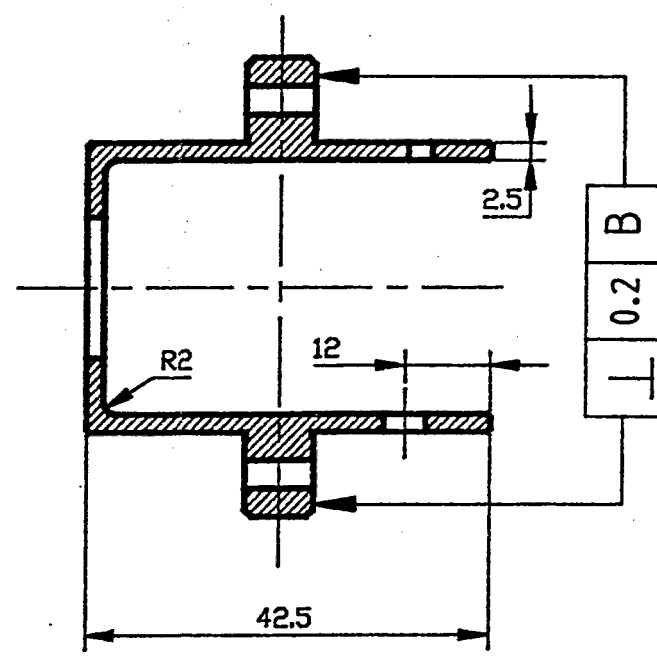
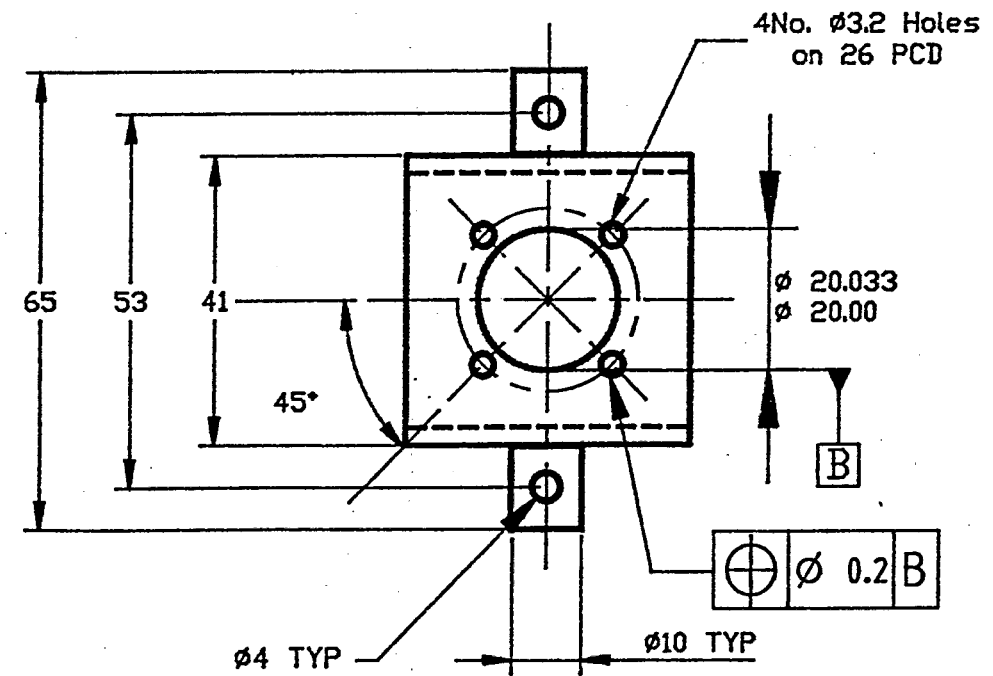
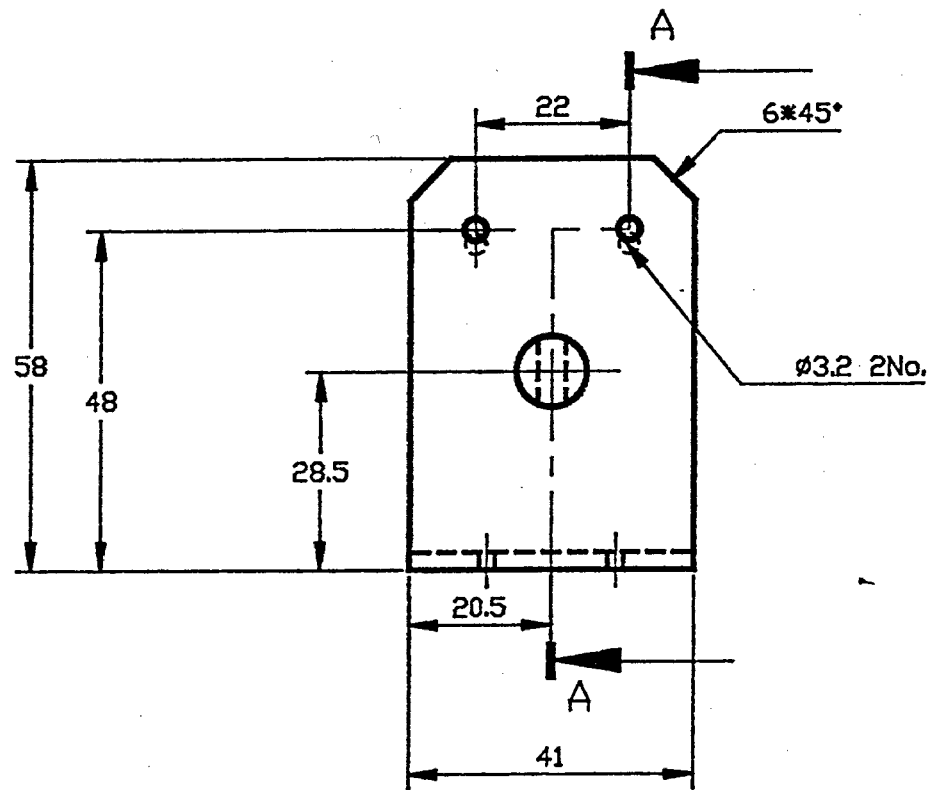


QUANTITY : ONE

Title		COUPLING			
Drawing No.		1019310013			
Drawn		Scale	DO NOT SCALE	Date	DEC 21 1993
Iss		Revision	Ref	DR	Date
Zone		Released for Fabrication			
Material and Heat Treatment ALUMINIUM Alloy 2014-T6					
Raw material- 45 ϕ x4.5mm long					

THE AUSTRALIAN NATIONAL UNIVERSITY FACULTY OF ENGINEERING AND INFORMATION TECHNOLOGY DEPARTMENT OF ENGINEERING		Sheet 1 Of 1
Canberra, ACT, 0200, ph 06-2493378, fax 06-2490506		Sheet Size A4

Drawing No.
1019310014



COMPUTER DRAWING - DRAWN TO AS1100	
Tolerances unless otherwise specified Linear + or - 0.1 Angular + or - 0.2°	DIMENSIONS MILLIMETRES
Surface Finish are in microns	Remove all burrs & sharp edges

1.6


ALL OVER

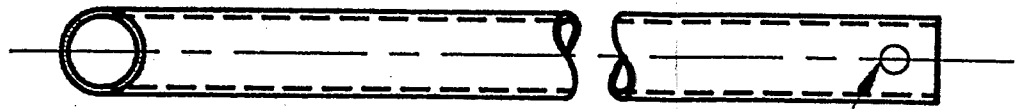
QUANTITY : TWO

A	Released for Fabrication	Y.N.
Iss	Revision	Ref DR Date
Drawn	Scale	Date
R BALE	1:1	DO NOT SCALE 21 DEC 1993
Material and Heat Treatment ALUMINIUM ALLOY-2014-T6		
Title BRACKET		
Drawing No. 1019310014		Sheet 1 Of 1
THE AUSTRALIAN NATIONAL UNIVERSITY FACULTY OF ENGINEERING AND INFORMATION TECHNOLOGY DEPARTMENT OF ENGINEERING Canberra, ACT, 0200, ph 06-2493378, fax 06-2490506		Sheet Size A3

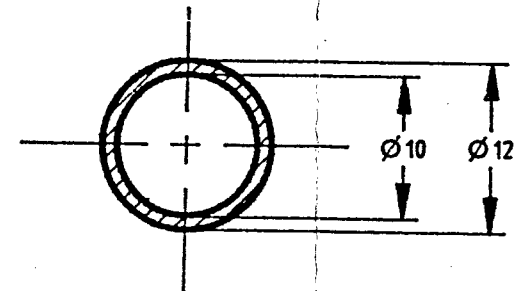
Drawing No.
1019310015

8 7 6 5 4 3 2 1

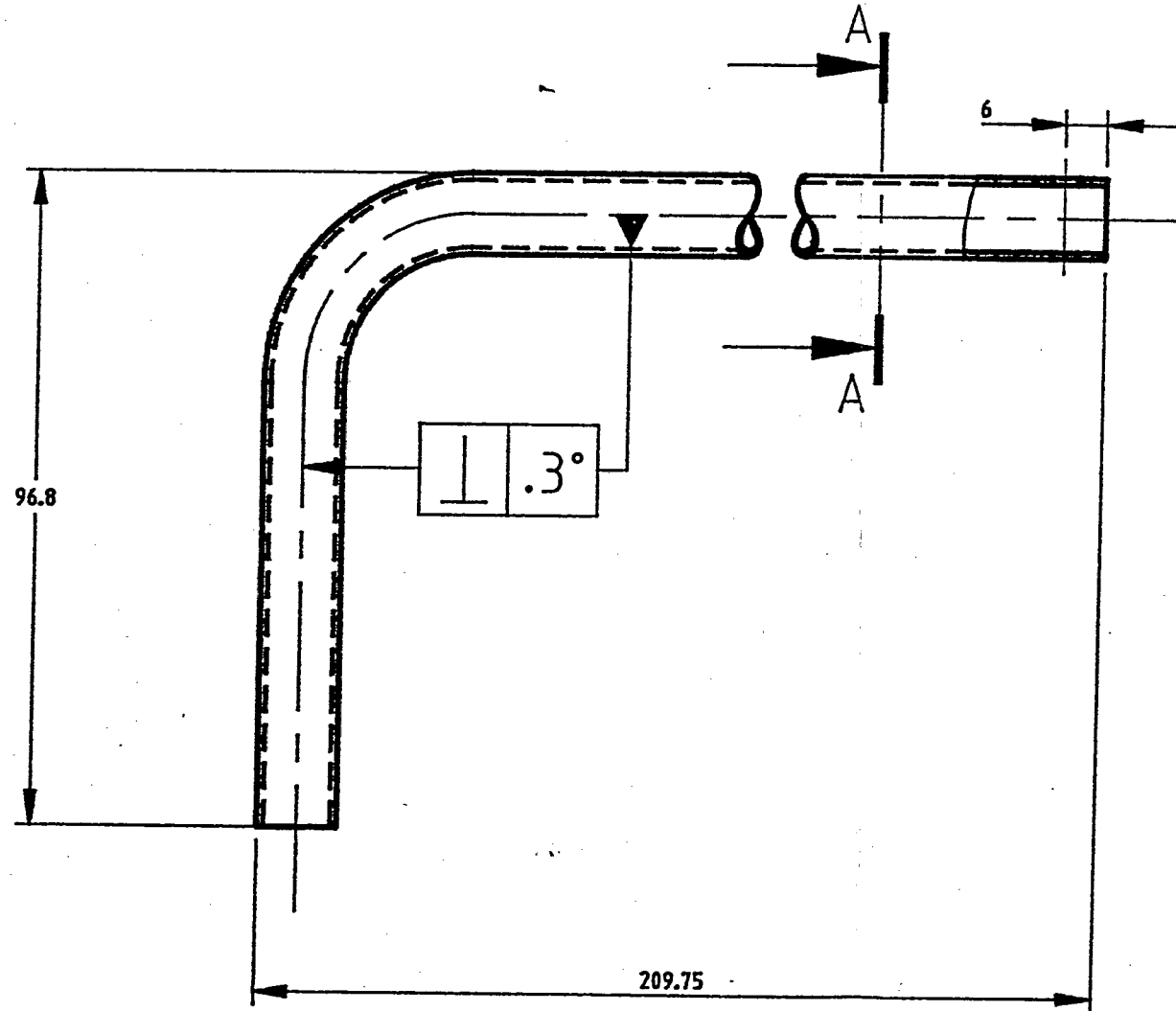
COMPUTER DRAWING - DRAWN TO AS1100		
Tolerances unless otherwise Specified Linear ± 0.25	DIMENSIONS MILLIMETRES	
Surface Finishes are in micro metres Ra	Remove all burrs & sharp edges	



Ø4



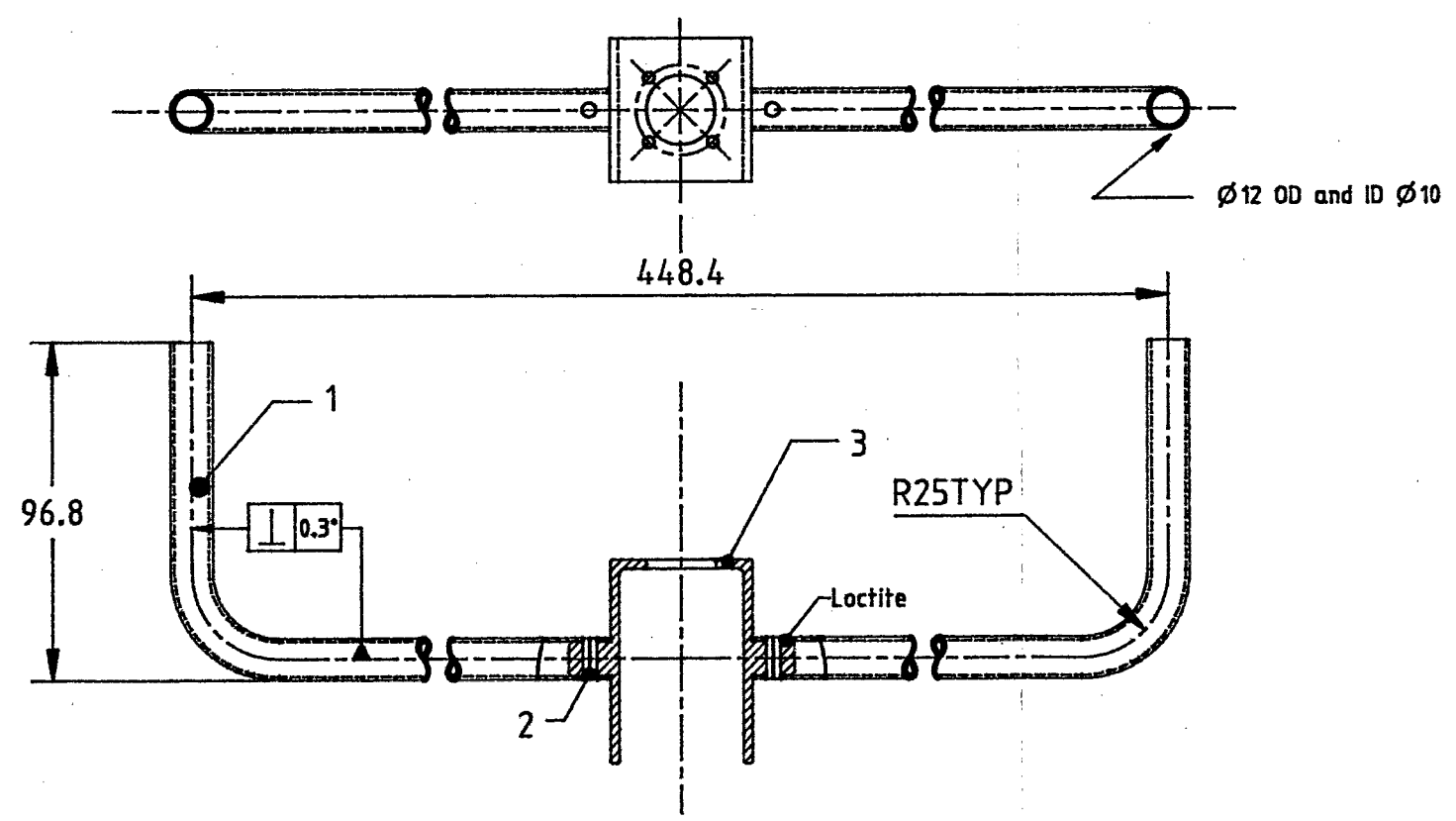
SECTION-AA
SCALE-2:1



Material : 6061-T6 OR T62
STD ALUMINIUM ALLOY TUBE
QUANTITY - FOUR

ITEM	QTY	DESCRIPTION	Ref	REMARKS
Drawn R BALE	Scale 1:1	DO NOT SCALE	Date DEC 22 1993	
Material and Heat Treatment				
Title		LEG		
Drawing No. 1019310015			Sheet 1 Of 1	
THE AUSTRALIAN NATIONAL UNIVERSITY FACULTY OF ENGINEERING AND INFORMATION TECHNOLOGY DEPARTMENT OF ENGINEERING				Sheet Size A3
Canberra, ACT, 0200, ph 06-2493378, fax 06-2490506				

Drawing No.
1019310016



COMPUTER DRAWING - DRAWN TO AS1100

Tolerances unless otherwise specified Linear ± 0.25	DIMENSIONS MILLIMETRES	
Surface Finishes are in micro metres Ra	Remove all burrs & sharp edges	

Note : Reduction unit + Motor + Encoder assembly is not shown here for clarity

QUANTITY : Two

ITEM	QTY	DESCRIPTION	Ref	REMARKS
3	2	ROLL PIN TO SUIT 4Ø		STD
2	1	BRACKET	1019310014	AL ALLOY
1	2	Leg	1019310017	STD +FAB

Drawn R BALE	Scale 1:2	DO NOT SCALE	Date DEC 22 1993
-----------------	--------------	--------------	---------------------

Material and Heat Treatment

Title **LEG ASSEMBLY**

Drawing No. **1019310016** Sheet 1 Of 1

THE AUSTRALIAN NATIONAL UNIVERSITY
FACULTY OF ENGINEERING AND INFORMATION TECHNOLOGY
DEPARTMENT OF ENGINEERING
Canberra, ACT, 0200, ph 06-2493378, fax 06-2490506

Sheet Size
A3